UNDERWATER MULTIPLE SCATTERING OF LIGHT FOR SYSTEM DESIGNERS

PART I. AN EXPONENTIAL MULTIPLE-SCATTERING MODEL.

PART II. EVALUATION OF THE EXPONENTIAL MULTIPLE-SCATTERING MODEL.

NAVAL UNDERSEA CENTER

NOVEMBER 1973

DISCLAIMER NOTICE

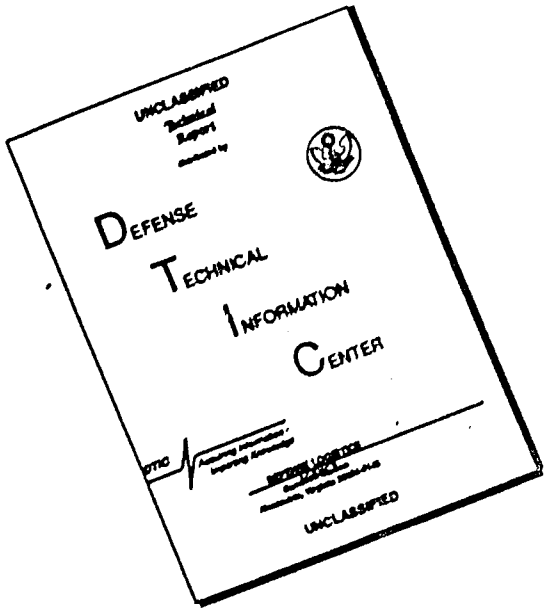

THIS DOCUMENT IS BEST QUALITY AVAILABLE. THE COPY FURNISHED TO DTIC CONTAINED A SIGNIFICANT NUMBER OF PAGES WHICH DO NOT REPRODUCE LEGIBLY.

NAVAL UNDERSEA CENTER, SAN DIEGO, CA. 92132

AN ACTIVITY OF THE NAVAL MATERIAL COMMAND

ROBERT H. GAUTIER, CAPT, USN
Commander

Wm. B. McLEAN, Ph.D.
Technical Director

ADMINISTRATIVE INFORMATION

The work reported was funded by Naval Undersea Center, Independent Research Funds, as part of the ongoing studies being pursued by the Advanced Systems Division, Ocean Technology Department, in the field of underwater optics. The work was performed during fiscal year 1972 from July 1971 to June 1972.

ACKNOWLEDGEMENTS

PART I

The author has profited greatly from informative discussions with Messrs. Tenny Keil and Richard Bocker and Drs. Clarence Funk and Paul Warnshuis. The encouragement of management, specifically Messrs. Ivor Lemaire and Paul Heckman and Dr. Eugene Cooper, throughout this project has been appreciated.

PART II

The author wishes to thank Drs. Alan Gordon and Clarence Funk for their assistance in generating and preparing the model predictions and experimental data for use in this report.

Released by
I. P. LEMAIRE, Head
Advanced Systems Division

Under authority of
H. R. TALKINGTON, Head
Ocean Technology Department

UNCLASSIFIED

Security Classification

DOCUMENT CONTROL DATA - R & D

(Security classification of title, body of abstract and indexing annotation must be entered when the overall report is classified)

1 ORIGINATING ACTIVITY (Corporate author)	2a. REPORT SECURITY CLASSIFICATION
Naval Undersea Center San Diego, California 92132	UNCLASSIFIED
	2b. GROUP

3 REPORT TITLE

UNDERWATER MULTIPLE SCATTERING OF LIGHT FOR SYSTEM DESIGNERS

4 DESCRIPTIVE NOTES (Type of report and inclusive dates)

Research and Development July 1971 – June 1972

5 AUTHOR(S) (First name, middle initial, last name)

Alan Gordon
Max R. Knittel

6 REPORT DATE	7a. TOTAL NO. OF PAGES	7b. NO. OF REFS
November 1973	97	14

8a. CONTRACT OR GRANT NO	9a. ORIGINATOR'S REPORT NUMBER(S)
b. PROJECT NO	NUC TP 371
c.	9b. OTHER REPORT NO(S) (Any other numbers that may be assigned this report)
d.	

10 DISTRIBUTION STATEMENT

Approved for public release; distribution unlimited

11 SUPPLEMENTARY NOTES	12 SPONSORING MILITARY ACTIVITY
	Naval Undersea Center San Diego, California 92132

13 ABSTRACT

An iterative method is presented which yields an exponential model for underwater multiple scattering in the forward direction. An easily evaluated effective attenuation coefficient is derived which allows rapid prediction of flux through an aperture and on-axis irradiance. Extensive comparison with experimental and Monte Carlo results indicate that our simple approximate expressions retain predictive value out to seven to ten attenuation lengths.

DD FORM 1 NOV 65 1473 (PAGE 1)

0102-014-6600

UNCLASSIFIED

Security Classification

14 KEY WORDS	LINK A		LINK B		LINK C	
	ROLE	WT	ROLE	WT	ROLE	WT
Underwater optics						
Multiple scattering						
Visibility models						

SUMMARY

PROBLEM

Provide the underwater optical systems designer with a physical description of multiple scattering of light. Derive simple approximate expressions for the target plane illumination which are valid in the region of present hardware viewing capabilities.

RESULTS

An iterative method is presented which yields an exponential model for underwater multiple scattering in the forward direction. An easily evaluated effective attenuation coefficient is derived which allows rapid prediction of flux through an aperture and on-axis irradiance. Extensive comparison with experimental and Monte Carlo results indicate that our simple approximate expressions retain predictive value out to seven to ten attenuation lengths.

RECOMMENDATIONS

Further studies into delimiting the range of validity, relaxing some approximations and providing more rigorous justification for others, could improve the predictive utility of the present model.

CONTENTS

INTRODUCTION 1

PART I. AN EXPONENTIAL MULTIPLE-SCATTERING MODEL 3

PART II. EVALUATION OF THE EXPONENTIAL MULTIPLE-SCATTERING MODEL 43

INTRODUCTION

Man's increased presence in the underwater environment has led to a need to increase the range of his sensory perceptions in this unfamiliar milieu. The Naval Undersea Center has been particularly active in this area, realizing that the ability to perform useful tasks underwater is determined to a great extent by the quantity and quality of sensory inputs. Recent years have seen great improvements in our ability to utilize and exploit the information contained in optical and acoustic signals.

In the field of underwater optics, many techniques have been introduced to enable viewing at greater distances. Though each has its disadvantages, the techniques of range-gating, volume scanning, and adaptive scanning have yielded imagery at greater distances than heretofore possible. Measurements of water parameters have led to an increased appreciation of the viewing problem and indicate that further improvements in viewing range are possible.

Increased optical hardware capability presents a mixed blessing to the systems designer. To advantage is that he can now specify systems which are certain to yield increased viewing ranges over prior techniques. However, he has difficulty predicting the performance of these systems since they operate deep in the multiple-scattering domain. Because the light is scattered many times in its travels from source to target to receiver, irradiance values become difficult to predict. The use of conventional single-scattering formulas can lead to predictions which are in error by orders of magnitude.

The systems designer is thus faced with the problem of designing an underwater viewing system which will perform in the complicated multiple-scattering domain. Often compounding the problem is the designer's lack of familiarity with multiple scattering and the mathematical tools necessary to interpret the vast literature on this subject. Lack of time and money resources, especially in the preliminary design stages, might also prevent implementation by the designer of Monte Carlo or other computer-based numerical methods.

Recognizing the system designer's dilemma, the Naval Undersea Center (NUC) has expended considerable effort to give him some methods that are applicable to problems in extended range viewing. A handbook has been published (reference 1) which uses a hybrid Monte Carlo model and the concept of effective attenuation coefficients to obtain a description of image quality. Also, a canonical design procedure, interrelating the various system and component parameters, is presented. Another NUC report (reference 2) documents the Monte Carlo program used in the handbook and, by listing the program, allows the user to generate effective attenuation coefficients for cross sections not considered in the handbook.

The work herein endeavors to aid the systems designer in two ways not included in the above reports. First, Part I of this work presents a simple analytic model of multiple scattering of light. It is hoped that this model will increase the designer's appreciation of the effects of the medium on the system's viewing capability. Second, Part I of this report provides simple exponential expressions for the flux through an aperture and for

the on-axis irradiance. These expressions are so easy to evaluate that the implications of different scattering cross sections, scattering coefficients, and scattering to absorption coefficient ratios can in turn be quickly and easily evaluated. A further advantage is that the functional dependence of the effective attenuation coefficient on the medium's inherent optical properties is explicitly displayed.

Part II of this report exhaustively compares the results of Part I with Monte Carlo simulations and experimental data. Part II shows, for the chosen scattering cross section, that all three methods give results in good agreement for ranges up to six scattering lengths (i.e., generally seven to ten attenuation lengths), but that the simple exponential model of Part I breaks down at longer ranges. Since almost all state-of-the-art viewing systems are limited to six scattering lengths or less, the failure of the model at longer ranges will probably be of little concern to all but the most advanced and highest powered viewing systems applications.

PART I

AN EXPONENTIAL MULTIPLE-SCATTERING MODEL

by

Alan Gordon

CONTENTS

	Page
Introduction	5
Analysis	6
Statement of Problem	6
Outline of the Iterative Method	10
Derivation of the Object Plane Light Distribution	12
Conclusion	32
Appendix A. The No-Return Backscatter Approximation	33
Appendix B. Proof of Equation 57	38
Appendix C. References	42

INTRODUCTION

The problem of evaluating the intensity of a beam which has passed through a multiple scattering environment has occurred repeatedly in widely varying areas. The passage of charged particles through thick foils, the shielding and moderating of neutrons, the scattering of high frequency sound by ship wakes, and the scattering of light both in the atmosphere and in water are all governed by multiple-scattering effects if the distances of interest are great enough. Because of the importance of multiple scattering in many fields and over a long time span, the scientific literature is replete with contributions on the subject. In contrast with most previous works, this report endeavors, at the sacrifice of some mathematical sophistication, to provide a rather intuitive approach and results which are computationally convenient.

The theoretical approach which will be used here is known as an iterative procedure. Preisendorfer (reference 3) has called such a procedure a natural tool ". . . because the light field N in any medium may be thought of as the superposition of component fields $N^{(i)}$ consisting of radiant energy having undergone i scatterings, i = 1, 2, 3, . . ., after entering the medium". In addition, this approach has other advantages as far as the underwater systems designer is concerned.

The iterative method as used here is strictly an integral approach, that is, it sums up the intensities due to rays traveling from the source plane to the target plane. Since there is no need to solve differential equations, no knowledge of this subject is required. All the quantities needed in the calculation are directly physically measurable; no artificial constructs such as scattering kernels or transmittance operators are introduced. Also, the iterative equations are subject to a simple implementation of the small angle and of the no-return backscatter approximation, which are a consequence of the highly peaked nature of the volume scattering function. Without any evaluation of integrals, the resulting expression for the irradiance yields a straightforward physical interpretation. Finally, the iterative procedure used here should have appeal to those readers who may be interested in Monte Carlo techniques, since there are many similarities in the two methods of obtaining intensities in terms of the ray paths.

In presenting the derivation, the author has tried to catalog all approximations as explicitly as possible. Physical and/or mathematical justifications are presented with the hope that the reader will be able to assess the applicability of the present results to his own particular problem.

ANALYSIS

STATEMENT OF PROBLEM

The geometry of the problem is shown in figure 1. Here, there is a source plane which contains an initially specified distribution of light. At a distance R from the source plane is the target plane on which we wish to know the light distribution. The space between these planes is filled with water of known optical properties. The problem is to find the distribution of the light on the target plane as a function of the distribution on the source plane, the optical properties of the water, and the distance R.

Two important restrictions allow us to simplify our problem immediately. First, we shall neglect diffractive effects. This is a reasonable approximation for most underwater applications and is discussed in reference 4. Second, we shall deal only with light intensities and not amplitudes, i.e., we assume an incoherent process.

In view of these restrictions, we can view light propagation in a very naive way. The source plane is a specified source of photons,* each of which propagates in a straight line through the medium until 1) it is absorbed and stops, 2) it is scattered and (possibly) changes direction and continues, or 3) it reaches the target plane and stops. Figure 1 shows a typical photon which undergoes two scatterings before reaching the target plane.

We define the light distribution and water parameters in terms of photons although they could be defined as easily in terms of energy flow. One can hop back and forth from one description to another through the use of Planck's expression for the energy of a photon.

The distribution of light on the source plane will be described in terms of the source plane's radiance, $N_O\ (x_O, y_O, \theta_1, \varphi_1)$, defined so that $N_O\ (x_O, y_O, \theta_1, \varphi_1)dx_O\, dy_O\, d\,\Omega_1$ is the number of photons per second leaving the area element $dx_O\, dy_O$ centered at (x_O, y_O) and heading into the solid angle $d\Omega_1$, centered at the angles θ_1 and φ_1. The symbols x_O, y_O refer to Cartesian coordinates and θ_1 and φ_1 to polar coordinates. The total flux, F_O, in photons per second leaving the source plane will be

$$F_O = \iint N_O\ (x_O, y_O, \theta_1, \varphi_1)d\vec{x_O}\, d\Omega_1, \qquad (1)$$

where the limits of integration are over all $\vec{x_O}$ and all Ω_1.

---

* *Photons in the sense of Newton's corpuscles, i.e., photons which contain energy but no phase information.*

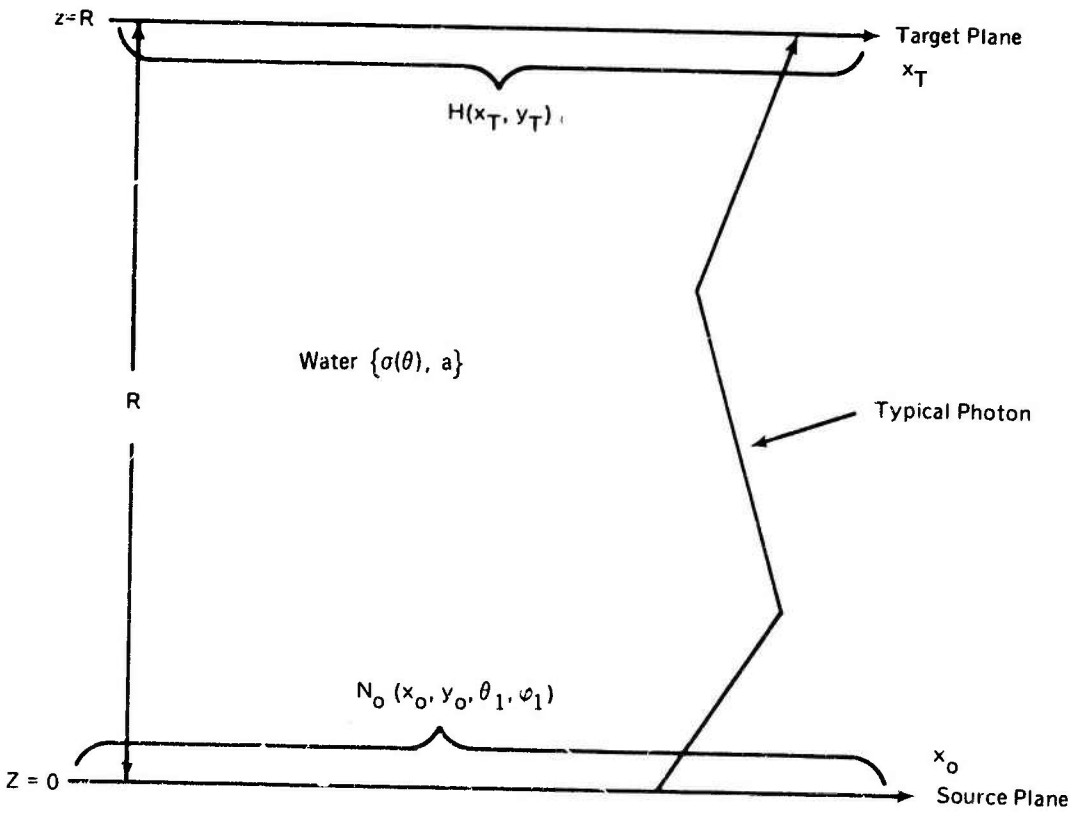

Figure 1. Scattering Geometry.

The light distribution at the target is described by the irradiance $H(x_T, y_T)$, where $H(x_T, y_T)dx_T\, dy_T$ is the number of photons per second arriving at the infinitesimal area $dx_T\, dy_T$ centered at (x_T, y_T). The flux, F, in photons per second entering a finite area (or aperture) A of the target plane is

$$F = \int_A H(x_T, y_T)dx_T. \tag{2}$$

The basic optical properties that we need are the water's absorption coefficient and its volume scattering function. The absorption coefficient, a, is defined such that $a \cdot d\ell$ is the probability of a photon being absorbed after traversing an infinitesimal distance $d\ell$. The volume scattering function, $\sigma(\theta)$, is defined schematically in figure 2 and algebraically by

$$\sigma(\theta) = \frac{J(\theta)}{HdV}, \tag{3}$$

where $J(\theta)d\Omega$ is the number of photons per second scattered into a solid angle $d\Omega$ centered at θ, and H is the number of photons per second per unit area (i.e., the irradiance) entering the scattering volume dV. Integrating equation 3 over Ω and using equation 2, we obtain

$$\frac{F_{scat}}{F_{in}} = \frac{\int J(\theta)d\Omega}{HdA} = \left[2\pi \int \sigma(\theta)\sin\theta d\theta\right]d\ell, \tag{4}$$

since

$$\left\{\begin{array}{l} F_{in} = \text{the number of photons per second incoming} = HdA \\ F_{scat} = \text{the number of photons per second scattered} = \int J(\theta)d\Omega \\ dV = dA \cdot d\ell \end{array}\right\}. \tag{5}$$

Because F_{scat}/F_{in} is just the probability of being scattered in the distance $d\ell$, we define the scattering coefficient s such that the probability of being scattered in the distance $d\ell$ is

$$sd\ell = \left[2\pi \int \sigma(\theta)\sin\theta d\theta\right]d\ell = \left[\int \sigma(\theta)d\Omega\right]d\ell. \tag{6}$$

We can also define the total attenuation coefficient, α, as

$$\alpha = a + s, \tag{7}$$

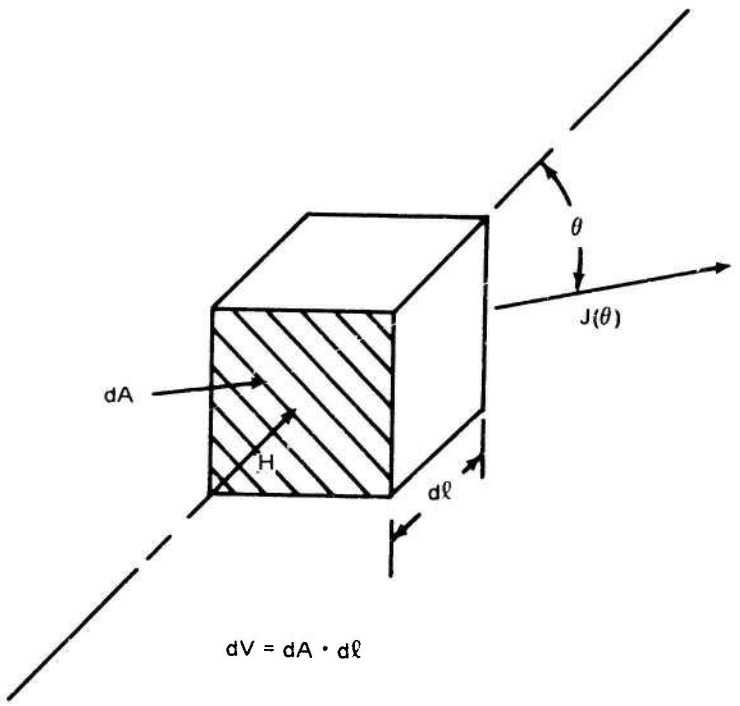

$$dV = dA \cdot d\ell$$

$$\sigma(\theta) = \frac{J(\theta)}{HdV}$$

Figure 2. Schematic of Scattering Process.

so that $\alpha \cdot d\ell$ is the probability of either being scattered or absorbed in the distance $d\ell$. Finally, we can define the backscatter coefficient b such that $bsd\ell$ is the probability of scattering in the distance $d\ell$ by an angle θ where $\pi/2 \leq \theta \leq \pi$:

$$b = \frac{2\pi}{s} \int_{\pi/2}^{\pi} \sigma(\theta) \sin\theta \, d\theta . \tag{8}$$

Having defined the problem and the quantities of interest, we shall now outline the procedure to be used in arriving at a solution.

OUTLINE OF THE ITERATIVE METHOD

The fundamental concept of the iterative method is that the irradiance on the object plane, H, can be regarded as being formed from the infinite series in equation 9 where H_i is the irradiance contribution from all photons which have undergone exactly i scatterings.

$$H = \sum_{i=0}^{\infty} H_i, \tag{9}$$

This decomposition is illustrated in figure 3 for i = 0, 1, 2. Here, the source plane is labeled by 0-coordinates, the target plane for the case of N scatterings is labeled by $\vec{x}_{N+1}$, and a set of N new planes, called scattering planes, is introduced and labeled by the coordinates i = 1, 2, ···N, where N is the number of scatterings for the geometry when the photons scatter exactly N times. All the planes are parallel and the origins of the planes' Cartesian coordinate systems $\{x_i, y_i\}$ are all collinear with a perpendicular joining all the planes. The distance between plane i and i + 1 is denoted by r_{i+1}. Also, each plane (except the target plane) has a set of polar coordinates assigned that will be used to reference the direction from which the photons leave the plane. The polar coordinates $\{\theta_i, \varphi_i\}$ will be assigned to the i - 1 plane.

The geometry just introduced allows us to describe the iterative method in a succinct fashion. First, equation 9 enables us to consider just those photons which have undergone exactly N scatterings. These photons will be broken down into groups, called configurations. Each configuration consists of all photons which 1) scatter exactly N times and 2) scatter within a distance dr of $r_1 = a_1$ and $r_2 = a_2$ and ··· $r_N = a_N$ and nowhere else. The no-return backscatter approximation discussed in the next section will allow us to write a simple expression for the target plane irradiance of each configuration. Summing (actually integrating) over the r_i's will then account for all photons which have scattered exactly N times, i.e., summing over all the configurations yields the irradiance due to exactly N scatterings, H_N. Finally, the total irradiance on the target plane due to all the photons leaving the source plane will be obtained by summing the H_N's, N = 0, 1, ··· ∞, according to equation 9. The iterative method thus involves segregating the light into small components, solving the problem for each component, and then obtaining the total solution by summing the component solutions. We can do this because of the linearity of the processes governing the transfer of radiance.

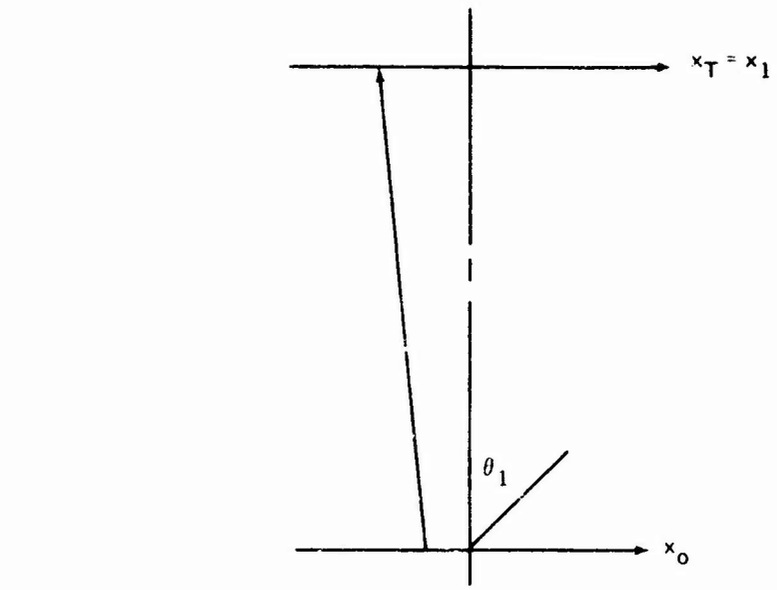

(a) geometry for photons undergoing no scatterings

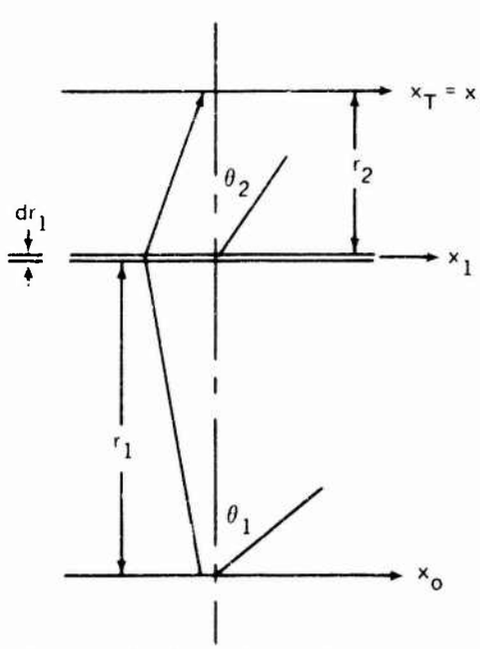

(b) geometry for photons undergoing exactly one scattering

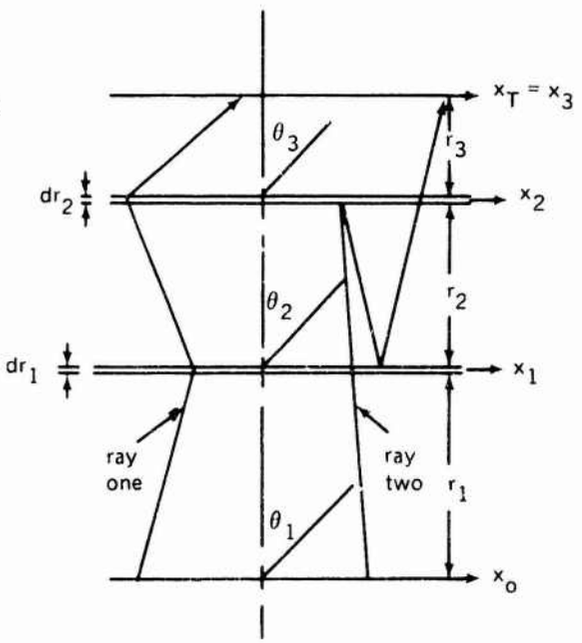

(c) geometry for photons undergoing exactly two scatterings

Figure 3. Geometry for Zero, One, and Two Scatterings.

DERIVATION OF THE OBJECT PLANE LIGHT DISTRIBUTION

THE NO-RETURN BACKSCATTER APPROXIMATION – Figure 3(c) illustrates two fundamentally different types of rays (i.e., photon paths) which can occur in a given configuration. Ray one has the property of $\theta_i \leq \pi/2$ for all i in the configuration, i.e. a ray such as ray one will never acquire a component of motion directed from the target plane to the source plane. As a consequence, all rays having this property also have the following properties: 1) all the photons enter each plane at which they are scattered from below (i.e., from a direction towards the source plane) and 2) each scattering occurs sequentially, i.e., the ray scatters from the first scattering plane, then the second and so on. Rays such as ray two have the property of $\theta_i > \pi/2$ for some i. For a given configuration, this implies that 1) type two rays can enter any scattering plane from either above or below and 2) type two rays can scatter from the scattering planes in any order (e.g., in figure 3(c) ray two scatters from the planes in the order 0-2-1-3). Clearly, type two rays undergo a more complex scattering behavior and make our problem of evaluating the object plane irradiance more difficult.

Fortunately, in typical oceanic waters type two rays are uncommon compared to type one rays. This is a direct consequence of the small value of the backscatter coefficient of ocean waters. An average of three readily available backscatter coefficients (references 5 through 7) indicates a value of b = 0.023. Using the results in appendix A, we can express the range R at which ignoring type two rays introduces an error ϵ in the flux reaching the target plane as

$$R = \frac{2\epsilon}{b^2 c}, \tag{10}$$

where c is the scattering to absorption coefficient (s/a) ratio and R is given in scattering lengths. Taking c = 5.0 (a rather large value), ϵ = 0.05, and b = 0.03, we have R = 22 scattering lengths, a distance much greater than distances of interest here. Thus, we will ignore the contribution of type two rays in all the following calculations.

The remaining type one rays have the important property of interacting with each scattering plane sequentially. This means that the radiance distribution emerging from the i + 1 scattering plane is completely determined by the radiance distribution on the i plane. Thus, to solve the problem of the irradiance on the target plane for a configuration containing N scattering planes, we need only compute 1) the radiance distribution emerging from a scattering plane due to the radiance distribution on the immediately preceding scattering (or source) plane and 2) the irradiance distribution on the target plane due to the radiance distribution on the last scattering plane.

TRANSFER OF RADIANCE AND IRRADIANCE – Figure 4 shows the geometry for which we will calculate the transfer of radiance between two planes. The geometry and symbols are similar to those shown in figure 3. The known quantities are N_0 $(x_0, y_0, \theta_1, \varphi_1)$, the radiance distribution on the 0-plane, the water parameters, and the distance r_1. It is desired to obtain the outgoing radiance of the 1-plane in terms of these parameters.

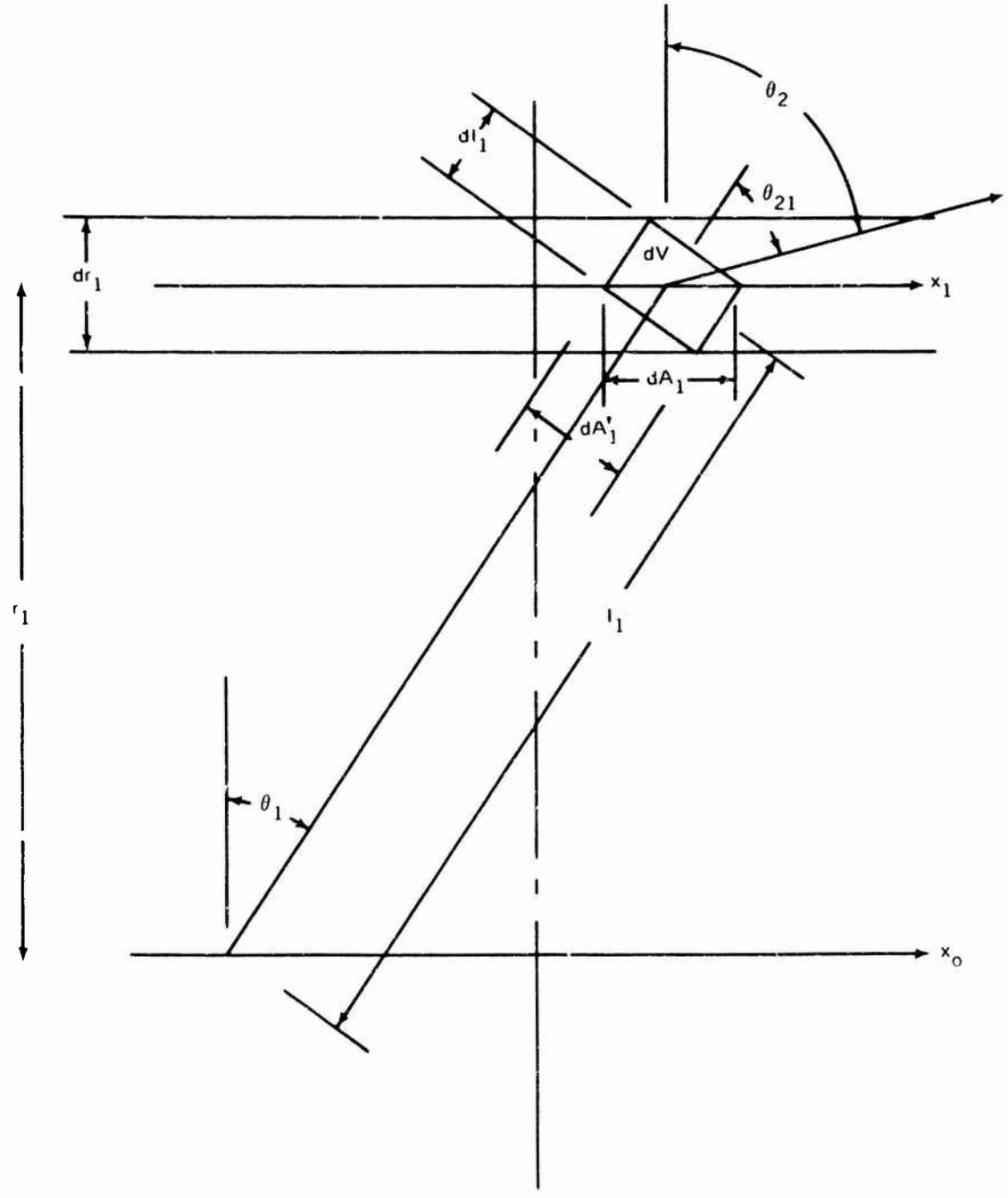

Figure 4. Radiance Transfer Geometry.

The radiant intensity emitted by a small area $dA_o = dx_o\, dy_o$ of the 0-plane centered at (x_o, y_o) is

$$N(x_o, y_o, \theta_1, \varphi_1)dx_o\, dy_o, \tag{11}$$

where

$$\theta_1 = \text{arc tan } \frac{[(x_1 - x_o)^2 + (y_1 - y_o)^2]^{1/2}}{r_1} \tag{12}$$

and

$$\varphi_1 = \text{arc tan } \left(\frac{y_1 - y_o}{x_1 - x_o}\right). \tag{13}$$

The total photon flux within the solid angle $d\Omega_1$, bounded by θ_1 to $\theta_1 + d\theta_1$ and φ_1 to $\varphi_1 + d\varphi_1$, is then

$$N_o(x_o, y_o, \theta_1, \varphi_1)dx_o\, dy_o\, d\Omega_1. \tag{14}$$

In free space equation 14 would represent the flux actually reaching the 1-plane. However, because of the scattering and absorptive properties of the water lying between the planes, not all of this flux reaches the 1-plane.

Considering the scattering interation first, the iterative model requires that in any given configuration we deal only with the rays that scatter within a distance dr of the scattering plane (in this case the 1-plane). By considering the probability of not scattering in the distance r_1, we will find the fraction of the flux (given by equation 14) which reaches the 1-plane unscattered.

If we make the usual assumption that the probability of scattering in a short distance $\Delta\ell$ is given by

$$s\Delta\ell, \tag{15}$$

then the probability of not scattering in that distance is

$$1 - s\Delta\ell \tag{16}$$

and the probability of not scattering in the distance $2\Delta\ell$ is

$$(1 - s\Delta\ell)(1 - s\Delta\ell) = (1 - s\Delta\ell)^2. \tag{17}$$

Now an arbitrary distance, ℓ_1, may be represented as

$$\ell_1 = n\Delta\ell. \tag{18}$$

Then, by generalizing equation 17, we obtain the probability of not scattering in the distance ℓ_1, $P_{ns}(\ell_1)$, as

$$P_{ns}(\ell_1) = \left(1 - \frac{s\ell_1}{n}\right)^n \tag{19}$$

for $n \to \infty$ $\Delta\ell \to d\ell$ and

$$P_{ns}(\ell_1) = \lim_{n\to\infty}\left(1 - \frac{s\ell_1}{n}\right)^n = e^{-s\ell_1}. \tag{20}$$

Early in this section we stated that the effects of absorption can be accounted for by terminating absorbed rays at the point where they are absorbed. Although this is proper, it is inconvenient to terminate rays in the iterative approach. Instead, we shall use an equivalent procedure (reference 8) which allows each ray to continue on through but weights its intensity by the probability of it not being absorbed in the distance traveled. Since the probability of being absorbed in the short distance $\Delta\ell$ is given as $a \cdot \Delta\ell$, we obtain by a procedure identical to equation 16 through 20, for the probability of not being absorbed in the finite distance ℓ_1, $P_{na}(\ell_1)$:

$$P_{na}(\ell_1) = e^{-a\ell_1}. \tag{21}$$

The probability of being neither scattered nor absorbed in the distance ℓ_1 is then

$$P_{ns,na}(\ell_1) = e^{-(a+s)\ell_1} = e^{-(a+s)\frac{r_1}{\cos\theta_1}} = e^{-\frac{\alpha r_1}{\cos\theta_1}}. \tag{22}$$

The amount of flux leaving the 1-plane from the element $dx_o\, dy_o$ in the direction $d\Omega_1$ which arrives at the 2-plane, is then

$$e^{-\frac{\alpha r_1}{\cos\theta_1}} N_o(x_o, y_o, \theta_1, \varphi_1)\, dx_o\, dy_o\, d\Omega_1. \tag{23}$$

Now from figure 4,

$$d\Omega_1 = \frac{dA_1'}{l_1^2} = \frac{dA_1' \cos^2\theta_1}{r_1^2}. \tag{24}$$

Using equation 23 and 24 we obtain for the irradiance on the frontal plane dA_1' of the scattering volume dV

$$H(dA_1') = e^{-\frac{\alpha r_1}{\cos\theta_1}} N_O(x_O, y_O, \theta_1, \varphi_1) dx_O\, dy_O \frac{\cos^2\theta_1}{r_1^2} . \tag{25}$$

Inserting this value into equation 3, we can calculate $dJ_1(x_1, y_1, \theta_2, \varphi_2)$, the scattered flux leaving the volume element dV on the 1-plane due to the flux arriving at dV from the vicinity of x_O, y_O, as

$$dJ_1(x_1, y_1, \theta_2, \varphi_2) = e^{-\frac{\alpha r_1}{\cos\theta_1}} N_O(x_O, y_O, \theta_1, \varphi_1)\, dx_O\, dy_O \frac{\cos^2\theta_1}{r_1^2} \sigma(\theta_{21}) dV, \tag{26}$$

where θ_{21} is the angle between the incoming and scattered photon, i.e.,

$$\theta_{21} = \arccos[\sin\theta_1 \cos\varphi_1 \sin\theta_2 \cos\varphi_2 + \sin\theta_1 \sin\varphi_1 \sin\theta_2 \sin\varphi_2 + \cos\theta_1 \cos\theta_2]. \tag{27}$$

At this point it is convenient to introduce the scattering probability density $p(\theta)$ such that

$$p(\theta) = \frac{\sigma(\theta)}{s} \tag{28}$$

so that

$$\int p(\theta) d\Omega = 1. \tag{29}$$

Noting that $dV = dA_1\, dr_1$, we can now write (using equations 26 and 28)

$$dJ_1(x_1, y_1, \theta_2, \varphi_2) = dA_1 \frac{s dr_1}{r_1^2} e^{-\frac{\alpha r_1}{\cos\theta_1}} N_O(x_O, y_O, \theta_1, \varphi_1) \cos^2\theta_1 p(\theta_{21})\, dx_O\, dy_O. \tag{30}$$

The radiance, $dN_1(x_1, y_1, \theta_2, \varphi_2)$, emerging from (x_1, y_1) and heading in the direction (θ_2, φ_2) due to photons entering the scattering volume dV from an elemental area surrounding (x_O, y_O) is

$$dN_1(x_1, y_1, \theta_2, \varphi_2) = \frac{s dr_1}{r_1^2} e^{-\frac{\alpha r_1}{\cos\theta_1}} N_0(x_0, y_0, \theta_1, \varphi_1)$$
$$\cos^2\theta_1 \, p(\theta_{21}) dx_0, dy_0. \tag{31}$$

Integrating equation 31 over the 0-plane coordinates we obtain the radiance, $N_1(x_1, y_1, \theta_2, \varphi_2)$, emerging from the point (x_1, y_1) and heading in the direction (θ_2, φ_2) as

$$N_1(x_1, y_1, \theta_2, \varphi_2) = \frac{s dr_1}{r_1^2} \iint e^{-\frac{\alpha r_1}{\cos\theta_1}} N_0(x_0, y_0, \theta_1, \varphi_1) \cdot$$
$$\cos^2\theta_1 p(\theta_{21}) dx_0 \, dy_0. \tag{32}$$

Noting that

$$d\Omega_1 = \frac{\cos^3\theta_1 dx_0 \, dy_0}{r_1^2}, \tag{33}$$

we arrive at

$$N_1(x_1, y_1, \theta_2, \varphi_2) = s dr_1 \int \frac{e^{-\frac{\alpha r_1}{\cos\theta_1}}}{\cos\theta_1} N_0 p(\theta_{21}) d\Omega_1, \tag{34}$$

which achieves our desired result of expressing the 1-plane radiance in terms of the 0-plane radiance. Since our derivation did not depend on the detailed properties of the 0-plane or 1-plane, the subscripts 0 and 1 are dummy indices and we can immediately write

$$N_2(x_2, y_2, \theta_3, \varphi_3) = s dr_2 \int \frac{e^{-\frac{\alpha r_2}{\cos\theta_2}}}{\cos\theta_2} N_1 p(\theta_{32}) d\Omega_2. \tag{35}$$

Substituting the results of equation 34 into equation 35 we obtain

$$N_2(x_2, y_2, \theta_3, \varphi_3) = s^2 dr_2 \, dr_1 \iint \frac{e^{-\frac{\alpha r_2}{\cos\theta_2}}}{\cos\theta_2} \frac{e^{-\frac{\alpha r_1}{\cos\theta_1}}}{\cos\theta_1}$$
$$N_0 p(\theta_{21}) p(\theta_{32}) d\Omega_1 d\Omega_2. \tag{36}$$

Clearly, by continuing this procedure, we can obtain the radiance emitted by the N^{th} scattering plane as

$$N_N(x_N, y_N, \theta_{N+1}, \varphi_{N+1}) = \left[\prod_{i+1}^{N} sdr_i \int \frac{e^{-\frac{\alpha r_i}{\cos\theta_i}}}{\cos\theta_i} p(\theta_{i+1}, _i)d\Omega_i \right] N_O, \qquad (37)$$

where $\prod_{i+1}^{N} a_i$ indicates the product of all the a_i's, i = 1, 2, ··· N, and where the quantity in brackets acts as an operator on N_O. Equation 37 thus provides us with an expression for the radiance leaving the last scattering plane of an N-scattering plane configuration in terms of the initial radiance, N_O, and the water characteristics.

To complete the solution for a given configuration we need the target plane irradiance in terms of the radiance leaving the N^{th} scattering plane. The geometry for this process is shown in figure 5. The flux, $d^2F(x_N, y_N, \theta_{N+1}, \varphi_{N+1})$, leaving an area surrounding the point (x_N, y_N) and heading into the element of solid angle centered at $(\theta_{N+1}, \varphi_{N+1})$ is expressed according to equation 23:

$$d^2F(x_N, y_N, \theta_{N+1}, \varphi_{N+1}) = e^{-\frac{\alpha r_{N+1}}{\cos\theta_{N+1}}} N_N(x_N, y_N, \theta_{N+1}, \varphi_{N+1})$$
$$dx_N dy_N d\Omega_{N+1}, \qquad (38)$$

where $N_N(x_N, y_N, \theta_{N+1}, \varphi_{N+1})$ is the radiance leaving the N^{th} scattering plane. Since

$$d\Omega_{N+1} = \frac{dA'_{N+1}\cos^2\theta_{N+1}}{r_{N+1}^2} \qquad (39)$$

and

$$dA'_{N+1} = \cos\theta_{N+1} dx_{N+1} dy_{N+1}, \qquad (40)$$

we have

$$d^2F(x_N, y_N, \theta_{N+1}, \varphi_{N+1}) = e^{-\frac{\alpha r_{N+1}}{\cos\theta_{N+1}}} N_N dA_{N+1} \left(\frac{dx_N dy_N \cos^3\theta_{N+1}}{r^2_{N+1}} \right). \qquad (41)$$

Letting $\mathcal{H}_N$ be the irradiance on the target plane due to a configuration containing N scattering planes, we have

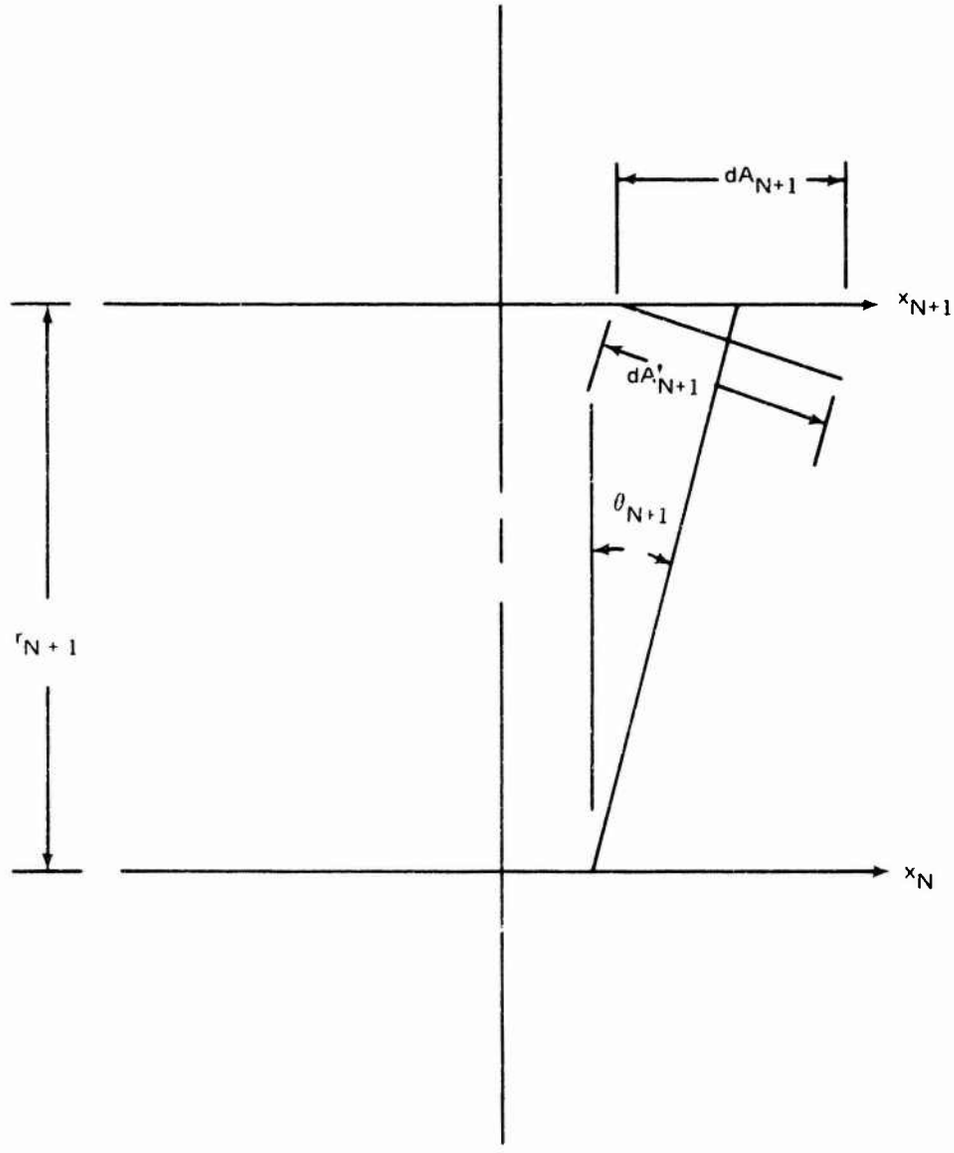

Figure 5. Target Plane Irradiance Geometry.

$$d\mathcal{H}_N = e^{-\frac{\alpha r_{N+1}}{\cos\theta_{N+1}}} N_N(x_N, y_N, \theta_{N+1}, \varphi_{N+1}) d\Omega_{N+1} \tag{42}$$

and the irradiance of the given configuration is

$$\mathcal{H}_N = \int_{\Omega_{N+1}} e^{-\frac{\alpha r_{N+1}}{\cos\theta_{N+1}}} N_N(x_N, y_N, \theta_{N+1}, \varphi_{N+1}) d\Omega_{N+1}. \tag{43}$$

To obtain the total target plane irradiance, H_N, of all configurations which involve exactly N scatterings, we must sum over all configurations, i.e., we must integrate $\mathcal{H}_N$ over all the dr_i, $i = 1 \cdots N$. For example,

for H_1

$$H_1 = \int_{r_1=0}^{r_1=R} \mathcal{H}_1, \tag{44}$$

for H_2

$$H_2 = \int_{r_2=0}^{r_2=R} \int_{r_1=0}^{r_1=R-r_2} \mathcal{H}_2, \tag{45}$$

for H_3

$$H_3 = \int_{r_3=0}^{r_3=R} \int_{r_2=0}^{r_2=R-r_3} \int_{r_1=0}^{r_1=R-r_3-r_2} \mathcal{H}_3. \tag{46}$$

and, in general,

$$H_N = \left[\prod_{i=1}^{N} \int_{r_i=0}^{r_i=R-\sum_{i+1}^{N} r_i} \right] \mathcal{H}_N, \tag{47}$$

with the conventions

$$\sum_{N+1}^{N} r_j = 0 \qquad \prod_{i+1}^{0} a_i = 1 \tag{48}$$

and where the quantity in brackets in equation 47 operates on $\mathcal{H}_N$.

Inserting the results of equations 37 and 43 into equation 47 yields H_N as

$$H_N = \left\{ s^N \left[\prod_{i=1}^{N+1} \int_{r_i=0}^{r_i = R - \sum_{i+1}^{N} r_j} \int_{\Omega_i} \frac{e^{-\frac{\alpha r_i}{\cos\theta_i}}}{f_i} p(\theta_{i+1,i}) d\Omega_i dr_i \right] N_o \right\} , \tag{49}$$

where the factor within the square brackets acts as an operator and the following convertions apply:*

$$\left\{ \begin{array}{ll} \int Q(r_{N+1}) dr_{N+1} & = Q(r_{N+1}) \\ p(\theta_{N+2,N+1}) & = 1 \\ \sum_{i=k}^{\ell} r_i & = 0 \quad \text{for } k > \ell \\ f_i & = \left\{ \begin{array}{ll} \cos\theta_i & i \leq N \\ 1 & i = N+1 \end{array} \right. \end{array} \right\} . \tag{50}$$

For example,

$$H_o = \int_{\Omega_1} N_o e^{-\frac{\alpha r_1}{\cos\theta_1}} d\Omega_1 \tag{51}$$

and

$$H_1 = s \int_0^R \int_{\Omega_2} \int_{\Omega_1} \frac{e^{-\frac{\alpha r_1}{\cos\theta_1}}}{\cos\theta_1} e^{-\frac{\alpha (R-r_1)}{\cos\theta_2}} N_o p(\theta_{21}) d\Omega_1 d\Omega_2 dr_1 . \tag{52}$$

---

* where $Q(r_{N+1})$ is an arbitrary function of r_{N+1}

We achieve our goal of expressing the target plane irradiance in terms of the initial radiance and the water parameters by summing equation 49 according to equation 9:

$$H = \sum_{N=0}^{\infty} \left[s^N \prod_{i=1}^{N+1} \int_0^{R - \sum_{i+1}^{N} r_j} \int_{\Omega} \frac{e^{-\frac{\alpha r_i}{\cos\theta_i}}}{f_i} p(\theta_{i+1,i}) d\Omega_i \, dr_i \right] N_o \quad . \quad (53)$$

In some cases we are interested in the flux, F, through an aperture, A, on the target plane. This is a somewhat cruder measure of the target light distribution and can be expressed as

$$F = \int_A H d\vec{x}_T, \quad (54)$$

where H is given by equation 53. Using that equation and interchanging summation and integration we obtain

$$\begin{aligned} F &= \sum_{N=0}^{\infty} F_N \\ &= \sum_{N=0}^{\infty} \int_A H_N \, d\vec{x}_T \\ &= \sum_{N=0}^{\infty} \int_A \left[s^N \prod_{i=1}^{N+1} \int_0^{R - \sum_{i+1}^{N} r_j} \int_{\Omega_i} \frac{e^{-\frac{\alpha r_i}{\cos\theta_i}}}{f_i} p(\theta_{i+1,\,i}) d\Omega_i dr_i \right] N_o d\vec{x}_{N+1} . \end{aligned} \quad (55)$$

From equation 55 we see that the flux, F, also consists of components, each component resulting from photons which have scattered exactly N times.

SMALL ANGLE APPROXIMATION – Although equation 53 provides a complete solution for the target plane irradiance, it suffers from two major difficulties. Being an infinite series, the N^{th} term of which involves a 2N–tuple integral, equation 53 poses serious computational problems. Second, the individual terms of the series are not in a form which is subject to the most fruitful physical interpretation. When the small angle approximation is employed, equation 53 can be cast in a form which is very revealing.

The small angle approximation involves the assumption that $\cos\theta_i \sim 1$ for all i. For moderate ranges and for angular apertures θ (as viewed from the source plane) which fulfill $\cos\theta \sim 1$, this approximation will be valid for the overwhelming majority of

the rays due to the highly peaked nature of oceanic scattering cross sections. For any range and ray, if θ is large, θ_i will clearly be large for some i, and the approximation does not describe the target irradiance at these angles. Also, as the range between target and source planes increases, the maximum angle θ_{max} at which the approximation holds becomes smaller. Because optical viewing systems often perform in the region of moderate θ and R. we shall employ the small angle approximation in all that follows.

Setting $\cos\theta_i = 1$ in equation 53 and noting that $\sum_{i=1}^{N} r_i = R$, we obtain

$$H = \sum_{N=0}^{\infty} s^N e^{-\alpha R} \left[\prod_{i=1}^{N+1} \int_0^{R - \sum_{i+1}^{N} r_j} \int_{\Omega_i} p(\theta_{i+1,\,i}) d\Omega_i \, dr_i \right] N_o. \qquad (56)$$

From appendix B we have the formula

$$\prod_{i=1}^{N+1} \int_0^{R - \sum_{i+1}^{N} r_j} dr_i = \frac{R^N}{N!} . \qquad (57)$$

Multiplying equation 56 by the right-hand side of equation 57 and dividing by the left-hand side, we obtain

$$\boxed{H = e^{-aR} \sum_{N=0}^{\infty} \frac{(sR)^N e^{-sR}}{N!} \langle h_N \rangle}, \qquad (58)$$

where

$$h_N = \left[\prod_{i=1}^{N+1} \int_{\Omega_i} p(\theta_{i+1,\,i}) d\Omega_i \right] N_o \qquad (59)$$

and

$$\langle h_N \rangle = \frac{\left[\prod_{i=1}^{N+1} \int_0^{R - \sum_{i+1}^{N} r_j} dr_i \right] h_N}{\prod_{i=1}^{N+1} \int_0^{R - \sum_{i+1}^{N} r_j} dr_i} . \qquad (60)$$

Equation 58 is a simple and readily interpretable form for the target plane irradiance. Imagine the target and source plane separated by vacuum rather than water. Into this vacuum we insert N scattering planes. Each scattering plane has the property of unity probability of scattering a photon with an angular probability density $p(\theta_{i+1,\,i})$. The planes are located at $r_1 = a_1$, $r_2 = a_2$ $\cdots$, $r_N = a_N$. The target plane irradiance due to the source plane's radiance propagating through these scattering planes is then h_N.

$\langle h_N \rangle$ is the value of the target plane irradiance averaged over all possible values of the r_i's. From equation 60 we note that this average takes place without a weighting factor dependent on any of the r_i's. This means that, given the fact that N scatterings occur, any of the configurations of the scattering planes is equally likely.

According to equation 58, we next compute the weighted sum of the $\langle h_N \rangle$'s. These weights are just the probability of scattering exactly N times. From equation 58 we see that this probability is given by the Poisson distribution with a mean number of scatterings equal to sR.

Finally, the target irradiance H is obtained from this weighted sum by multiplying by e^{-aR}. All the effects of absorption are accounted for by this factor which represents the fraction of flux that reaches the target plane without being absorbed.

The simplicity of equation 58 is due to the small angle and no-return backscatter approximations. Unfortunately, except for the first two terms, it cannot be directly evaluated. In the next section we shall establish some preliminary relations between the flux through an aperture and on-axis irradiance, leading to approximations for these quantities which can be easily evaluated.

RELATIONSHIP BETWEEN FLUX AND ON-AXIS IRRADIANCE – One of the factors that makes equation 58 difficult to evaluate is the possible generality of the source plane irradiance N_O. This difficulty can be alleviated by restricting equation 58 to the case where N_O is a unidirectional, unipotent point source located at the origin and symbolized by N_O^{ups}.

$$N_O^{ups} = \delta(\cos\theta_1 - 1)\delta(\varphi_1)\delta(\vec{x_O}) \quad , \tag{61}$$

where N_O^{ups} is of unit strength since

$$\int N_O^{ups}\, d\Omega_O d\vec{x_O} = 1. \tag{62}$$

The restriction of N_O to N_O^{ups} can be made without loss of generality in the small angle approximation. If $H^{ups}(x_T, y_T, R)$ is the target plane irradiance resulting from a source plane radiance $N_O^{ups}(x_O, y_O, \theta_1, \varphi_1)$, then the target plane irradiance

$H(x_T, y_T, R)$ of an arbitrary source $N_O(x_O, y_O, \theta_1, \varphi_1)$ can be expressed as

$$H(x_T, y_T, R) = \left\{ \iint H^{ups}(x_T - x_O - R\theta_1 \cos\varphi_1, y_T - y_O - R\theta_1 \sin\varphi_1, R) \cdot N_O(x_O, y_O, \theta_1, \varphi_1) d\vec{x}_O d\Omega_1 \right\} \tag{63}$$

in the small angle approximation. Equation 63 is just a convolution between H^{ups} and N_O, with H^{ups} serving as an impulse response function.

The function H^{ups} has much utility in the field of underwater optics and is known as the beam spread function. Due to the reciprocity theorem for underwater optics (reference 9), H^{ups} also yields (aside from scale factors) the point spread function, which is the image plane irradiance due to light radiated by an omnidirectional point source. The Fourier transform of the point spread function, known as the modulation transfer function (MTF), is used to describe contrast degradation as a function of range and spatial frequency.

Our main use of H^{ups} will be in conjunction with equation 63 and for the case where N_O becomes the radiance distribution, N_C, due to a point source conical beam of strength F_O and solid angle Ω_C expressed as

$$N_C = \begin{cases} \frac{F_O}{\Omega} \delta(\vec{x_O}) & \theta_1, \varphi_1 \in \Omega_C \\ 0 & \theta_1, \varphi_1 \notin \Omega_C \end{cases} . \tag{64}$$

The on-axis (i.e., $x_T = 0$, $y_T = 0$) irradiance due to this source is, from equation 63,

$$H(O, O, R) = \left\{ \iint H^{ups}(-x_O - R\theta_1 \cos\varphi_1, -y_O - R\theta_1 \sin\varphi_1, R) \cdot \frac{F_O}{\Omega_C} \delta(\vec{x_O}) dx_O d\Omega_1 \right\} . \tag{65}$$

Letting

$$x = R\theta_1 \cos\varphi_1 ; \quad y = R\theta_1 \sin\varphi_1 \tag{66}$$

and dropping the dummy index 1, we have

$$\boxed{H(O,O,R) = \frac{F_O F(\Omega_C)}{\Omega_C R^2}} , \tag{67}$$

where

$$F(\Omega_c) = \int_{\Omega_c} H^{ups}(x,y,R)dxdy. \tag{68}$$

Equation 67 has been previously derived by Funk (reference 10) for the case of a spherical geometry.

Equation 67 allows us to evaluate the on-axis irradiance of conical beams. The restriction to on-axis irradiance is usually of little practical consequence since it is common to evaluate imaging systems on the basis of on-axis performance (reference 11). Equation 67 may be used to delimit the on-axis irradiance of a square beam by considering the irradiance of the inscribed and circumscribed cones.

The most important property of the on-axis irradiance is that it is proportional to the integral of the "ups" irradiance across the beamwidth. The significance of this result is that the spatial derivative of the flux (i.e., the irradiance) can be expressed in terms of the flux alone. In view of the approximations we are about to make, this is a welcome property since a function itself is often less sensitive to certain approximations than its derivative.

FLUX THROUGH AN APERTURE — The primary goal of this section is to compute $F(\Omega)$ (equation 68). Knowledge of this function will allow evaluation of the on-axis irradiance as well as energy distribution contours in the target plane.

Using equation 58 to express H^{ups}, we have

$$H^{ups} = e^{-aR} \sum_{N=0}^{\infty} \frac{(sR)^N e^{-sR}}{N!} \left\langle h_N^{ups} \right\rangle , \tag{69}$$

where from equation 59

$$h_N^{ups} = \prod_{i=1}^{N+1} \int_{\Omega_i} p(\theta_{i+1,\,i})\, N_o^{ups}\, d\Omega_i. \tag{70}$$

Substituting equation 69 into equation 68, we obtain

$$F(\Omega) = e^{-aR} \sum_{N=0}^{\infty} \frac{(sR)^N e^{-sR}}{N!} \left\langle f_N^{ups} \right\rangle \tag{71}$$

with

$$f_N^{ups} = \int h_N^{ups} \, d\vec{x}_{N+1}. \tag{72}$$

Although equation 71 is simple in form, consideration of equations 72 and 70 shows that its evaluation is non-trivial. To obtain an indication of how to proceed, we rearrange equation 71:

$$F(\Omega) = e^{-aR} \, e^{-sR} \sum_{N=0}^{\infty} \frac{(sR)^N \left\langle f_N^{ups} \right\rangle}{N!}. \tag{73}$$

It is now clear that approximating $\left\langle f_N^{ups} \right\rangle$ by a quantity of the form

$$\left\langle f_N^{ups} \right\rangle \sim aP^N \tag{74}$$

will make equation 73 summable (to a exponential) and also will require the evaluation of only two quantities (a and P) rather than the infinite set $\left\{ f_N^{ups} \right\}$. Some justifications for approximating $\left\langle f_N^{ups} \right\rangle$ by

$$\left\langle f_N^{ups} \right\rangle \sim \left\langle f_O^{ups} \right\rangle \left\{ \frac{f_1^{ups}}{f_O^{ups}} \right\}^N \tag{75}$$

will now be given.

Inspecting equation 75 shows that $\left\langle f_N^{ups} \right\rangle$ is reproduced exactly for N = 0 or 1 and thus the approximation is correct for small distances, i.e., for $sR \ll 1$.

Second, equation 75 is correct when the scattering function $p(\theta)$ is a delta function, i.e., when

$$p(\theta) = \frac{\delta(\cos\theta - 1)}{2\pi}. \tag{76}$$

Since oceanic scattering functions are highly peaked, agreement of equation 75 in the limit of equation 76 is reassuring.

Finally, equation 75 is subject to a simple physical interpretation. It states that the amount of the flux ($\langle f_N^{ups} \rangle$) reaching the aperture Ω after N scatterings equals the original source strengtn ($\langle f_o^{ups} \rangle$) times a factor ($\langle f_1^{ups} \rangle / \langle f_o^{ups} \rangle$), which equals the probability of being scattered by less than an angle Ω, this probability being raised to the N^{th} power. Thus, equation 75 assumes that the result of N scatterings is the same as the result of N consecutive single scatterings. For these scatterings only the flux within an angle Ω contributes to the source term for the next scattering, and the flux distribution resulting from any given scattering can be consolidated into a point source. This interpretation seems reasonable for scattering at moderate ranges by a volume scattering function which is highly peaked. At longer ranges, equation 75 must break down since some of the flux originally scattered outside Ω will return and the succeeding source distributions will depart significantly from point sources.

A rigorous mathematical argument concerning the domain of validity of equation 75 is beyond the scope of this work. Our main justification for this approximation lies in Part II of this report, in which formulas based on this approximation show good agreement with both Monte Carlo and experimental results. Utilizing equations 75 and 73, we obtain

$$F(\Omega) = \left\langle f_o^{ups} \right\rangle e^{-\alpha R + s \left\langle f_1^{ups} \right\rangle / \left\langle f_o^{ups} \right\rangle R}. \tag{77}$$

To proceed, we must evaluate $\left\langle f_1^{ups} \right\rangle$ and $\left\langle f_o^{ups} \right\rangle$. From equations 61, 70, and 72 we have

$$\begin{aligned} \left\langle f_o^{ups} \right\rangle &= \iint N_o^{ups} \, d\Omega_1 \\ &= \iint \delta(\cos\theta_1 - 1)\delta(\varphi_1)\delta(\vec{x_o}) d\Omega_1 \, d\vec{x_1}. \end{aligned} \tag{78}$$

Now,

$$\delta(\vec{x_o}) = \delta(x_o)\delta(y_o) = \delta(x_1 - R\theta_1 \cos\varphi_1)\delta(y_1 - R\theta_1 \sin\varphi_1). \tag{79}$$

Evaluating the delta function over $d\Omega_1$ we obtain

$$\left\langle f_o^{ups} \right\rangle = \int \delta(x_1)\delta(y_1) d\vec{x_1}, \tag{80}$$

so

$$\left\langle f_o^{ups} \right\rangle = 1. \tag{81}$$

For $\left\langle f_1^{ups} \right\rangle$,

$$\left\langle f_1^{ups} \right\rangle = \frac{\int\int\int\int p(\theta_{21})\, N_O^{ups}\, d\Omega_1 d\Omega_2 d\vec{x}_2 dr_1}{\int dr_1} . \tag{82}$$

Integrating over $d\Omega_1$,

$$\left\langle f_1^{ups} \right\rangle = \frac{\int\int\int p(\theta_2)\delta(x_1)\delta(y_1) d\Omega_2 d\vec{x}_2 dr_1}{\int dr_1} . \tag{83}$$

Writing

$$d\Omega_2 = \frac{dx_1 dy_1 \cos^3\theta_2}{r_2^2} \equiv \frac{dx_1 dy_1}{r_2^2} \tag{84}$$

and integrating over $\vec{x}_1$, we obtain

$$\left\langle f_1^{ups} \right\rangle = \frac{\int\int \frac{p(\theta_2)}{r_2^2} d\vec{x}_2 dr_1}{\int dr_1} . \tag{85}$$

Using

$$\theta_2 = \arctan \frac{[x_2^2 + y_2^2]^{1/2}}{r_2^2} \tag{86}$$

and

$$\frac{d\vec{x}_2}{r_2^2} = \frac{dx_2 dy_2}{r_2^2} \equiv \theta_2 d\theta_2 d\varphi_2 \equiv d\Omega_2 \tag{87}$$

and dropping the subscript 2, we obtain

$$\left\langle f_1^{ups} \right\rangle = \frac{\int_0^R \left[\int_{\theta_A} p(\theta) d\Omega \right] dr_1}{\int_0^R dr_1} , \tag{88}$$

where θ_A is the half-angle subtended by a circular aperture (or by the intersection of a conical beam) centered on the target plane as viewed from the first scattering plane, i.e.,

$$\theta_A = \arctan \frac{r_A}{r_2} , \tag{89}$$

where r_A is the radius of the aperture.

We note that the quantity in square brackets in equation 88 is just the distribution function associated with the normalized cross section $p(\theta)$. The distribution function is the form in which underwater cross sections are often tabulated; however, evaluation of $\langle f_1^{ups} \rangle$ requires the value of the distribution function to be averaged over r_1. In line with our attempt to present the simplest possible description of multiple scattering which retains some predictive value, we shall now approximate $\langle f_1^{ups} \rangle$ by

$$\langle f_1^{ups} \rangle \sim f_1^{ups} \Big|_{r_1 = R/2} . \tag{90}$$

That is, we shall drop the average over the scattering plane's location in favor of evaluating the function f_1^{ups} for the case of the scattering plane located exactly halfway between the source plane and the target plane. This yields

$$\langle f_1^{ups} \rangle \sim f_1^{ups} \Big|_{r_1 = R/2} = \int_{\theta'} p(\theta) d\Omega, \tag{91}$$

where θ' is the polar half-angle subtended by the circular aperture for an on-axis observer located midway between the source and target plane.

Using equations 91, 81, and 77, we obtain for $F(\Omega)$, the flux through a circular aperture due to a unidirectional point source of unit strength,

$$F(\Omega) = e^{\left[-\alpha + s \int_{\theta'} p(\theta) d\Omega\right] R} . \tag{92}$$

Due to the linearity of the scattering process, for a source of strength F_0 equation 88 becomes

$$F(\Omega) = F_o \, e^{\left[-\alpha + s \int_{\theta'} p(\theta) d\Omega\right] R} \quad . \tag{93}$$

Using equations 92 and 67, we obtain for H(O,O,R), the on-axis target plane irradiance due to a point conical beam of solid angle Ω_c and strength F_o,

$$H(O,O,R) = \frac{F_o}{\Omega_c R^2} \, e^{\left[-\alpha + s \int_{\theta'} p(\theta) d\Omega\right] R} \quad . \tag{94}$$

We note that both the flux through an aperture and the on-axis irradiance are governed by an effective attenuation coefficient, α_{eff}, defined by

$$\alpha_{eff} = \alpha - s \int_{\theta'} p(\theta) d\Omega \quad . \tag{95}$$

In addition to being easily calculable, α_{eff} also has reasonable limiting forms. For $\theta' \to 0$, $\alpha_{eff} \to \alpha$, as would be expected from a narrow beam where almost all scattered photons remain outside the beam. For $\theta' \to \pi$, $\alpha_{eff} \to a$, which corresponds to the intuitive statement that if all the scattered light remains in the beam, this light is then attenuated by the absorption coefficient.

CONCLUSION

Equations 93 and 94 represent the main formulas of computational interest to the systems designer. With very little computational investment, they provide useful expressions for flux and on-axis irradiance. Part II of this report shows that (for the cross section tested) equation 93 retains predictive value out to six scattering lengths or seven to ten attenuation lengths, depending on the s/a ratio.

We have used equation 58 as a starting point for deriving expressions for on-axis irradiance and flux through an aperture. It also serves as an excellent departure for the derivation of the water's MTF. By taking the Fourier transform of equation 58 and applying the small angle approximation consistently, a series expression for the MTF can be obtained. By suitably applying and extending the model other quantities, such as off-axis irradiance, can also be derived.

The iterative method has shown its ability to yield results in agreement with Monte Carlo, experimental, and analytic approaches and should thus be considered a useful and important approach to multiple scattering problems.

APPENDIX A
THE NO-RETURN BACKSCATTER APPROXIMATION

We will confine our attention to scattering on a line since for this case the problem is exactly solvable. In figure A-1, F_o is a source of photons located at x = 0, where all these photons initially travel to the right on the line [0, ∞] and

u(x)	=	flux at point x traveling to the right
v(x)	=	flux at point x traveling to the left
b,a,s	=	backscatter, absorption, and scattering coefficient, respectively
Δ	=	a small increment in length along the x-axis
bsΔ	=	probability of being backscattered in the interval Δ
aΔ	=	probability of being absorbed in the interval Δ.

By considering the various loss and gain processes, we can write for u(x)

$$u(x + \Delta) = u(x) - a\Delta u(x) - bs\Delta u(x) + bs\Delta v(x + \Delta). \tag{A-1}$$

In this equation, u(x) is the original flux, aΔu(x) is the amount lost by absorption, bsΔu(x) is the amount lost by backscatter, and bsΔv(x + Δ) is the amount of flux gained by the rightward-moving beam due to backscatter of the leftward-moving beam (i.e., the returned backscatter).

Noting that

$$v(x + \Delta) \sim v(x) + \left.\frac{dv}{dx}\right|_{x=x} \Delta \quad , \tag{A-2}$$

we have, to first order in Δ,

$$u(x + \Delta) = u(x) - (a + bs)\Delta u(x) + bs\Delta v(x) \ . \tag{A-3}$$

Similarly, for v,

$$v(x) = v(x + \Delta) - (a + bs)\Delta v(x) + bs\Delta u(x) \quad . \tag{A-4}$$

Dividing equations A-3 and A-4 by Δ, and rearranging and letting Δ→0, we obtain

$$\frac{du}{dx} = -qu(x) + bsv(x) \tag{A-5}$$

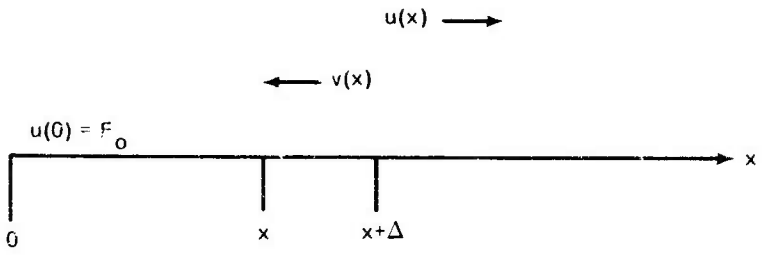

Figure A-1. One-Dimensional Backscatter Geometry.

and

$$\frac{dv}{dx} = +qv(x) - bsu(x) \quad , \tag{A-6}$$

where $q = a + bs$.

Differentiating equation A-5 and using equations A-5 and A-6, we obtain

$$\frac{d^2u}{dx^2} = -q\,\frac{du}{dx} + bs\,\frac{dv}{dx}$$

$$= -q(-qu(x) + bsv(x)) + bs(qv(x) - bsu(x))$$

$$\frac{d^2u}{dx^2} = (q^2 - (bs)^2)u(x) \quad . \tag{A-7}$$

Similarly, for v(x),

$$\frac{d^2v}{dx^2} = (q^2 - (bs)^2)v(x) \quad . \tag{A-8}$$

Therefore, u and v have solutions of the form

$$u(x) = Ae^{-\sqrt{q^2 - (bs)^2}\,x} + Be^{+\sqrt{q^2 - (bs)^2}\,x} \tag{A-9}$$

and

$$v(x) = Ce^{-\sqrt{q^2 - (bs)^2}\,x} + De^{+\sqrt{q^2 - (bs)^2}\,x} \quad . \tag{A-10}$$

Because of the absorptive properties, we require u(x) and v(x)→0 as $x \to +\infty$, so that

$$u(x) = Ae^{-\sqrt{q^2 - (bs)^2}\,x} \tag{A-11}$$

and

$$v(x) = Ce^{-\sqrt{q^2 - (bs)^2}\,x} \quad , \tag{A-12}$$

but $u(x = 0) = F_o \Rightarrow A = F_o$, whence

$$\boxed{u(x) = F_o e^{-\sqrt{q^2 - (bs)^2}\, x}} \quad . \tag{A-13}$$

And by substituting equations A-13 and A-12 into equations A-5 and A-6, we obtain

$$C = \frac{q - \sqrt{q^2 - (bs)^2}}{bs} F_o = \frac{bs}{q + \sqrt{q^2 - (bs)^2}} F_o \quad . \tag{A-14}$$

Now making the no-return backscatter approximation means we drop the term $+ bs\Delta v(x)$ from equation A-3, obtaining

$$u(x + \Delta) = u(x) - (a + bs)\Delta u(x) \tag{A-15}$$

and rearranging and letting $\Delta \rightarrow 0$, we obtain

$$\frac{du}{dx} = -qu(x) \ , \tag{A-16}$$

which has the solution

$$u(x) = F_o e^{-qx} \ . \tag{A-17}$$

The question is, at what range $x = r$ does the flux predicted by the simplified result, equation A-17, begin to depart significantly from equation A-13, which includes the effects of returned backscatter. If we define a fractional error $\epsilon \ll 1$ as a significant departure, then we require

$$\frac{F_o e^{-\sqrt{q^2 - (bs)^2}\, r} - F_o e^{-qr}}{F_o e^{-qr}} = \epsilon \tag{A-18}$$

or

$$e^{+(-\sqrt{q^2 - (bs)^2} + q)r} = 1 + \epsilon \, . \qquad \text{(A-19)}$$

Letting

$$\left.\begin{aligned} a &= s/c \\ c &= s/a \text{ ratio} \\ sr &= R \end{aligned}\right\} \, , \qquad \text{(A-20)}$$

we have

$$e^{+(-1/c\sqrt{1 + 2bc} + 1/c + b)R} = 1 + \epsilon \qquad \text{(A-21)}$$

for ocean waters

$$2bc \ll 1 \, , \qquad \text{(A-22)}$$

so that

$$(1 + 2bc)^{1/2} \cong 1 + bc - \frac{(bc)^2}{2} \, . \qquad \text{(A-23)}$$

Inserting equation A-23 into A-21,

$$e^{\frac{b^2 cR}{2}} = 1 + \epsilon \, , \qquad \text{(A-24)}$$

but since $\epsilon \ll 1$ we obtain

$$\boxed{R = \frac{2\epsilon}{b^2 c}} \qquad \text{(A-25)}$$

APPENDIX B
PROOF OF EQUATION 57

Equation 57 asserts that

$$\prod_{i=1}^{N+1} \int_0^{R-\sum_{i+1}^{N} r_j} dr_i = \frac{R^N}{N!} \quad .$$

First, we will verify this formula for N = 1, 2, 3.

For N = 1,

$$\prod_{i=1}^{1} \int_0^{R-\sum_{i+1}^{1} r_j} dr_i = \int_0^R dr_1 = R = \frac{R^1}{1!} \quad .$$

For N = 2,

$$\prod_{i=1}^{2} \int_0^{R-\sum_{i+1}^{2} r_j} dr_i = \int_0^R \int_0^{R-r_2} dr_1 dr_2$$

$$= \int_0^R (R - r_2) dr_2$$

$$= \left(Rr_2 - \frac{r_2^2}{2} \right) \Bigg|_0^R$$

$$= R^2 - \frac{R^2}{2} = \frac{R^2}{2!} \quad .$$

For N = 3,

$$\prod_{i=1}^{3} \int_0^{R-\sum_{i+1}^{3} r_j} dr_i = \int_0^R \int_0^{R=r_3} \int_0^{R-r_3-r_2} dr_1 dr_2 dr_3$$

$$= \int_0^R \int_0^{R-r_3} (R - r_3 - r_2) dr_2 dr_3$$

$$= \int_0^R \left(Rr_2 - r_3 r_2 - \frac{r_2^2}{2} \right) \Bigg|_0^{R-r_3} dr_3$$

$$= \int_0^R \left[\frac{(R - r_3)^2}{2} \right] dr_3$$

$$= 1/2 \left[R^2 r_3 - Rr_3^2 + \frac{r_3^3}{3} \right]_0^R$$

$$= \frac{R^3}{6} = \frac{R^3}{3!} .$$

Now, if we define

$$\prod_{i=1}^{N} \int_0^{R - \sum_{i+1}^{N} r_j} dr_i = \int_0^R \int_0^{R-r_N} \int_0^{R-r_N-r_{N+1}} \cdots \int_0^{R-\cdots-r_2} .$$

$$dr_1 \cdots dr_N \equiv F_N(R)$$

and assume

$$F_N(R) = \frac{R^N}{N!} ,$$

we need only prove that

$$F_{N+1}(R) = \frac{R^{N+1}}{(N+1)!} .$$

But

$$F_{N+1}(R) = \int_0^R \int_0^{R-r_{N+1}} \int_0^{R-r_{N+1}-r_N} \cdots \int_0^{R-\cdots-r_2} dr_1 \cdots dr_{N+1}$$

$$= \int_0^R \left[\int_0^{R-r_{N+1}} \cdots \int_0^{R-\cdots-r_2} dr_1 \cdots dr_N \right] dr_{N+1} .$$

Letting $R - r_{N+1} = R'$,

then

$$F_{N+1}(R) = \int_0^R \left[\int_0^{R'} \cdots \int_0^{R'-\cdots-r_2} dr_1 \cdots dr_N \right] dr_{N+1} ,$$

but the quantity in brackets is $F_N(R')$,

so

$$F_{N+1}(R) = \int_0^R \frac{(R')^N}{N!} dr_{N+1} .$$

But

$$dr_{N+1} = -dR'$$

for

$$r_{N+1} = 0 \qquad R' = R$$

$$r_{N+1} = R \qquad R' = 0$$

so that

$$F_{N+1}(R) = -\int_R^0 \frac{(R')^N}{N!} dR' ,$$

and evaluating the integral yields

$$F_{N+1}(R) = \frac{R^{N+1}}{(N+1)!} \quad .$$

APPENDIX C. REFERENCES

1. Naval Undersea Center, NUC TP 303. *Handbook of Underwater Optical Imaging Systems*, by S. Bryant, C. Funk, P. J. Heckman, Jr. San Diego, California. July 1972.

2. Naval Undersea Center, NUC TP. *Monte Carlo Simulation of Underwater Light Propagation*, by T. J. Keil, Jr., C. Funk. San Diego, California. To be published.

3. R. W. Preisendorfer, "A Survey of Theoretical Hydrologic Optics, " *J. Quant. Spectrosc. Radiat. Transfer*, Vol. 8, pp. 325-338, 1968.

4. C. J. Funk, *Energy Propagation Constraints on Underwater Optical and Acoustical Imaging Systems*, PhD Thesis, University of California, Los Angeles, 1972.

5. Scripps Institution of Oceanography, SIO Ref. No. 71-1. *Underwater Lighting by Submerged Lasers and Incandescent Sources*, by S. Q. Duntley, San Diego, California. June 1971.

6. M. V. Kozlyaninov, "New Instrument for Measuring the Optical Properties of Seawater," *Tr. Inst. Okeanol., Akad. Nouk. S.S.S.R.*, Vol. 25, p. 134, 1957.

7. R. E. Morrison, *Studies on the Optical Properties of Seawater at Argus Island in the North Atlantic Ocean and in Long Island and Block Island Sounds*, PhD Thesis, New York University, June 1967.

8. Naval Undersea Warfare Center, NUWC TN 138. *Monte Carlo Simulation of the Underwater Light Field Distribution from a Point Source*, by Clarence Funk. Pasadena, California. September 1968.

9. I. M. Levin, "Observation of Objects Illuminated by a Narrow Light Beam in a Scattering Medium," *Izv. Atmos. and Oceanic Physics*, Vol. 5, No. 1, pp. 62-76, 1969.

10. C. J. Funk, "Multiple Scattering Calculations of Light Propagation in Ocean Water," *Journal of the Optical Society of America*, To be published.

11. Naval Undersea Research and Development Center, NUC TP 275. *Design Study of Advanced Underwater Optical Imaging Systems*, by A. Gordon, D. Cozen, C. Funk, P. Heckman, Jr. San Diego, California. January 1972.

PART II

EVALUATION OF THE EXPONENTIAL MULTIPLE-SCATTERING MODEL

by

Max R. Knittel

CONTENTS

	Page
Introduction	45
Comparison Sources	46
Exponential Multiple-Scattering Model	46
Monte Carlo Simulation Model	47
Data from Duntley's Experiments	48
Comparison of Exponential Model with Two Other Sources	49
Relative Error as a Function of Range	49
Relative Error as a Function of Aperture Angle	50
Conclusions	52
Figures	53
Tables	81
References	94

INTRODUCTION

The purpose of this section is to evaluate the predictions of radiant energy flux through an aperture developed from Gordon's exponential model. This will be done by comparing them with the predictions of a Monte Carlo simulation model and with experimental data.

The radiant energy flux passing through an aperture has significance in underwater optics for two reasons. First, it is important in areas concerning the power distribution of a collimated source (e.g., a laser) after the beam has travelled a given distance underwater; for example, target illumination or amount of energy reaching a receiver. Second, the flux through an aperture is related to the on-axis irradiance of a conical beam, which is significant because the available irradiance is an important design parameter for underwater optical imaging systems.

Because of the significance of the radiant energy flux, rather lengthy comparisons will be made of this quantity as a function of aperture angle, range, and scattering to absorption coefficient (s/a) ratio. It is hoped that these comparisons will serve as a guide to the various regions of validity for the results of Gordon.

EXPONENTIAL MULTIPLE-SCATTERING MODEL

The exponential multiple-scattering model developed by Gordon in Part I is presently formulated to predict the radiant energy flux produced by a unidirectional point source for a given combination of range, aperture angle, and s/a ratio.

To illustrate the geometry of this model, let a unidirectional point source illuminate a screen placed perpendicular to the light source axis. If F_o is the radiant energy emitted by the unidirectional point source and F is the energy flux intercepted by the screen placed at a distance R inside a cone of half-angle γ (a circular aperture of radius r), then the ratio of these will yield the fraction of energy that remains inside the circular aperture. This arrangement is shown in figure 1.*

The basic equation of the model as given by Gordon is

$$\frac{F}{F_o} = e^{\left\{\left[-\alpha + s\int_{\gamma'} P(\sigma)d\Omega\right]R\right\}}, \tag{1}$$

where

α ≡ total attenuation coefficient (meters^{-1}),
$P(\sigma)$ ≡ (σ) (θ)/s ≡ probability density function of volume scattering,
R ≡ range (meters),
γ' ≡ half-angle of the cone measured from the midpoint of the range (degrees),
$\frac{F}{F_o}$ ≡ normalized radiant energy flux through the target aperture.

It has been established that the ratio c = s/a is easily measured, but the quantity s itself is not. To write equation 1 in terms of the ratio c, the quantity αR, which defines the range as measured in attenuation lengths, must be written in terms of c. Substituting the definition of the total attenuation coefficient

$$\alpha = a + s, \tag{2}$$

αR can be written as

$$\alpha R = (a + s)R$$

$$= aR(1 + c). \tag{3}$$

---

*Figures are placed at the end of Part II.

Rewriting equation 1, we obtain

$$\frac{F}{F_o} = e^{[-\alpha R + sR\int_{\gamma'} P(\sigma)d\Omega]}$$

$$= e^{[-\alpha R + caR\int_{\gamma'} P(\sigma)d\Omega]}$$

$$= e^{\left[-\alpha R + \frac{c\alpha R}{1+c}\int_{\gamma'} P(\sigma)d\Omega\right]}$$

$$= e^{-\alpha R\left[1 - \frac{c}{1+c}\int_{\gamma'} P(\sigma)d\Omega\right]}. \quad (4)$$

From equation 4 it can be seen that the radiant energy flux for a unidirectional point source decreases exponentially with distance. It can also be seen that an effective attenuation coefficient, α_{eff}, can be defined such that

$$\alpha_{eff} = \alpha\left[1 - \frac{c}{1+c}\int_{\gamma'} P(\sigma)d\Omega\right]. \quad (5)$$

Single-scatter underwater visibility models predict a normalized radiant energy flux given by

$$\frac{F}{F_o} = e^{-\alpha R},$$

which corresponds to

$$\int_{\gamma'} P(\sigma)d\Omega = 0.$$

Therefore, the effective attenuation coefficient α_{eff} is bounded on one side by α. On the other side, the effective attenuation coefficient is bounded by $\alpha - s$ since

$$1 \geq \int_{\gamma'} P(\sigma)d\Omega \geq 0$$

and

$$\frac{c}{1+c} = \frac{s}{\alpha}.$$

Hence,

$$\alpha \geq \alpha_{eff} \geq a. \quad (6)$$

MONTE CARLO SIMULATION MODEL

In order to simulate increasingly complex underwater imaging systems, Funk has developed a method for describing the propagation of light underwater that includes the effects of multiple-scatterings (references 1 and 2). In this method Monte Carlo techniques are used to calculate effective attenuation coefficients for illuminating, image-forming, and backscattered light; these coefficients permit the most significant effects of multiple-scattering to be incorporated into an underwater visibility model.

The simplest form of the Monte Carlo calculations for predicting the radiant energy flux from a unidirectional point source is a specialized three-dimensional random walk. The scattering and absorption properties of the water are found in terms of probability distribution functions that characterize the direction and length of each step in the random walk.

DATA FROM DUNTLEY'S EXPERIMENTS

For a number of years, S. Q. Duntley of Scripps Institution of Oceanography, Visibility Laboratory, has been investigating the propagation of light in water. During this investigation, numerous experiments were performed in both fresh water at Diamond Island, New Hampshire, and simulated ocean water of various s/a ratios in a laboratory tank. A laser was used as the light source, and measurements of the radiant energy flux were made at varying ranges and collector angles. The experimental procedure was to measure the energy at an off-axis collector angle γ' at a radius r from the source. The data were then integrated to obtain the total power on a spherical cap, with γ' as the half angle of the cap. These experiments are described in reference 3.

COMPARISON OF EXPONENTIAL MODEL WITH TWO OTHER SOURCES

Using equation 4, it is now possible to compare the predictions of the exponential model with those of the Monte Carlo multiple-scattering model and the experimental data accumulated by Duntley.

Theoretical predictions were provided by Funk for the chosen cases from the Monte Carlo simulation model, and equation 4 was programmed on a desk calculator to give predictions from the exponential model. Representative sets were chosen from Duntley's data to serve as a basis from which to assess the accuracy of the two visibility models.

The $\int_{\gamma'} P(\sigma)d\Omega$ was interpolated from the table of the experimental volume scattering distribution function as calculated by Duntley (table 1*). The seven aperture cone half-angles chosen by Funk for the Monte Carlo model were used here. The angles that Duntley defines in his experiments and those used in Gordon's theoretical model are related through the expression

$$\tan \gamma' = 2 \tan \gamma.$$

The angles γ (and γ') and the corresponding scattering probabilities are shown in table 2.

Tables 3 through 11 show the radiant energy flux as a function of aperture and range for three s/a ratios. The results of the calculations using equation 4 are shown in tables 3, 6, and 9 for the ratios 3.56, 2.28, and 1.48, respectively. In a similar manner, tables 4, 7, and 10 display the predictions of the Monte Carlo simulation model, and tables 5, 8, and 11 display the experimental results as compiled by Duntley.

Figures 2 through 22 show the predictions of the exponential multiple-scattering model (designated as E-model in the graphs for brevity) as straight lines on semi-logarithmic paper. For comparison, the predictions of the Monte Carlo simulation model (designated as M-model) and the experimental data of Duntley (designated as D-data) appear as crosses and circles, respectively, on the appropriate exponential model line.

RELATIVE ERROR AS A FUNCTION OF RANGE

Figures 2 through 22 indicate that both the exponential and Monte Carlo simulation model predictions give very close agreement with the set of selected experimental data. In order to see this agreement more easily, a simple type of error analysis was performed to give an idea of the relative differences between the results of the two models and the experimental data.

**Tables are placed at the end of Part II.*

Because the exponential model of Gordon is based upon the assumption of small angle forward scattering, the validity of the small angle approximation is reduced as the number of scatterings increases, which tends to make the model predictions less accurate. To show this, the unit of measurement for the range was changed from attenuation length to scattering length. Now, the exponential model should tend to break down at the same range in all cases; i.e., the model should break down after the same number of scattering lengths, regardless of the s/a ratio. The scattering length, sR, can be found from the attenuation length αR through

$$sR = \frac{\alpha R}{1 + \frac{a}{s}} , \tag{8}$$

where

sR ≡ range (scattering lengths),
αR ≡ range (attenuation lengths),
a ≡ absorption coefficient,
s ≡ scattering coefficient.

To find this average error, an error equation of the form

$$\text{Error} = \frac{\left\{ \sum_{i=1}^{7 \text{ angles}} \left[\ln\left(\frac{\text{theoretical model flux}}{\text{experimental flux}} \right) \right]^2 \right\}^{1/2}}{7} \tag{9}$$

was used to find an average error value over all of the seven aperture cone half-angles. Table 12 shows the results of these calculations. The errors between the exponential model predictions and the experimental values are denoted by E/D, while the errors between the Monte Carlo simulation model predictions and the experimental values are denoted by M/D. Figures 23 through 25 display these results for the three s/a ratios investigated.

RELATIVE ERROR AS A FUNCTION OF APERTURE ANGLE

Another way of examining the differences between the predicted radiant energy flux and the experimental data is to calculate the error averaged over all the ranges for the various aperture cone half-angles. In this case, the formula used to calculate the average error is given by

$$\text{Error} = \frac{\left\{ \sum_{i=1}^{10 \text{ ranges}} \left[\ln\left(\frac{\text{theoretical model flux}}{\text{experimental flux}} \right) \right]^2 \right\}^{1/2}}{10} \tag{10}$$

The results of these calculations for the exponential model (E/D) and the Monte Carlo simulation model (M/D) are summarized in table 13. Figures 26 through 28 display these results for the three s/a ratios investigated.

CONCLUSIONS

By examining figures 23 through 25, it can be seen that the differences between the predictions of the exponential model and the multiple-scattering simulation model for ranges up to six scattering lengths are not very significant. In terms of attenuation lengths, this range corresponds to seven to ten attenuation lengths, depending on the s/a ratio. The exponential model does tend here to slightly better predict this particular set of experimental data, but it is also apparent from these graphs that when the exponential model does break down at the longer ranges, the Monte Carlo simulation method still continues to offer reasonable predictions for calculating effective attenuation coefficients.

Looking at figures 26 through 28, it is apparent that the accuracy of the exponential model is greater for small angles (less than 2°) and large angles (greater than 10°), but that the Monte Carlo simulation model appears better able to predict the experimental results for the intermediate angles. Again, the differences are undoubtedly not very significant.

In addition, it must be stressed that the accuracy of the two models has been assessed here on the basis of only one set of experimental data. While there is no reason to believe that the data are biased in any manner, such a limited comparison may not yield the same results as one supported on a broader base of experiment. Such a comparison may show slight differences in the relative accuracy of the two models.

Therefore, in the final analysis, it can be stated that the ranges up to seven to ten attenuation lengths, this simple, exponential formula rivals the Monte Carlo model in accuracy of predicting radiant energy flux or on-axis irradiance due to conical beams and surpasses it in ease of use. When supplied with a table of volume scattering distribution functions, one can easily predict what fraction of the energy produced by a narrow-beam light source will reach a target of known size located at selected distances from the source. The limitation to ranges of less than seven to ten attenuation lengths is not a disabilitating one since the most sophisticated underwater viewing systems now available can detect an object at a maximum range of only about seven attenuation lengths. However, for questions other than flux through an aperture or on-axis irradiance or for ranges greater than six scattering lengths, one must at present look for tools other than the exponential model, such as Monte Carlo analysis.

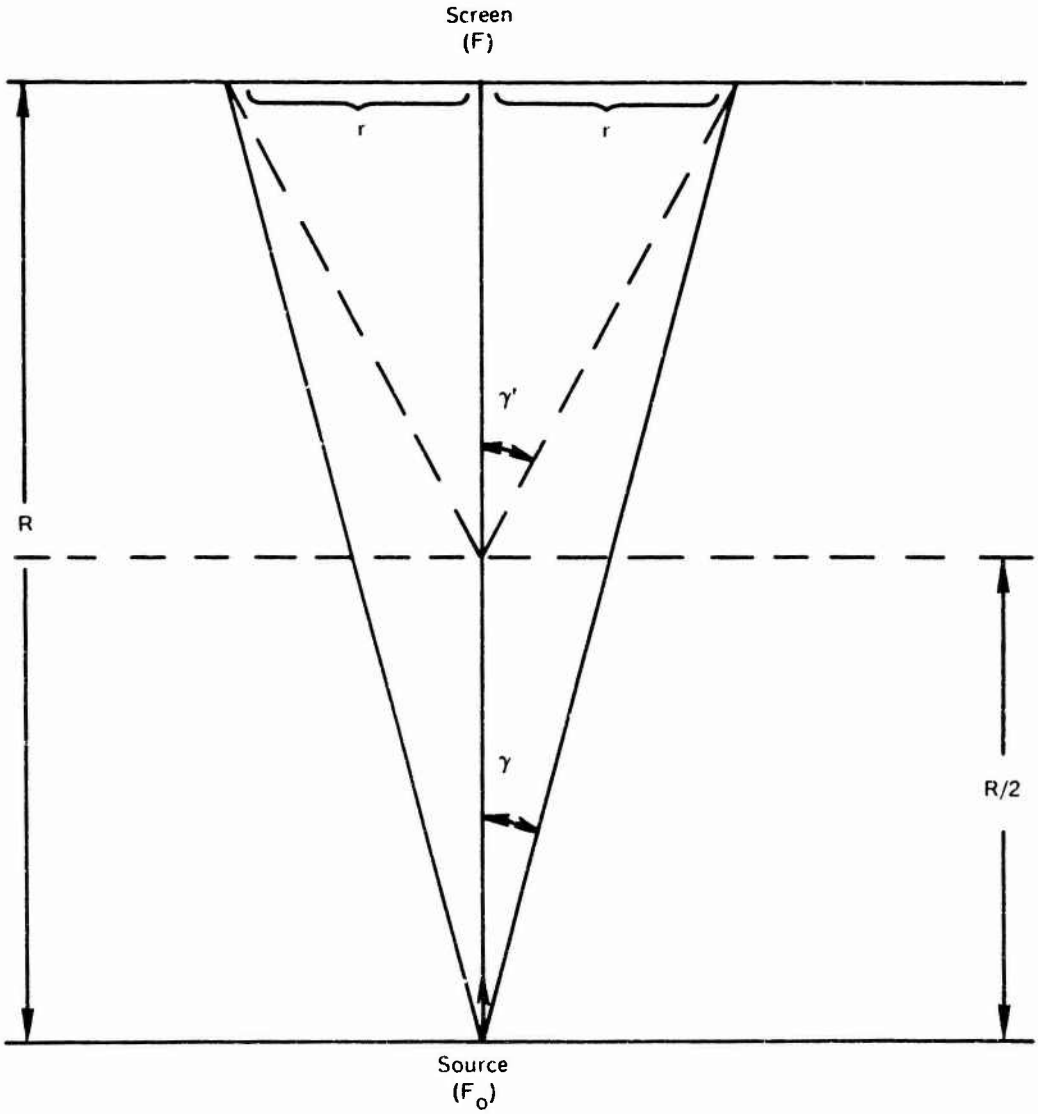

Figure 1. Geometry of the Exponential Model.

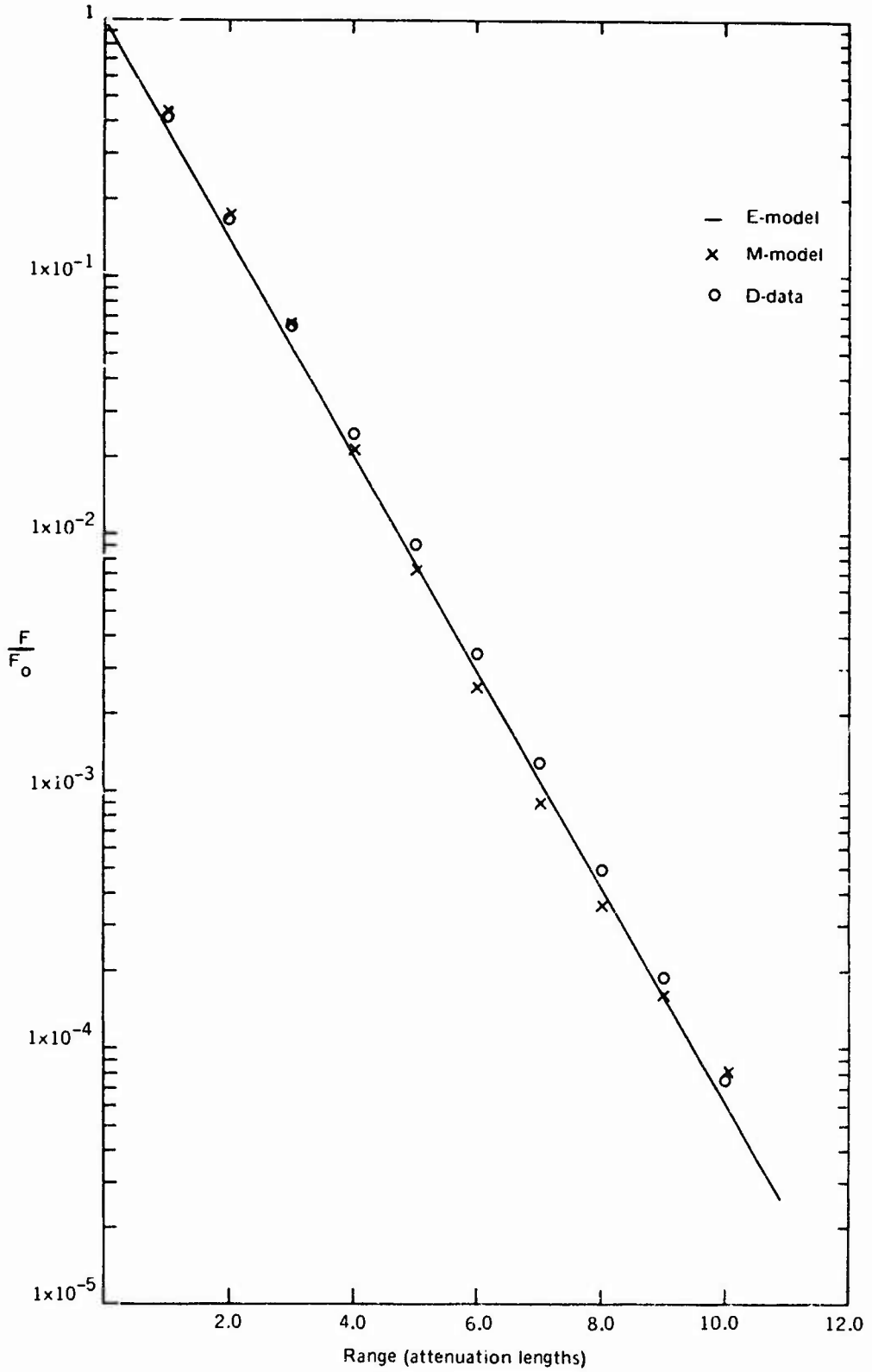

Figure 2. Radiant Energy Flux as a Function of Range for s/a = 3.56, $\gamma = 0.10^{\circ}$.

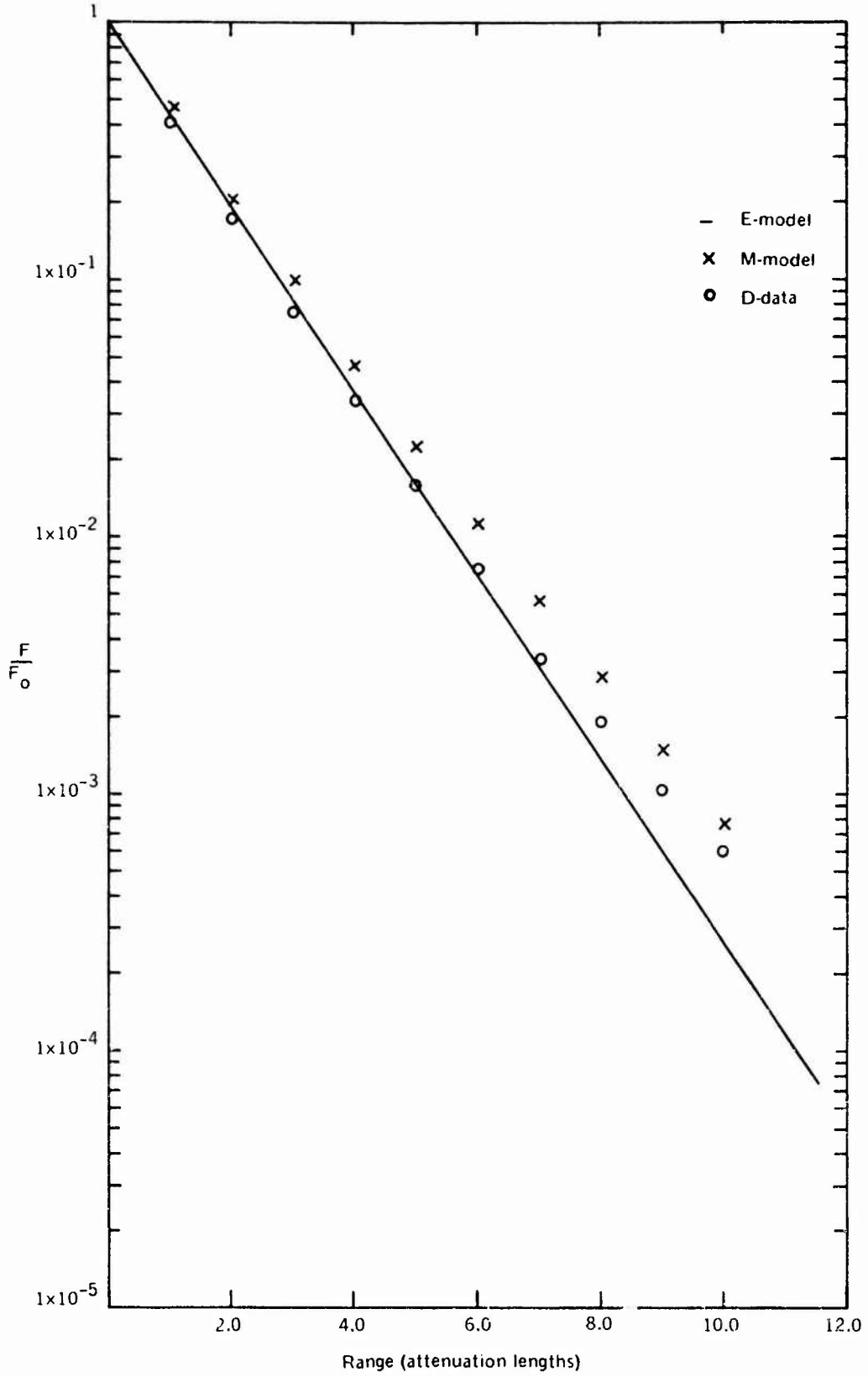

Figure 3. Radiant Energy Flux as a Function of Range for s/a = 3.56, $\gamma = 1.00^{\circ}$.

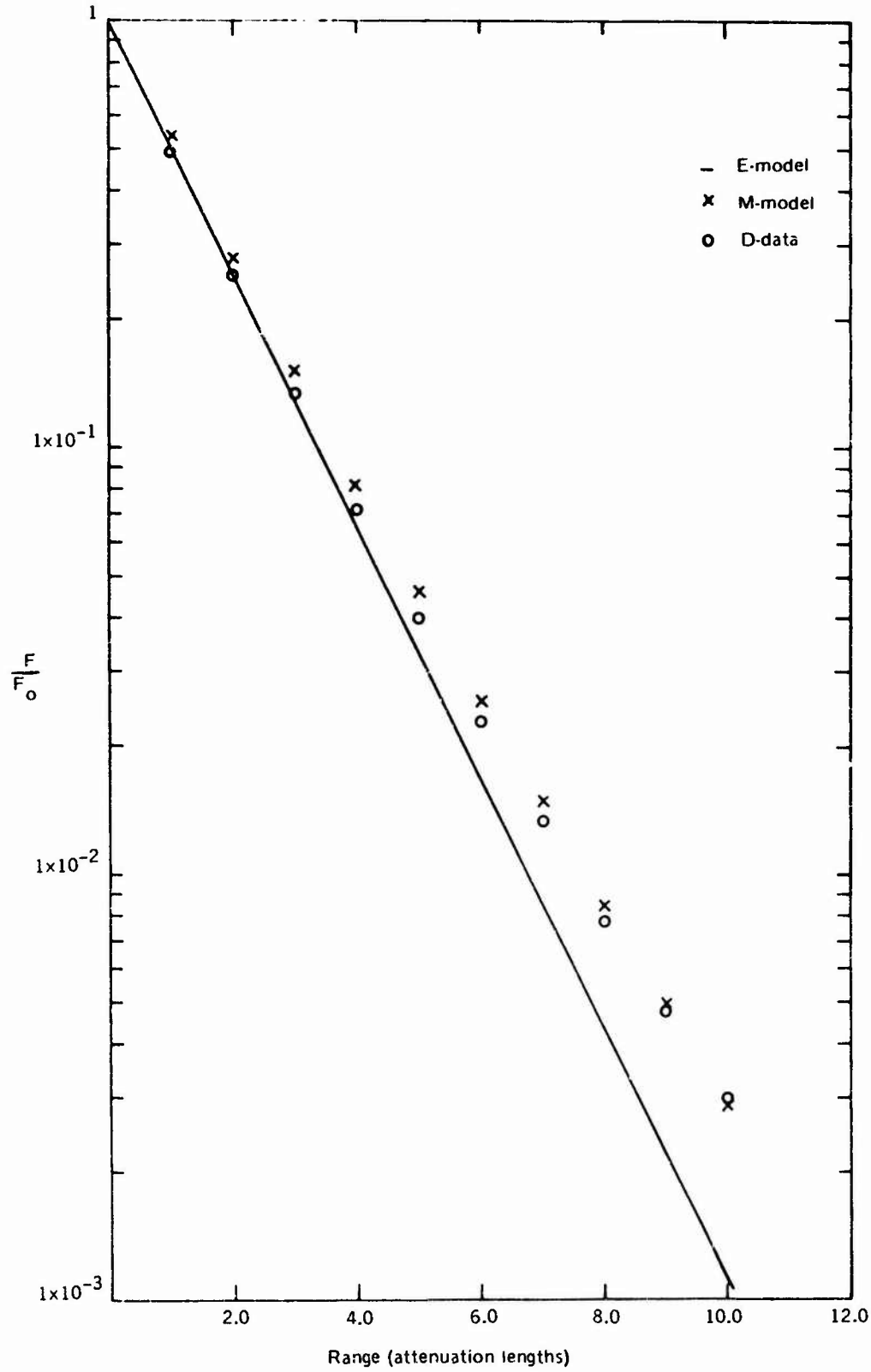

Figure 4. Radiant Energy Flux as a Function of Range for s/a = 3.56, $\gamma = 2.51^{\circ}$.

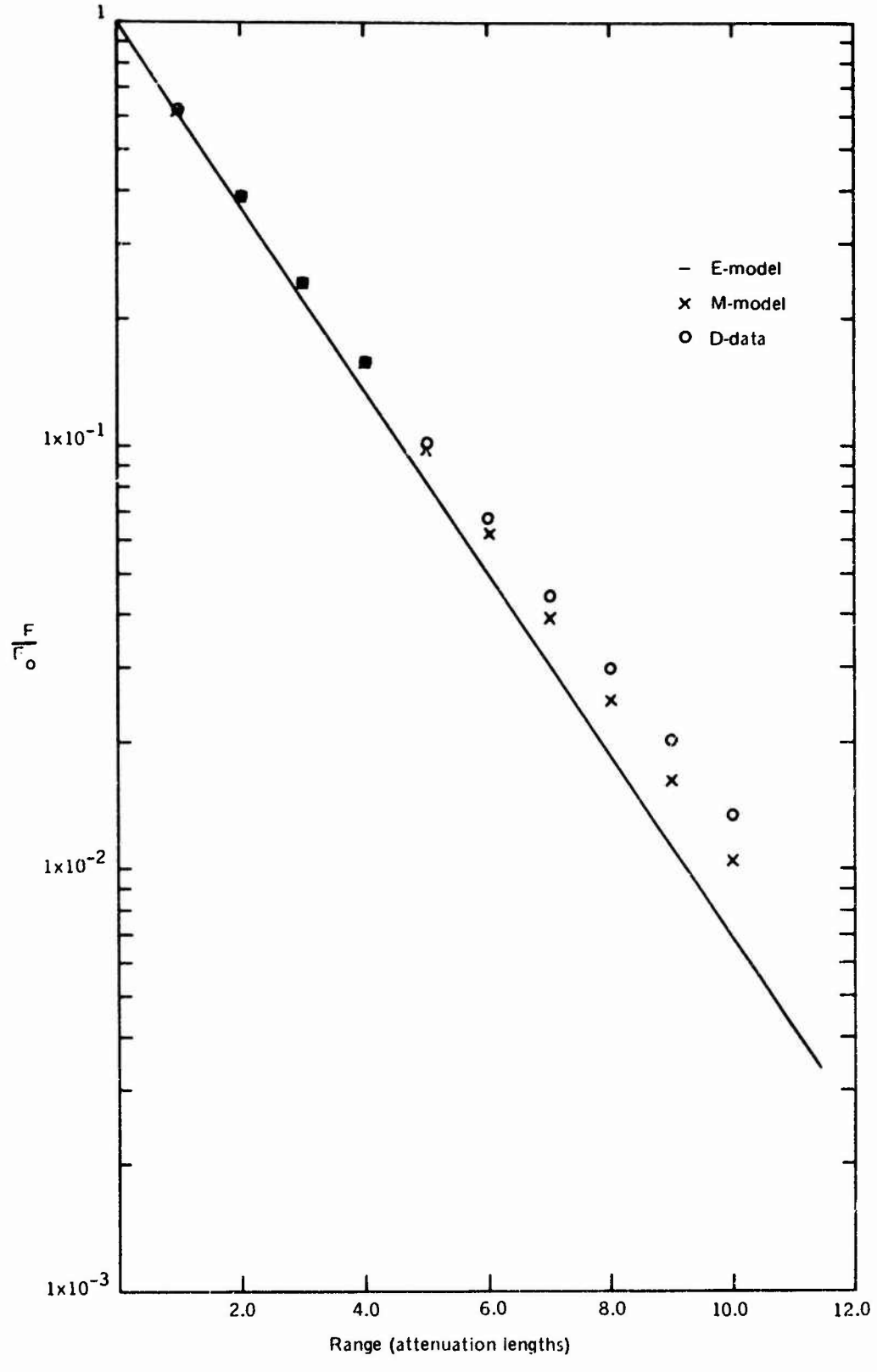

Figure 5. Radiant Energy Flux as a Function of Range for s/a = 3.56, $\gamma = 6.31^{\circ}$.

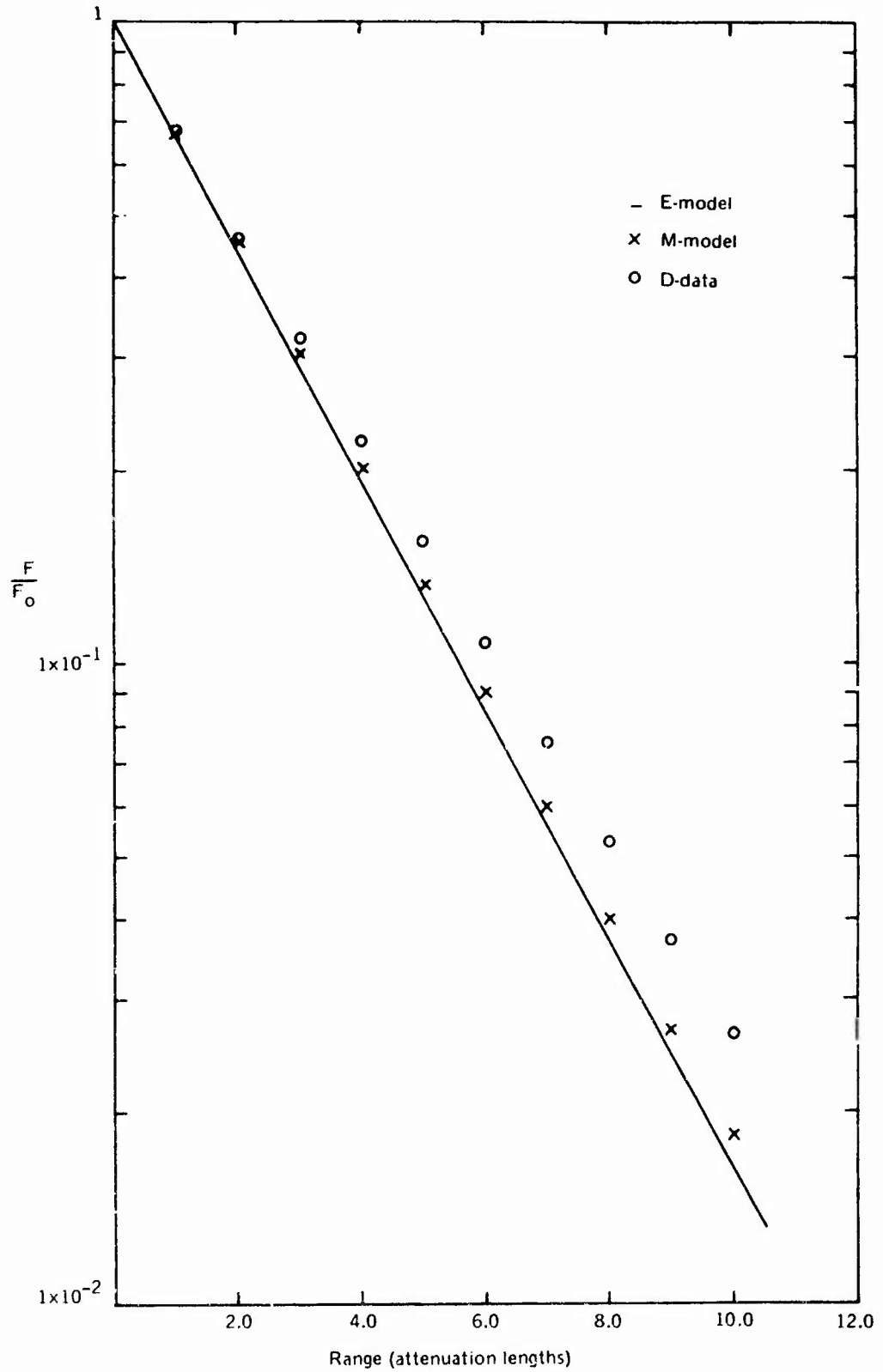

Figure 6. Radiant Energy Flux as a Function of Range for s/a = 3.56, $\gamma = 10.00^{\circ}$.

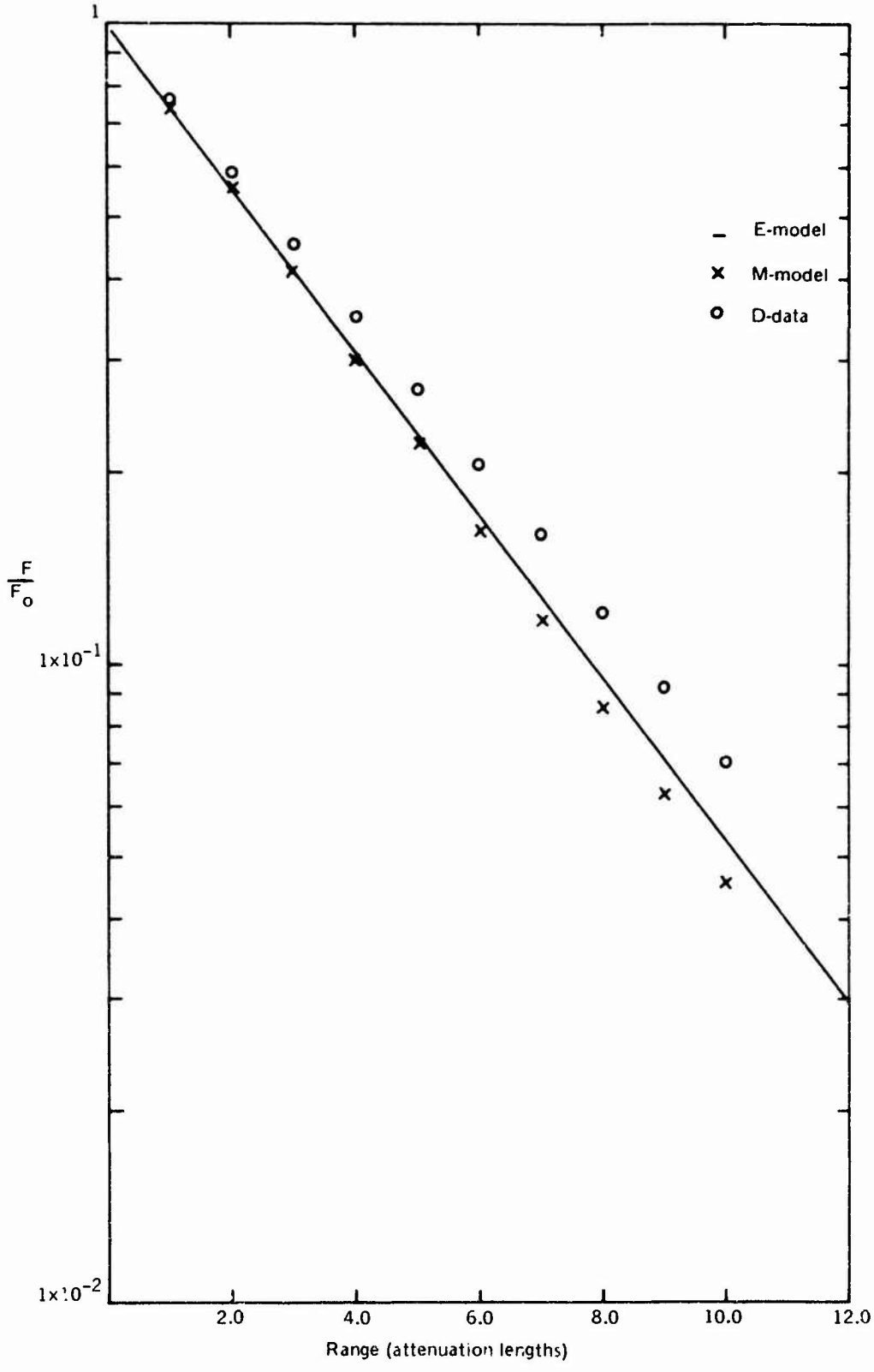

Figure 7. Radiant Energy Flux as a Function of Range for s/a = 3.56, $\gamma = 25.11^{\circ}$.

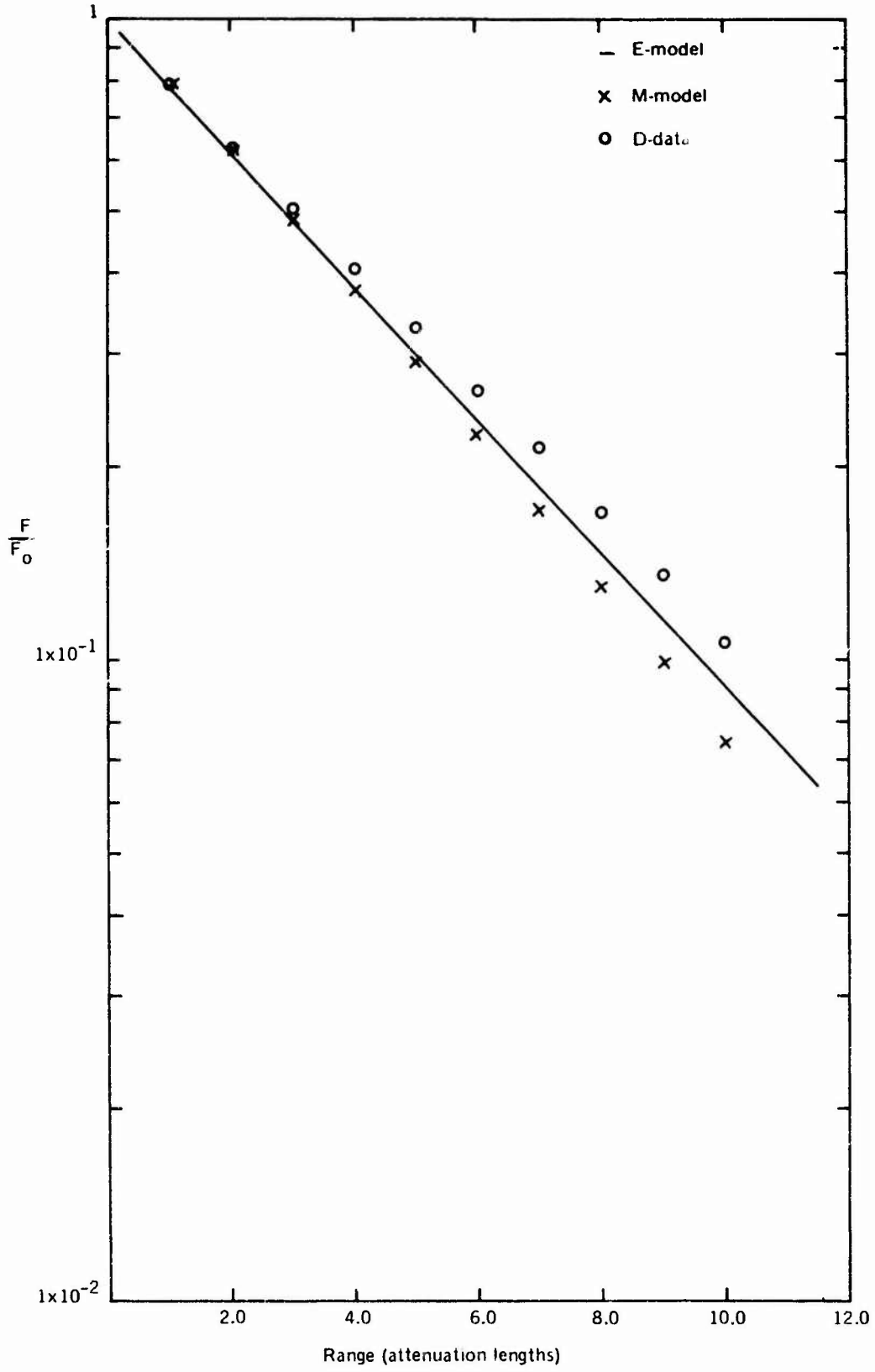

Figure 8. Radiant Energy Flux as a Function of Range for $s/a = 3.56$, $\gamma = 100.00^{\circ}$.

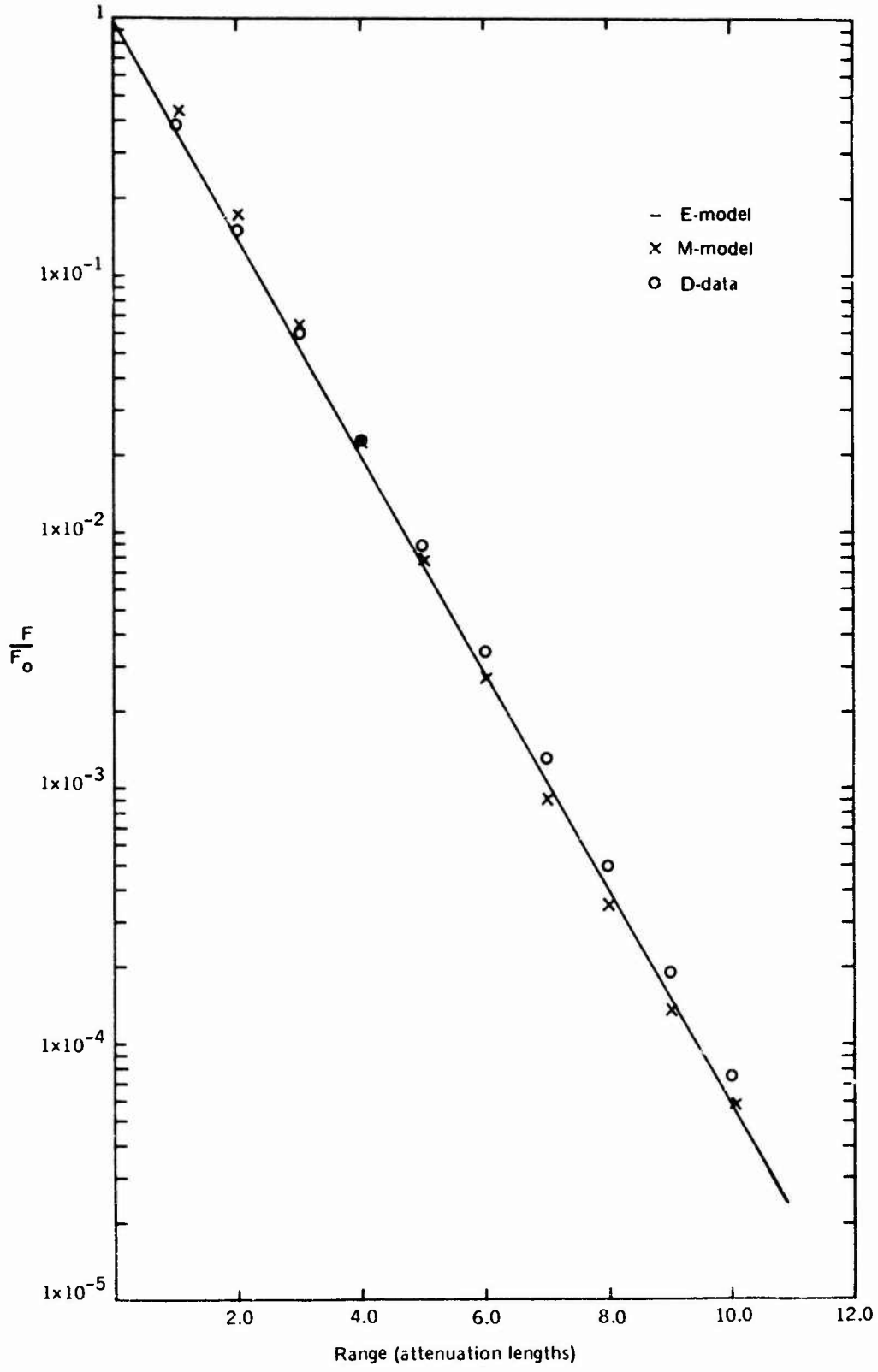

Figure 9. Radiant Energy Flux as a Function of Range for s/a = 2.28, $\gamma = 0.10^{\circ}$.

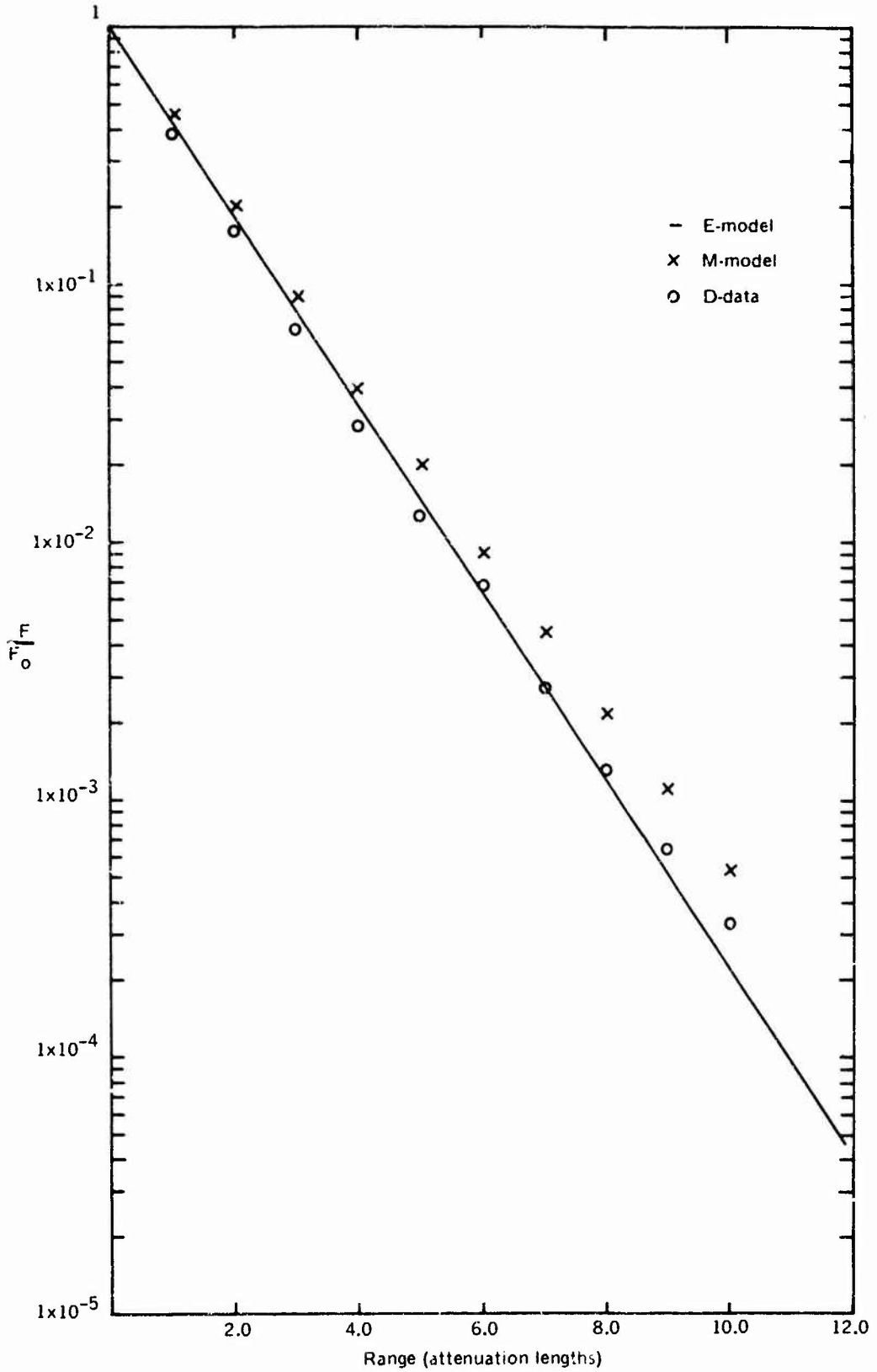

Figure 10. Radiant Energy Flux as a Function of Range for s/a = 2.28, $\gamma = 1.00^{\circ}$.

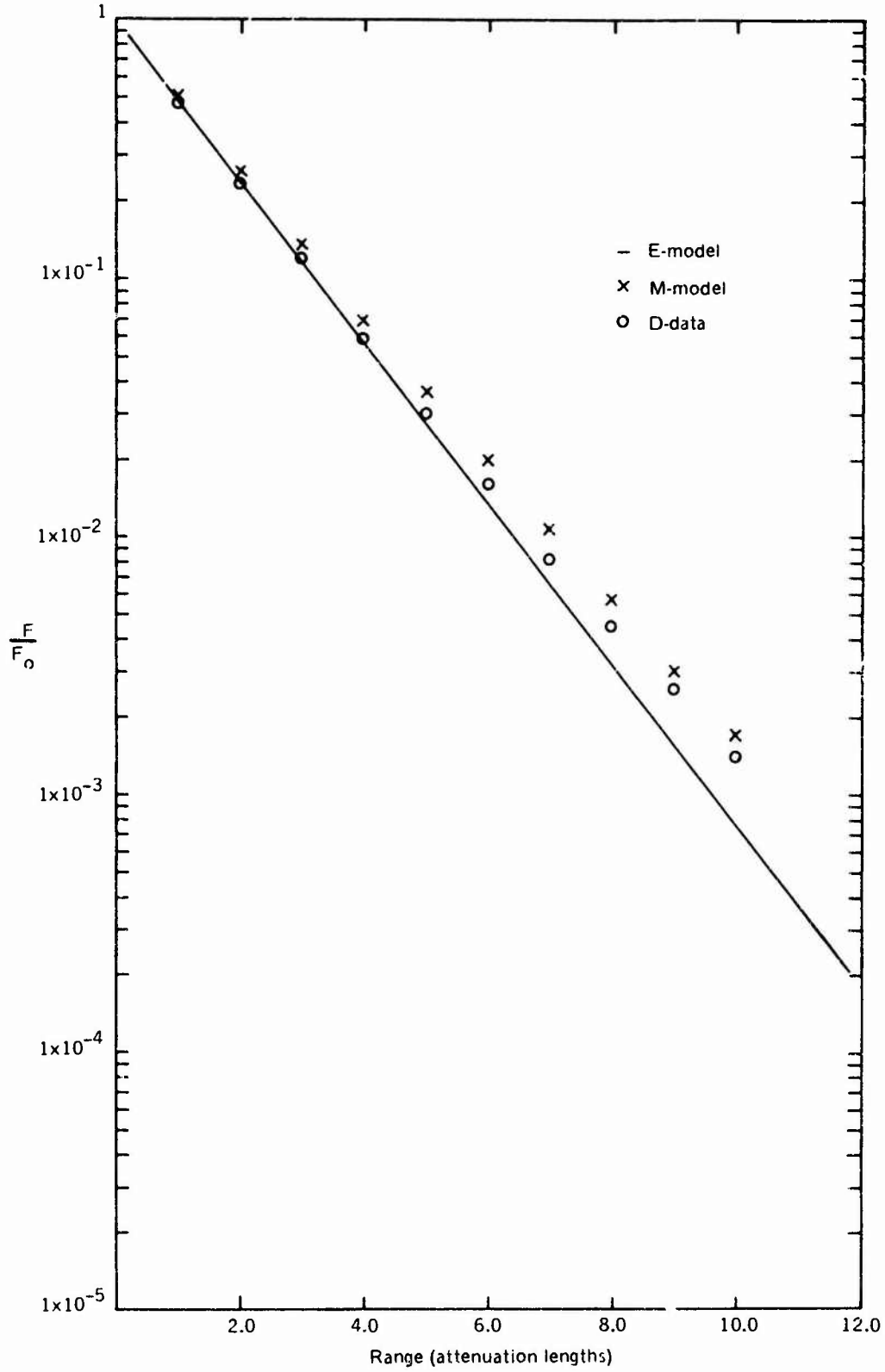

Figure 11. Radiant Energy Flux as a Function of Range for s/a = 2.28, $\gamma = 2.51^{\circ}$.

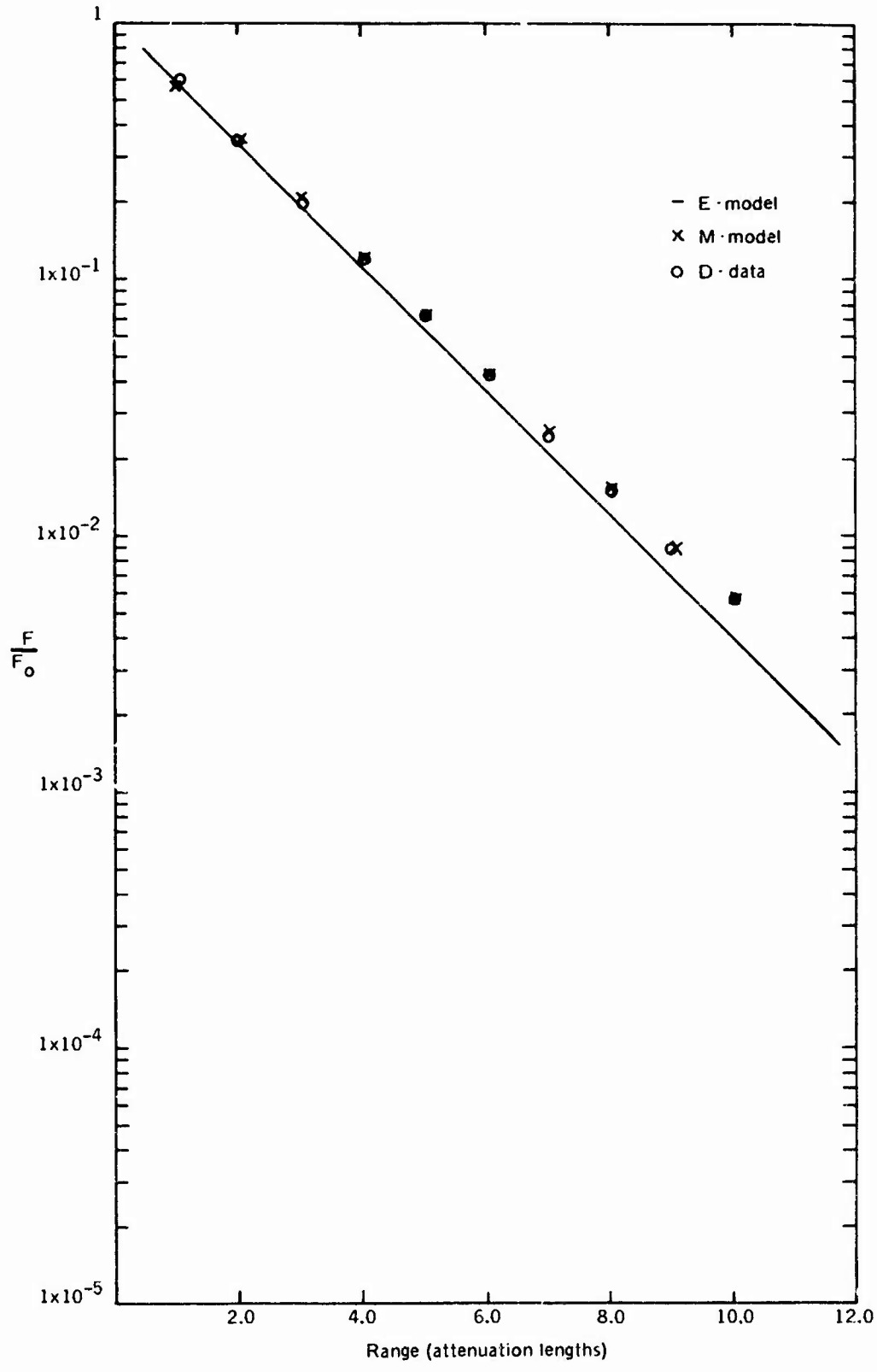

Figure 12. Radiant Energy Flux as a Function of Range for s/a = 2.28, $\gamma = 6.31^{\circ}$.

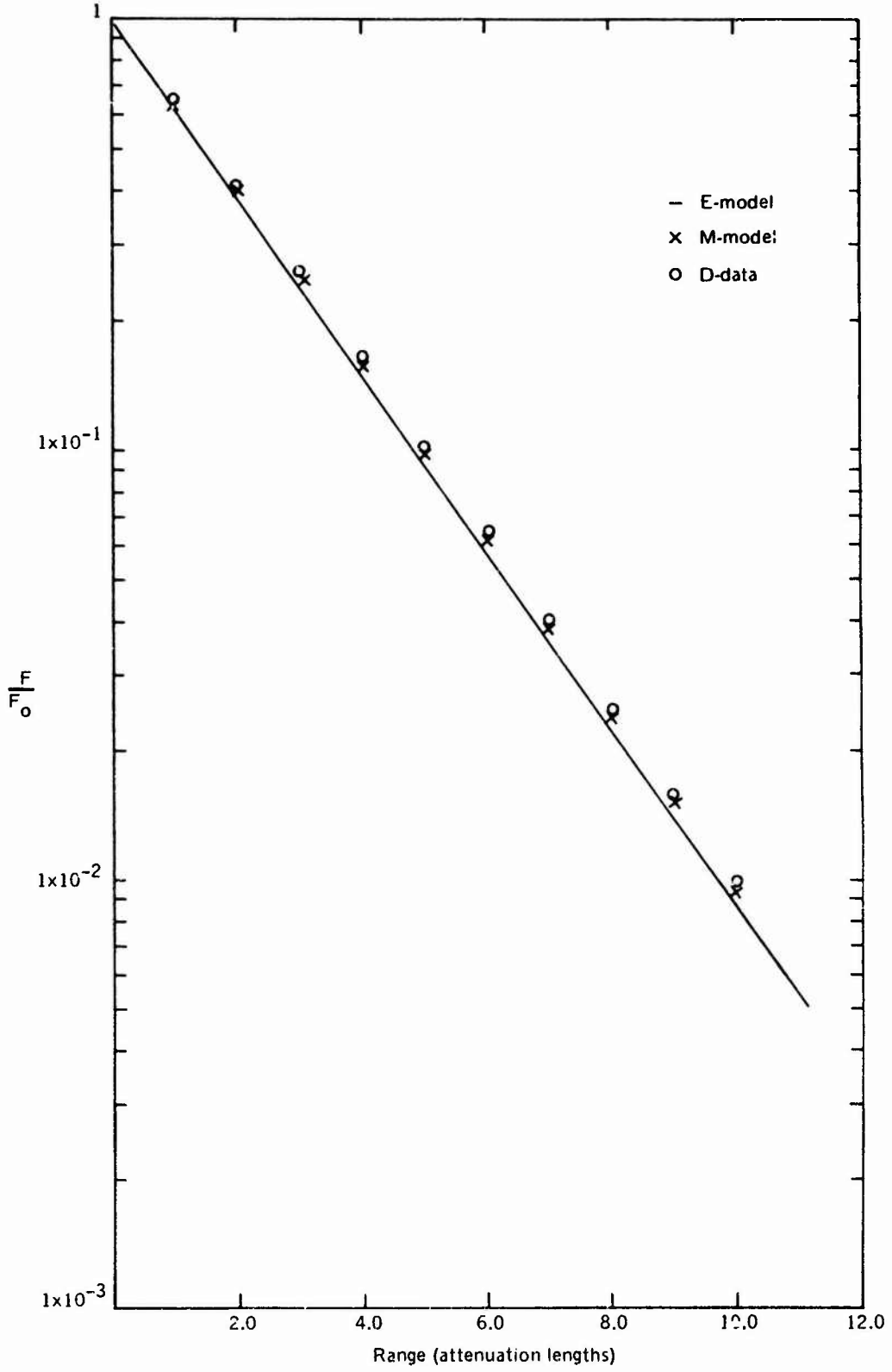

Figure 13. Radiant Energy Flux as a Function of Range for s/a = 2.28, $\gamma = 10.00^{\circ}$.

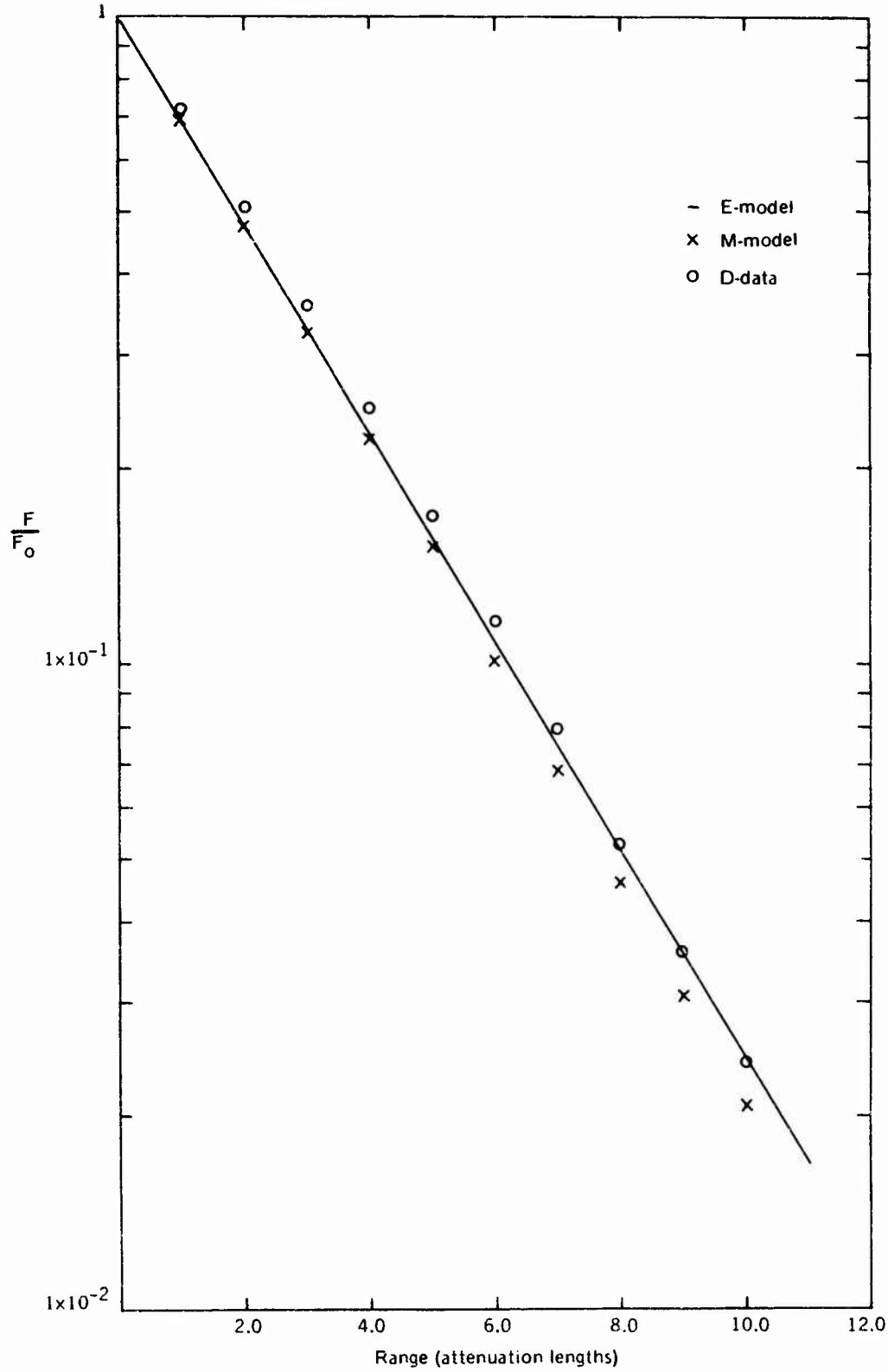

Figure 14. Radiant Energy Flux as a Function of Range for s/a = 2.28, $\gamma = 25.11^{\circ}$.

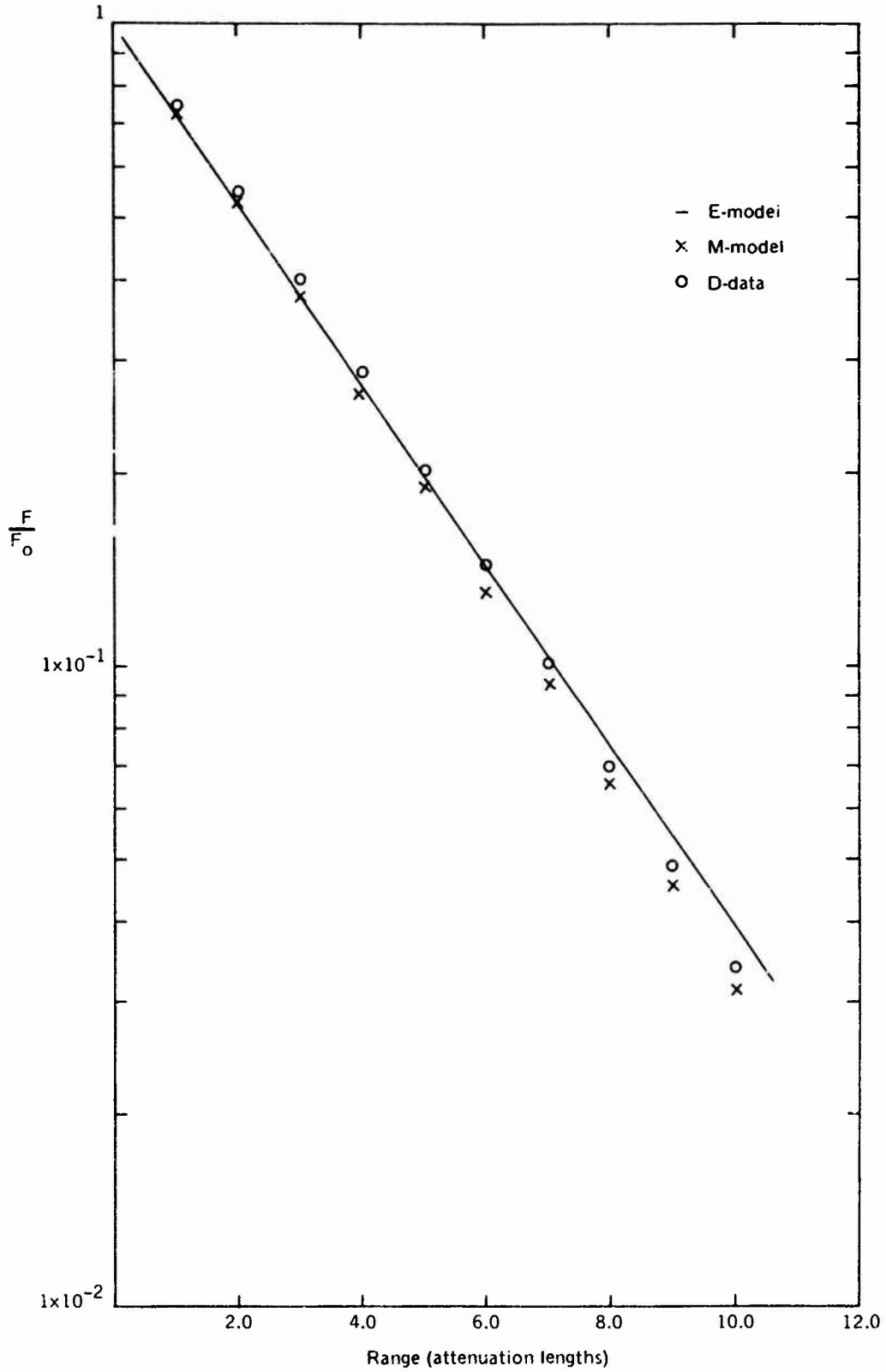

Figure 15. Radiant Energy Flux as a Function of Range for s/a = 2.28, $\gamma = 100.00^{\circ}$.

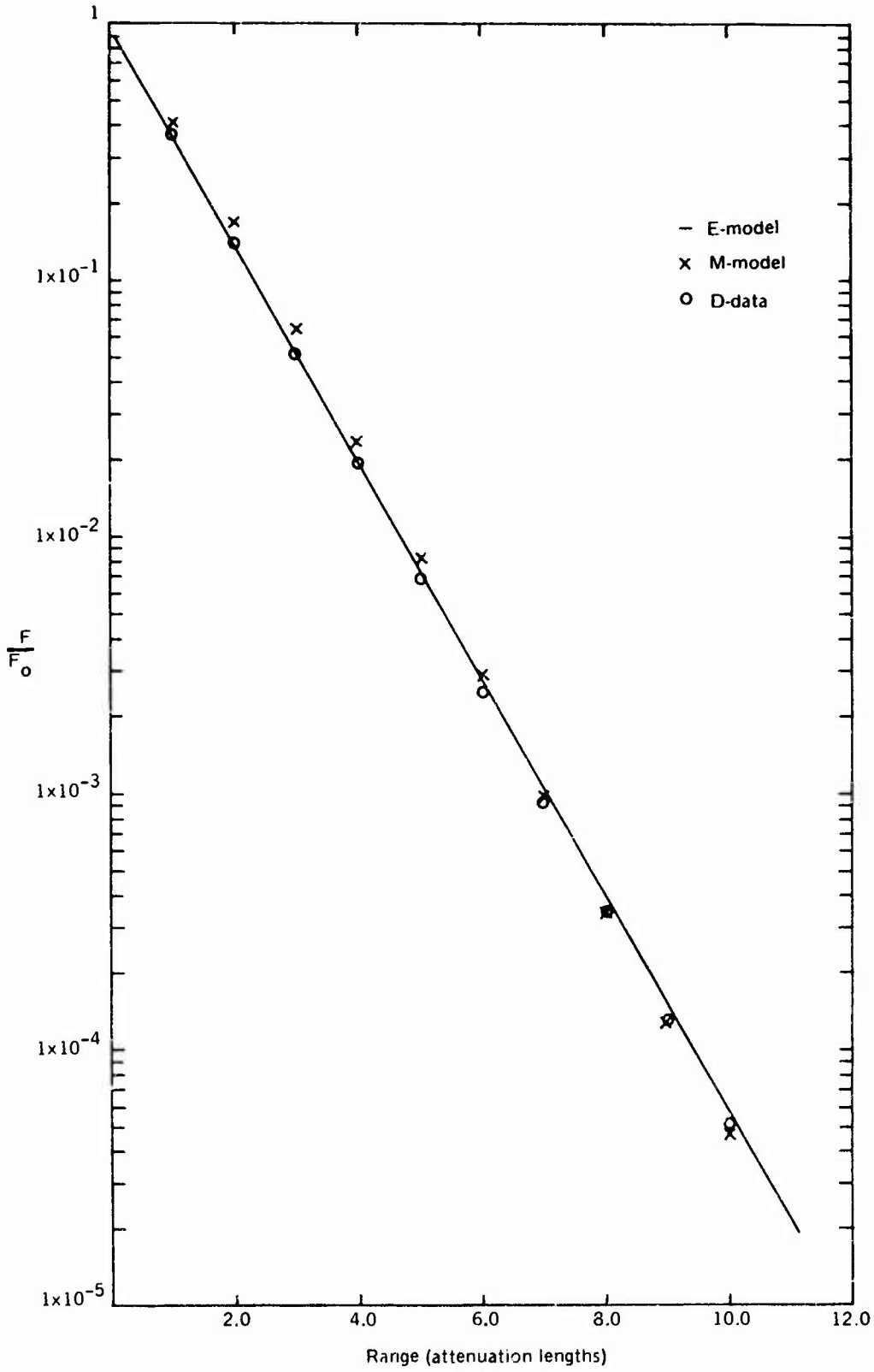

Figure 16. Radiant Energy Flux as a Function of Range for s/a = 1.48, $\gamma = 0.10^{\circ}$.

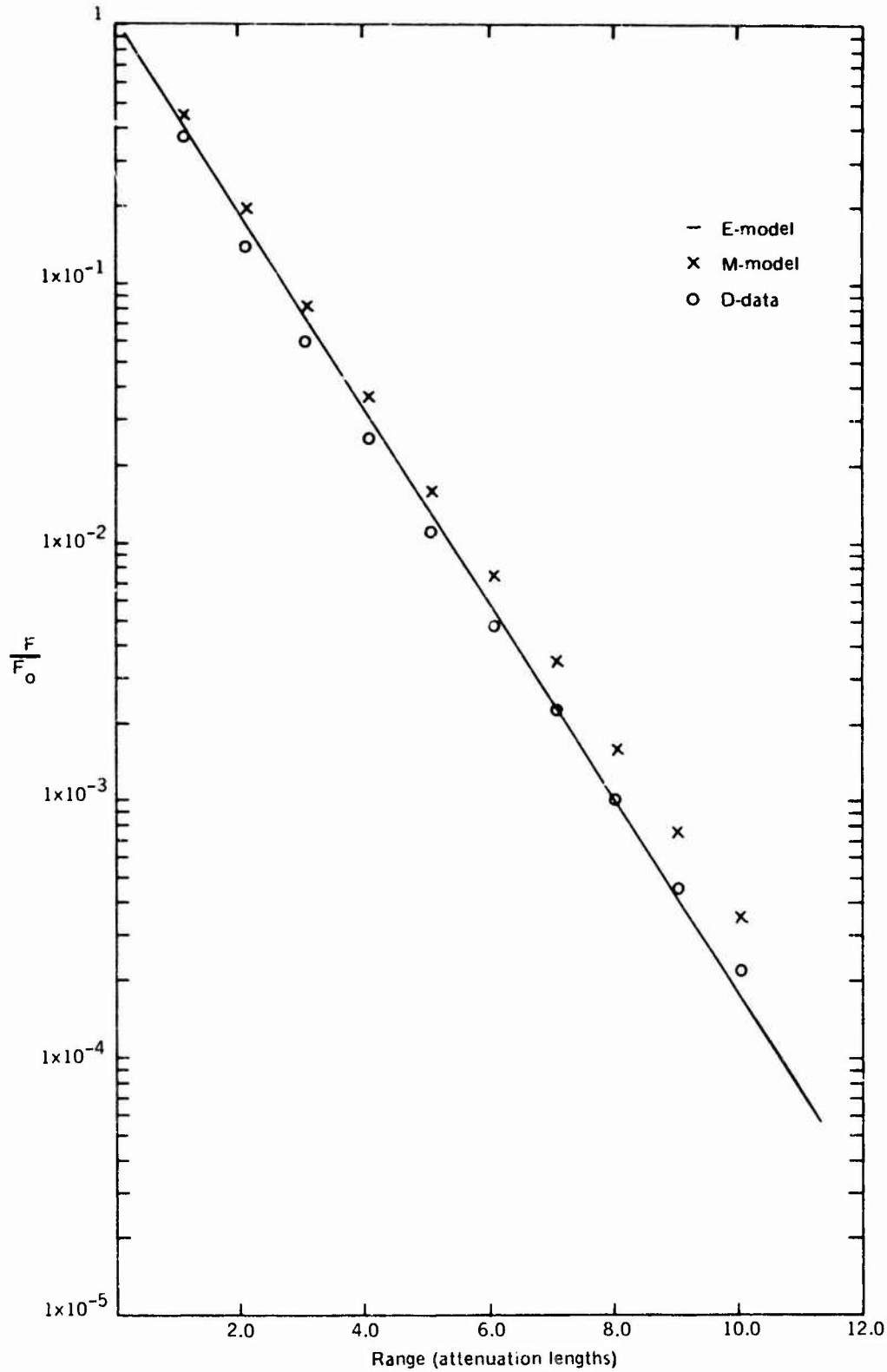

Figure 17. Radiant Energy Flux as a Function of Range for s/a = 1.48, $\gamma = 1.00^{\circ}$.

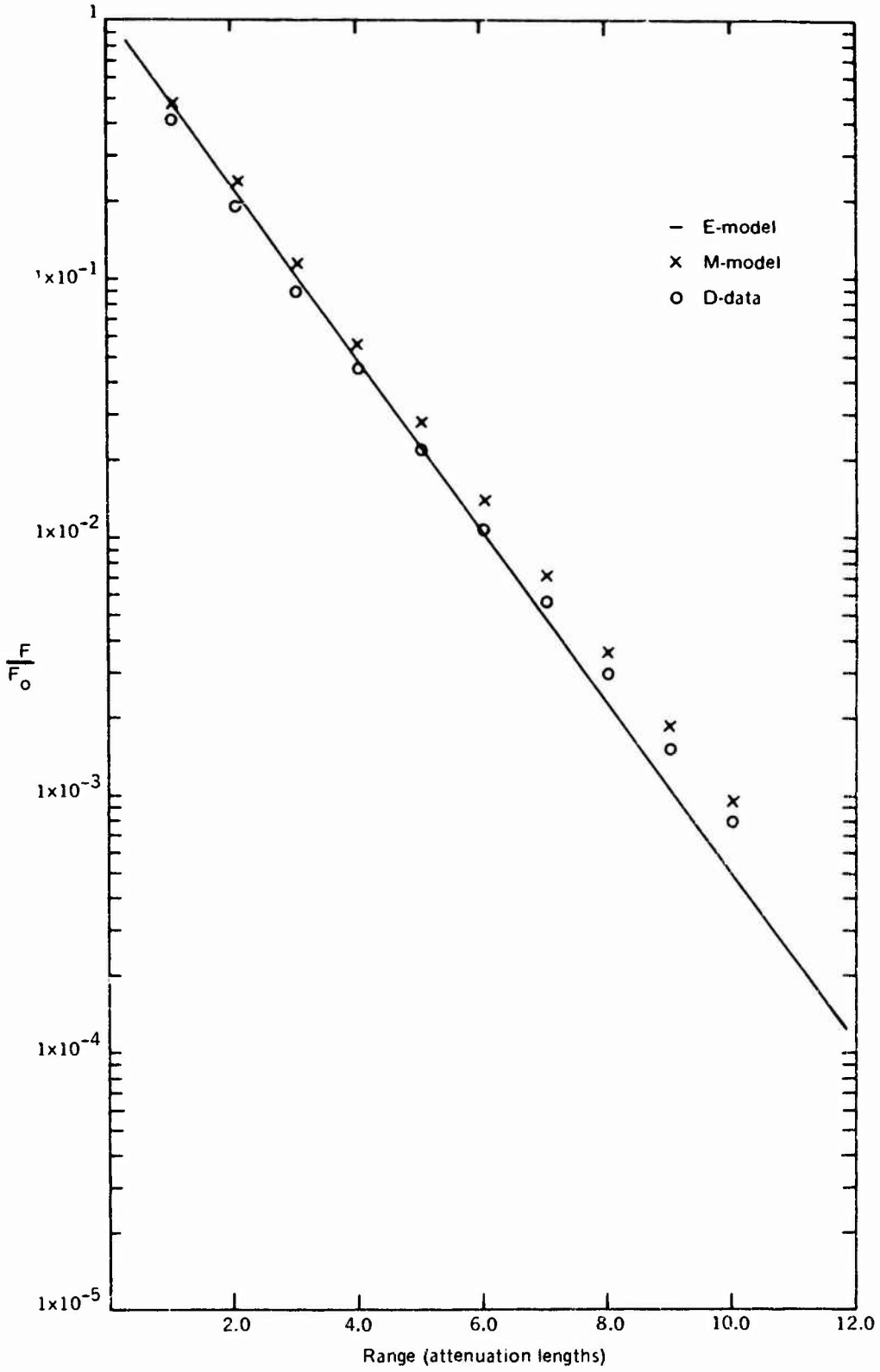

Figure 18. Radiant Energy Flux as a Function of Range for s/a = 1.48, $\gamma = 2.51^{\circ}$.

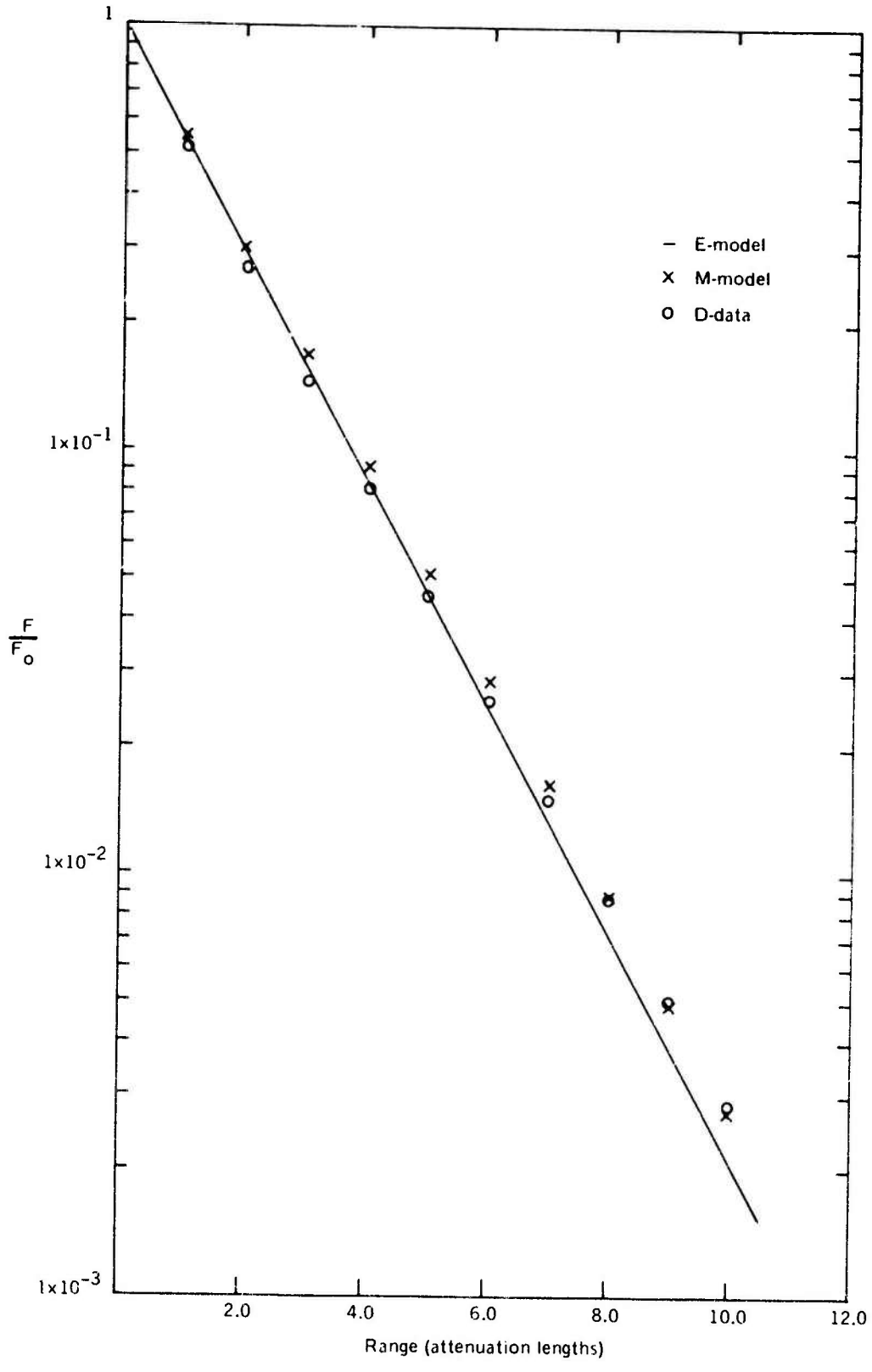

Figure 19. Radiant Energy Flux as a Function of Range for s/a = 1.48, $\gamma = 6.31^{\circ}$.

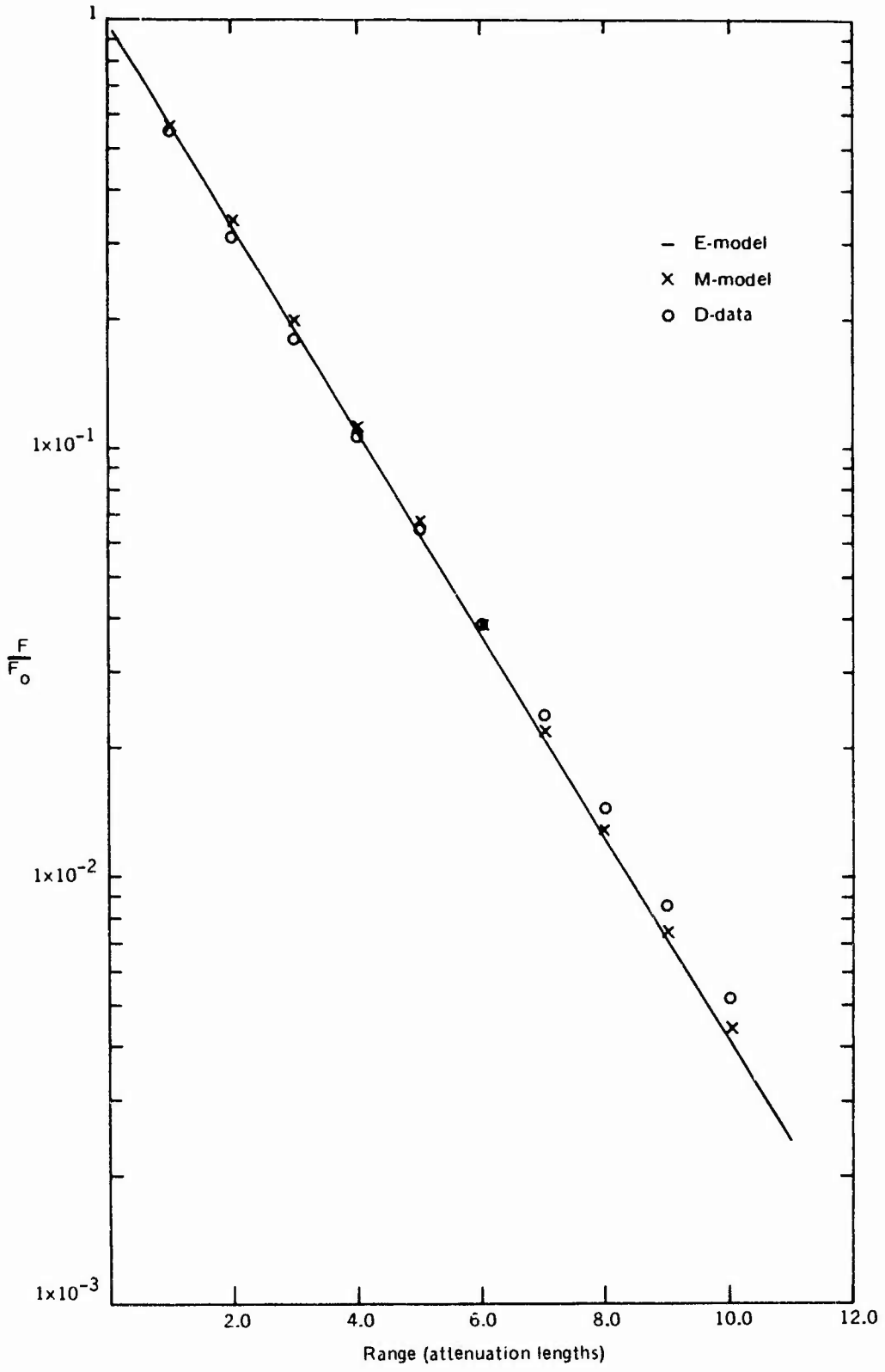

Figure 20. Radiant Energy Flux as a Function of Range for s/a = 1.48, $\gamma = 10.00^{\circ}$.

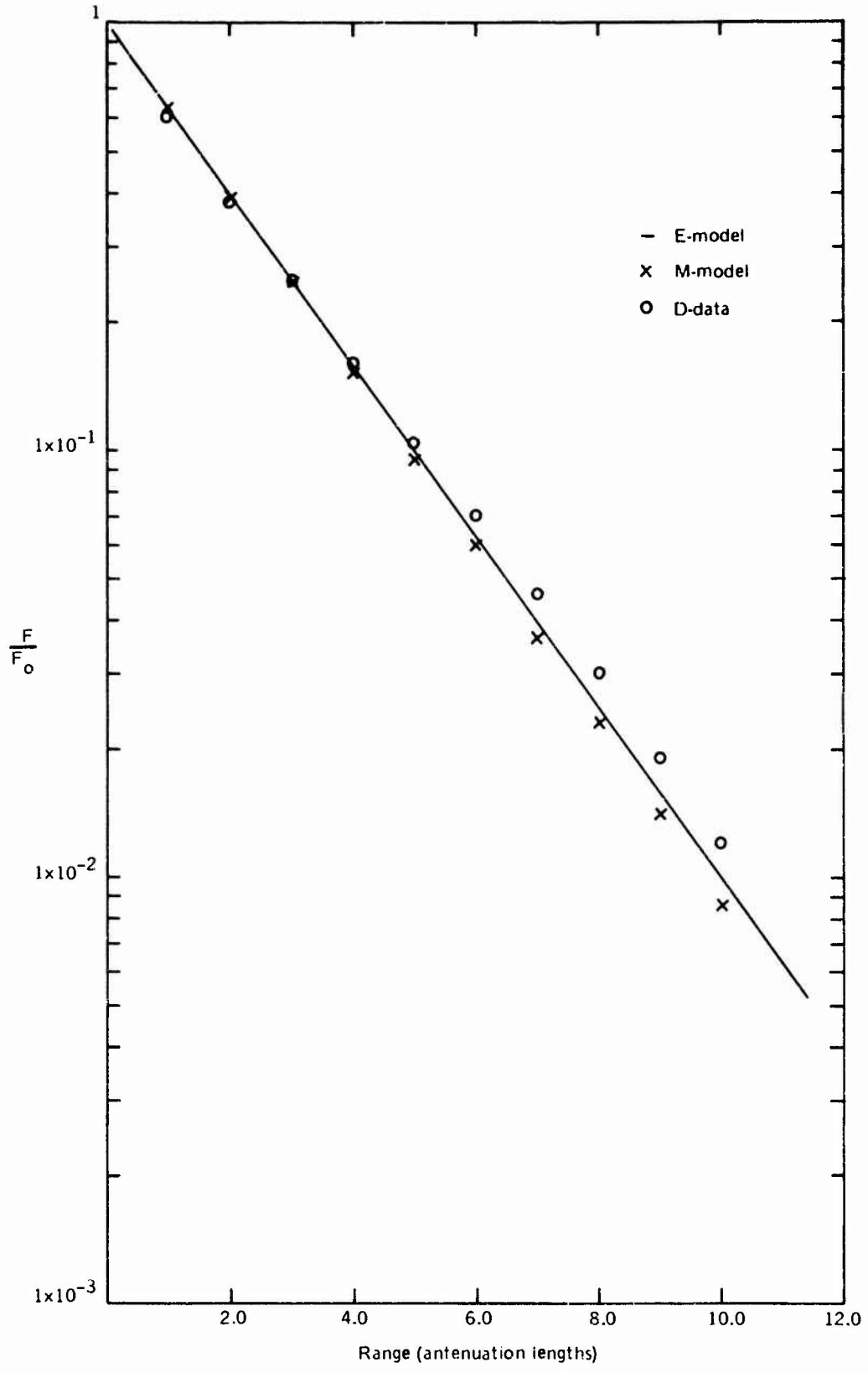

Figure 21. Radiant Energy Flux as a Function of Range for s/a = 1.48, $\gamma = 25.11^{\circ}$.

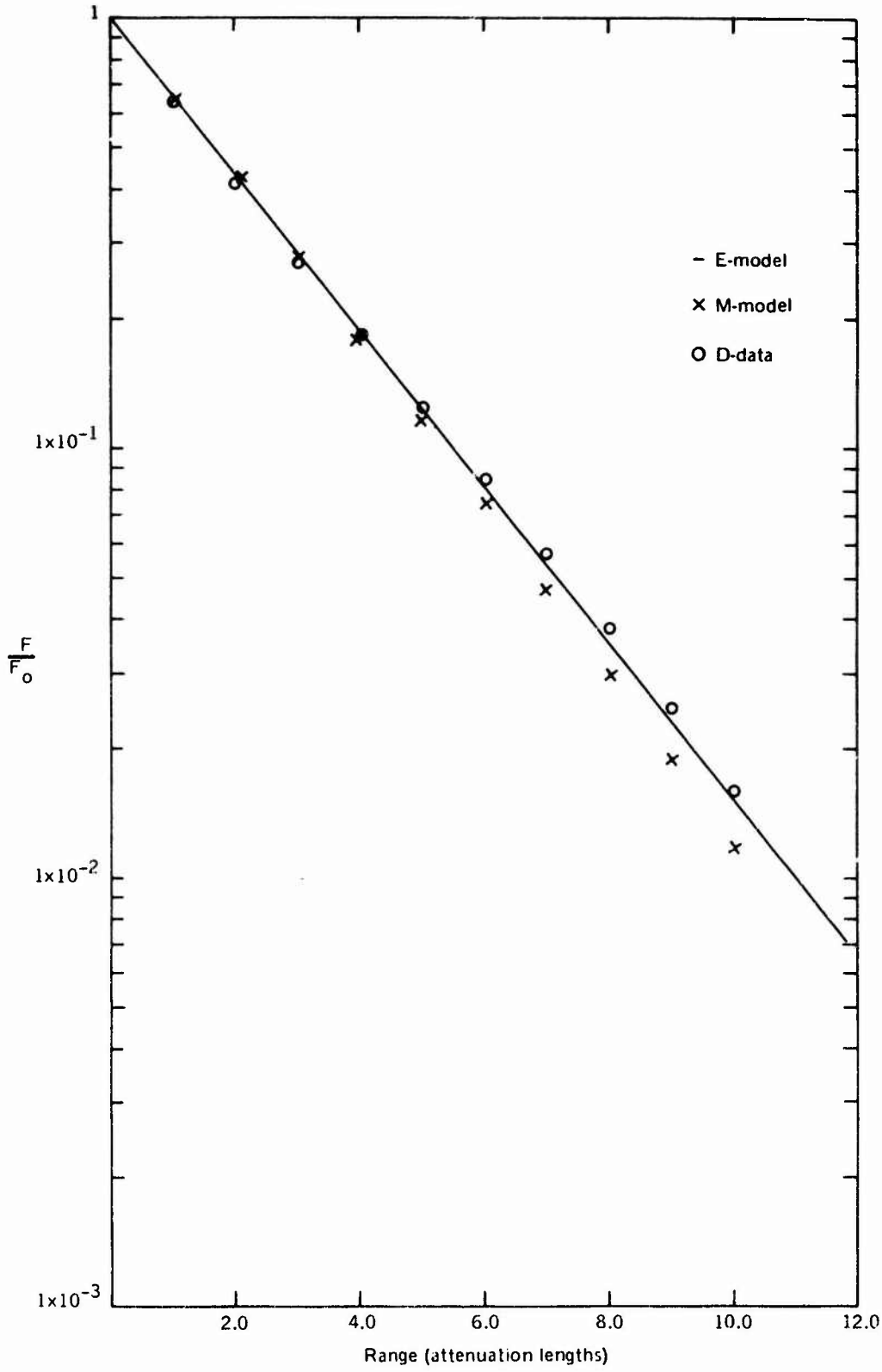

Figure 22. Radiant Energy Flux as a Function of Range for s/a = 1.48, $\gamma = 100.00^{\circ}$.

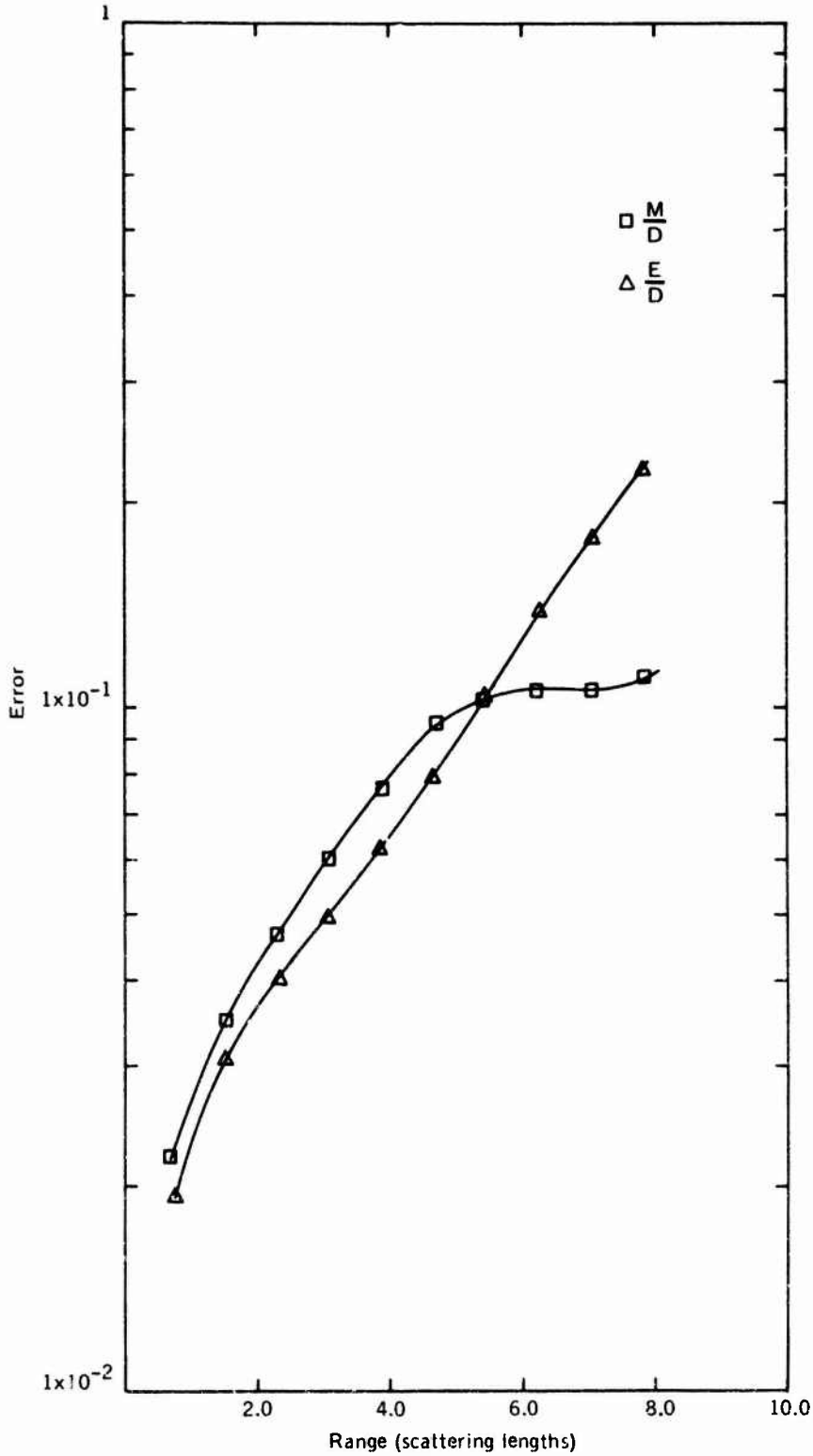

Figure 23. Average Error as a Function of Range for s/a = 3.56.

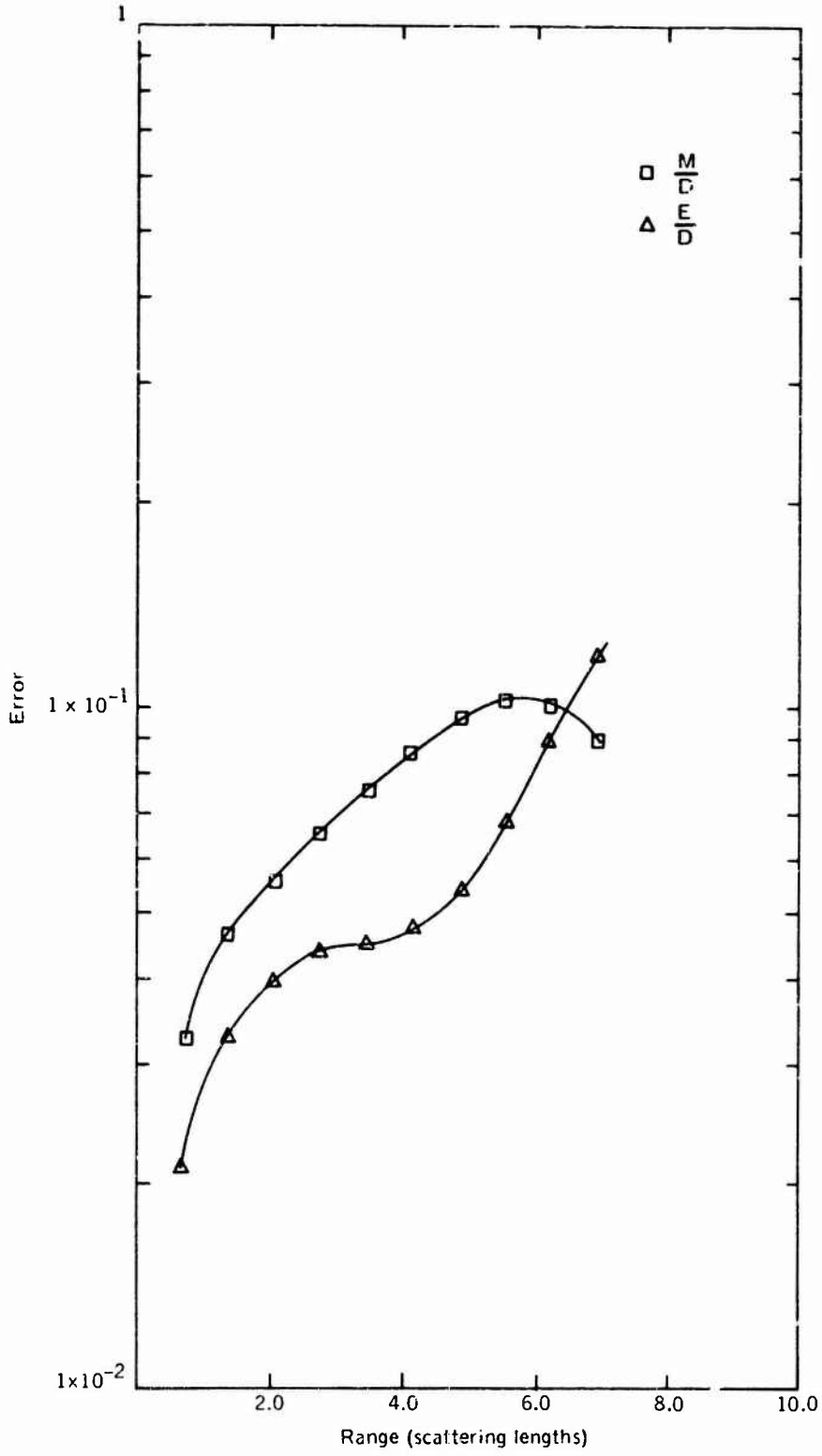

Figure 24. Average Error as a Function of Range for s/a = 2.28.

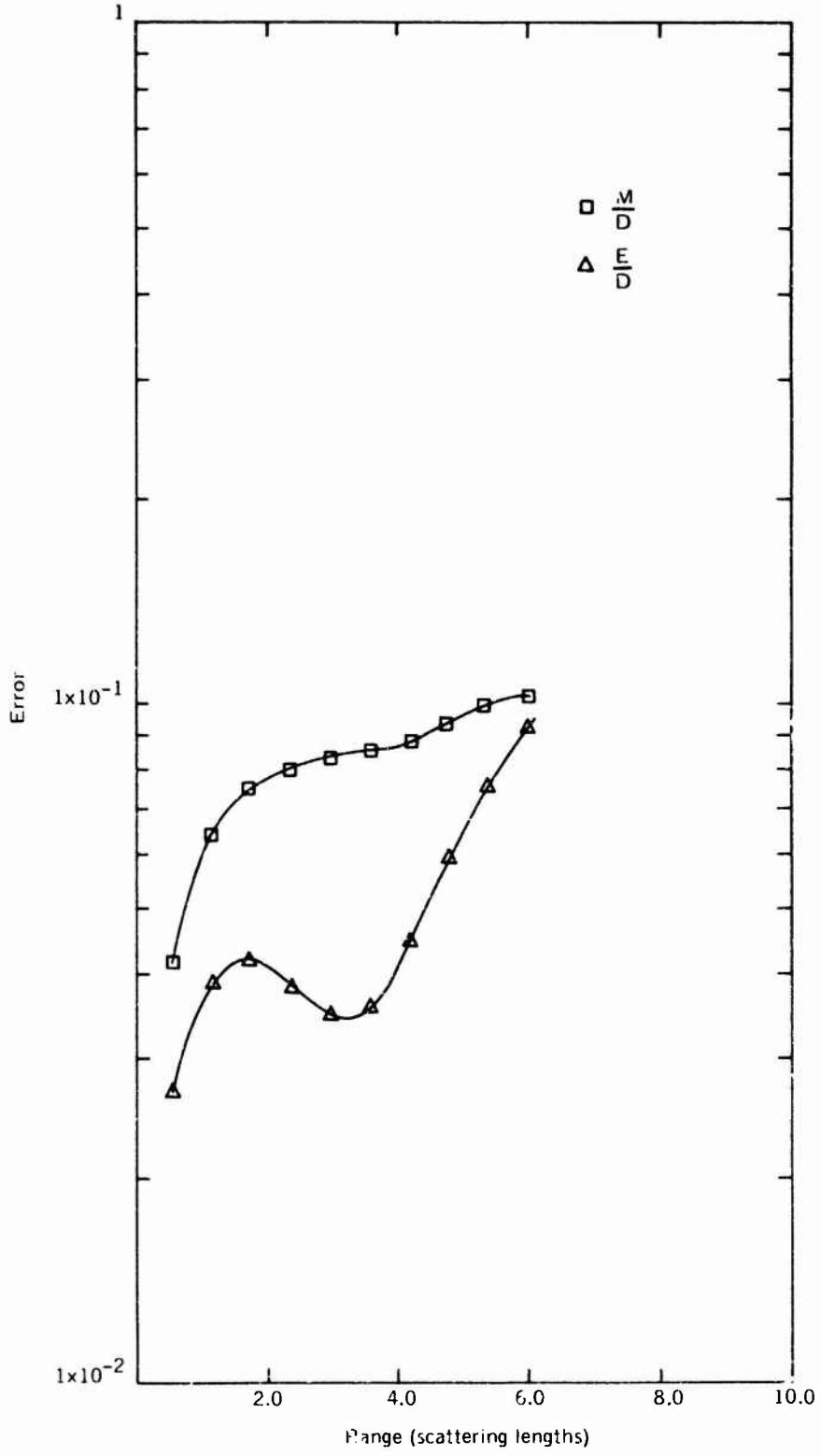

Figure 25. Average Error as a Function of Range for s/a = 1.48.

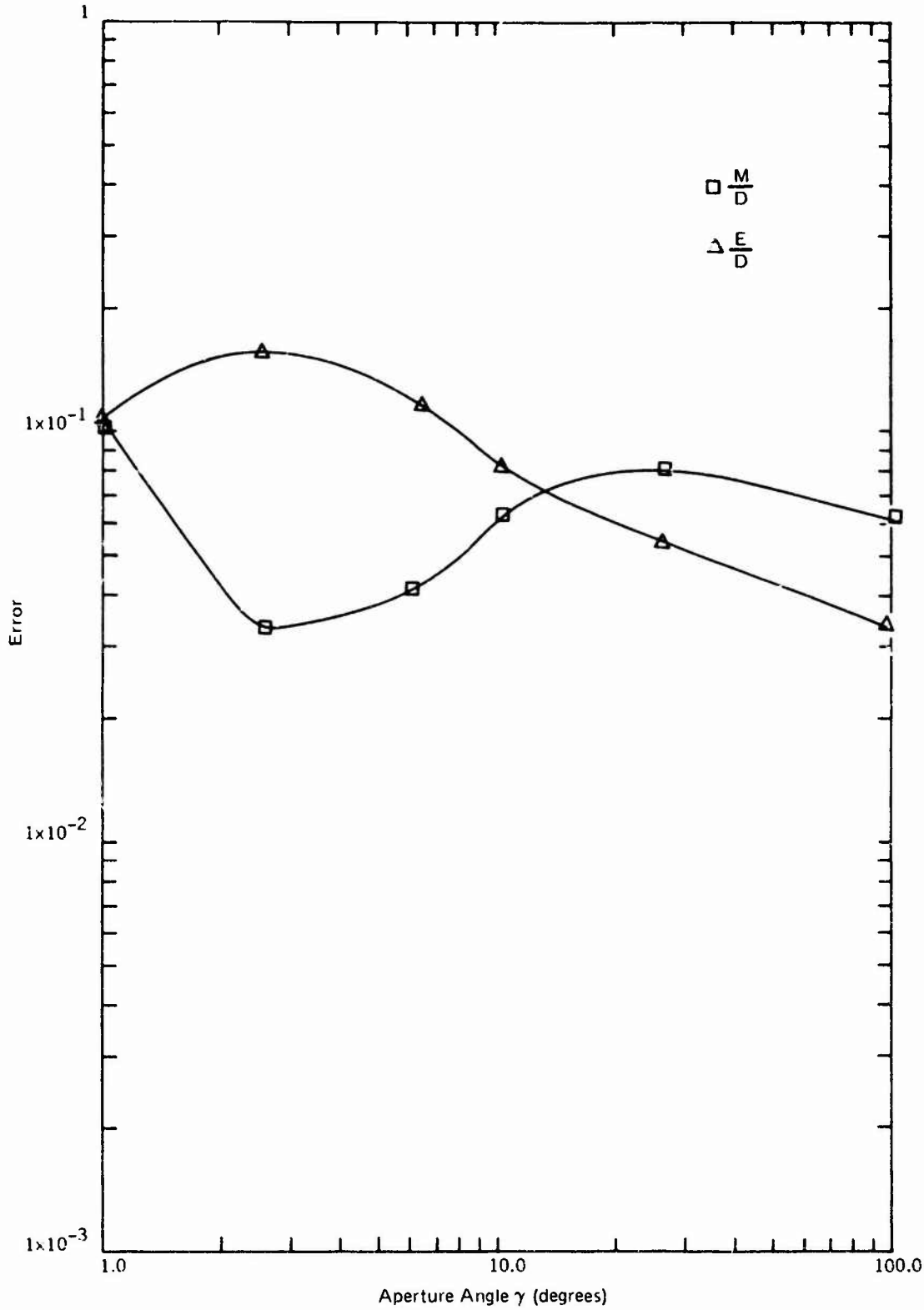

Figure 26. Average Error as a Function of Aperture Angle for s/a = 3.56.

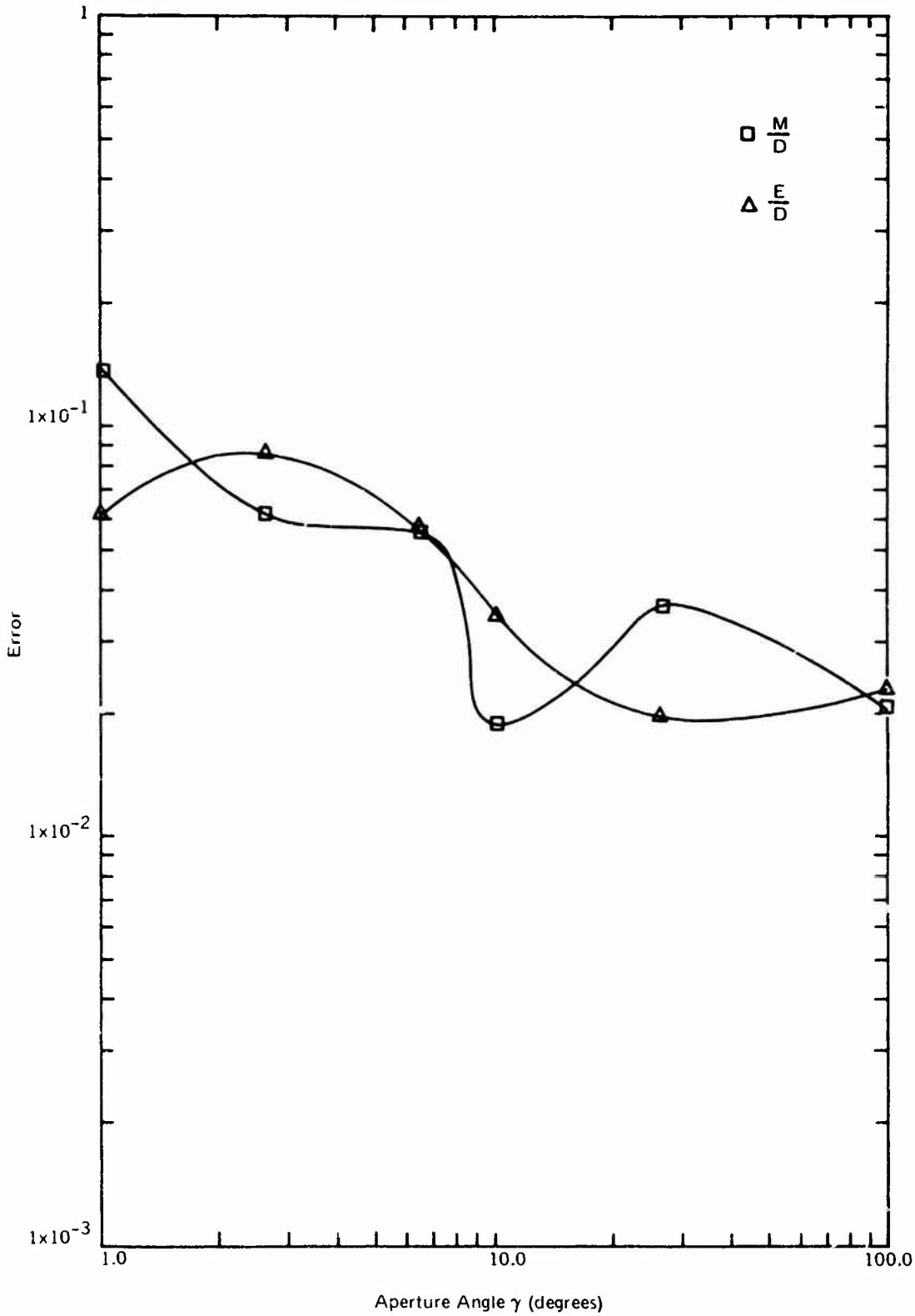

Figure 27. Average Error as a Function of Aperture Angle for s/a = 2.28.

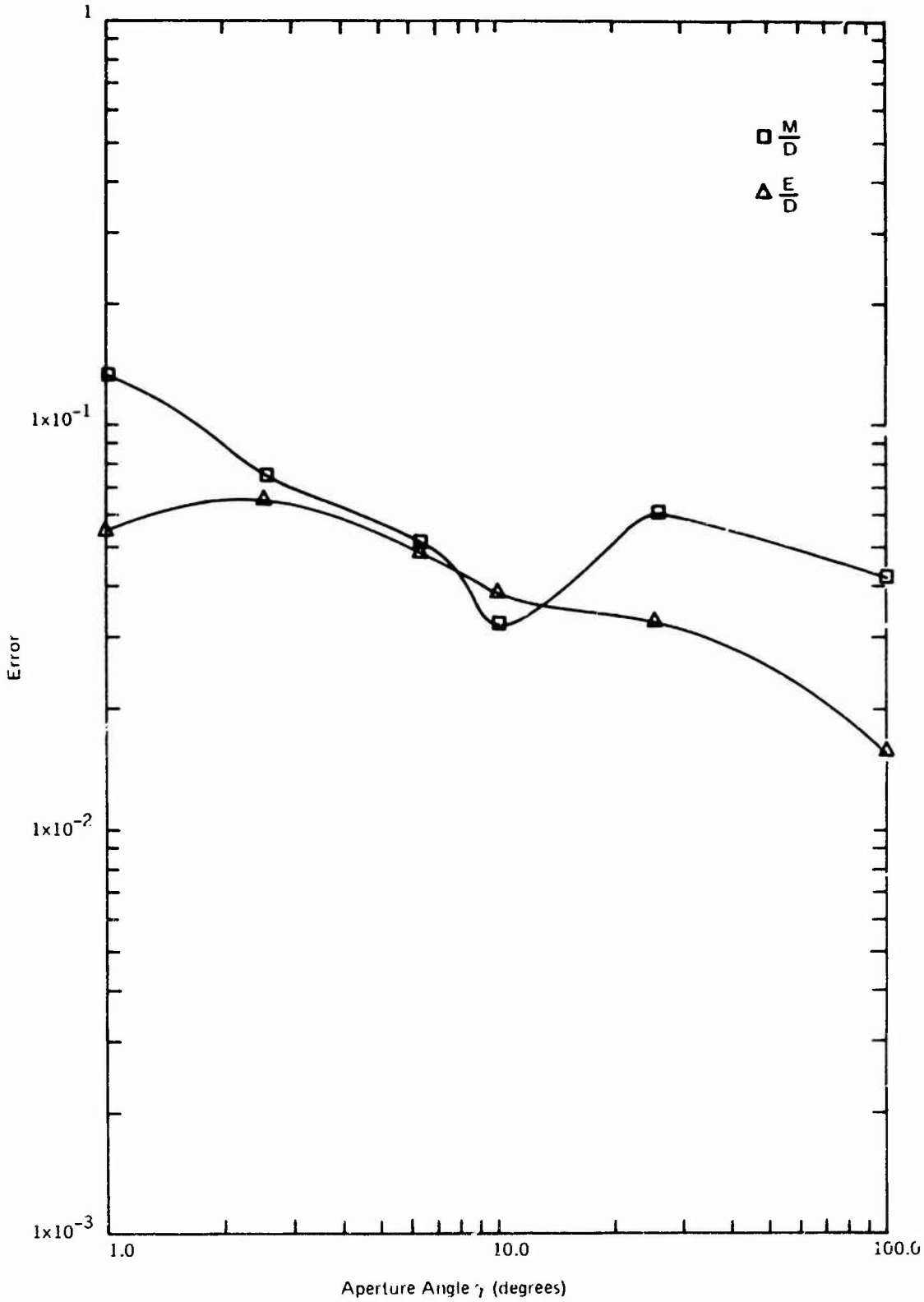

Figure 28. Average Error as a Function of Aperture Angle for s/a = 1.48.

Table 1. Volume Scattering Distribution Functions From S. Q. Duntley.

γ'	$\int_{\gamma'} P(\theta)d\Omega$	γ'	$\int_{\gamma'} P(\theta)d\Omega$
0.000	0.00000	0.100	0.01530
0.120	0.02040	0.150	0.02720
0.170	0.03170	0.200	0.03790
0.250	0.04700	0.300	0.05570
0.350	0.06380	0.400	0.07150
0.500	0.08520	0.600	0.09800
0.700	0.11000	0.800	0.12130
0.900	0.13240	1.000	0.14220
1.200	0.16130	1.500	0.18630
1.700	0.20290	2.000	0.22760
2.500	0.26050	3.000	0.29180
3.500	0.32350	4.000	0.35390
5.000	0.40510	6.000	0.45030
7.000	0.49300	8.000	0.52790
9.000	0.56050	10.000	0.58990
12.000	0.63490	15.000	0.68760
17.000	0.72070	20.000	0.76180
25.000	0.81170	30.000	0.84650
35.000	0.87540	40.000	0.89670
50.000	0.92590	60.000	0.94370
75.000	0.96090	90.000	0.97160
105.000	0.97970	120.000	0.98600
135.000	0.99140	150.000	0.99580
165.000	0.99880	180.000	1.00000

Table 2. Interpolated Volume Scattering Distribution Functions.

γ	γ'	$\int_{\gamma'} P(\theta) d\Omega$
0.10°	0.20°	0.0379
1.00°	2.00°	0.2276
2.51°	5.01°	0.4055
6.31°	12.47°	0.6432
10.00°	19.43°	0.7540
25.11°	43.15°	0.9059
100.00°	109.43°	0.9816

Table 3. Exponential Model Predictions of Radiant Energy Flux for s/a = 3.56.

Range (attenuation lengths)	Aperture Cone Half-Angle γ (degrees)						
	0.10	1.00	2.51	6.31	10.00	25.11	100.00
1.0	0.3789E+00	0.4394E+00	0.5919E+00	0.6078E+00	0.6627E+00	0.7462E+00	0.7871E+00
2.0	0.1436E+00	0.1931E+00	0.2519E+00	0.3694E+00	0.4392E+00	0.5568E+00	0.6196E+00
3.0	0.5441E-01	0.8481E-01	0.1287E+00	0.2246E+00	0.2911E+00	0.4155E+00	0.4877E+00
4.0	0.2062E-01	0.3728E-01	0.6499E-01	0.1365E+00	0.1929E+00	0.3100E+00	0.3839E+00
5.0	0.7812E-02	0.1638E-01	0.3281E-01	0.8296E-01	0.1279E+00	0.2314E+00	0.3022E+00
6.0	0.2960E-02	0.7199E-02	0.1657E-01	0.5042E-01	0.8474E-01	0.1726E+00	0.2379E+00
7.0	0.1217E-02	0.3163E-02	0.8365E-02	0.3065E-01	0.5616E-01	0.1288E+00	0.1872E+00
8.0	0.4251E-03	0.1390E-02	0.4223E-02	0.1863E-01	0.3722E-01	0.9612E-01	0.1474E+00
9.0	0.1611E-03	0.6108E-03	0.2132E-02	0.1132E-01	0.2467E-01	0.7173E-01	0.1600E+00
10.0	0.6103E-04	0.2684E-03	0.1077E-02	0.6882E-02	0.1635E-01	0.5352E-01	0.9131E-01

Table 4. Monte Carlo Model Predictions of Radiant Energy Flux for s/a = 3.56.

Range (attenuation lengths)	Aperture Cone Half-Angle γ (degrees)						
	0.10	1.00	2.51	6.31	10.00	25.11	100.00
1.0	0.4363E+00	0.4695E+00	0.5373E+00	0.6230E+00	0.6761E+00	0.7499E+00	0.7926E+00
2.0	0.1765E+00	0.2137E+00	0.2843E+00	0.3940E+00	0.4552E+00	0.5576E+00	0.6242E+00
3.0	0.6475E-01	0.9979E-01	0.1530E+00	0.2474E+00	0.3048E+00	0.4124E+00	0.4882E+00
4.0	0.2233E-01	0.4766E-01	0.8361E-01	0.1558E+00	0.2034E+00	0.3036E+00	0.3794E+00
5.0	0.7535E-02	0.2323E-01	0.4638E-01	0.9847E-01	0.1355E+00	0.2226E+00	0.2931E+00
6.0	0.2577E-02	0.1153E-01	0.2607E-01	0.6241E-01	0.9038E-01	0.1627E+00	0.2251E+00
7.0	0.9279E-03	0.5807E-02	0.1484E-01	0.3968E-01	0.6041E-01	0.1187E+00	0.1720E+00
8.0	0.3653E-03	0.2964E-02	0.8540E-02	0.2532E-01	0.4056E-01	0.8636E-01	0.1308E+00
9.0	0.1632E-03	0.1528E-02	0.4963E-02	0.1620E-01	0.2741E-01	0.6279E-01	0.9906E-01
10.0	0.8591E-04	0.7944E-03	0.2910E-02	0.1041E-01	0.1867E-01	0.4564E-01	0.7471E-01

Table 5. Experimental Data of Radiant Energy Flux for s/a = 3.56.

Range (attenuation lengths)	Aperture Cone Half-Angle γ (degrees)						
	0.100	1.000	2.511	6.309	10.600	25.110	100.060
1.0	0.4238E+00	0.4136E+00	0.4980E+00	0.6212E+00	0.6823E+00	0.7691E+00	0.7919E+00
2.0	0.1688E+00	0.1745E+00	0.2549E+00	0.3908E+00	0.4682E+00	0.5916E+00	0.6316E+00
3.0	0.6544E-01	0.7585E-01	0.1311E+00	0.2486E+00	0.3228E+00	0.4556E+00	0.5067E+00
4.0	0.2488E-01	0.3402E-01	0.7245E-01	0.1598E+00	0.2236E+00	0.3510E+00	0.4080E+00
5.0	0.9343E-02	0.1578E-01	0.4017E-01	0.1038E+00	0.1555E+00	0.2702E+00	0.3291E+00
6.0	0.3489E-02	0.7580E-02	0.2284E-01	0.6801E-01	0.1085E+00	0.2078E+00	0.2654E+00
7.0	0.1305E-02	0.3787E-02	0.1330E-01	0.4496E-01	0.7587E-01	0.1594E+00	0.2134E+00
8.0	0.4928E-03	0.1968E-02	0.7927E-02	0.2995E-01	0.5318E-01	0.1219E+00	0.1709E+00
9.0	0.1890E-03	0.1066E-02	0.4832E-02	0.2010E-01	0.3734E-01	0.9284E-01	0.1360E+00
10.0	0.7417E-04	0.6037E-03	0.3009E-02	0.1358E-01	0.2625E-01	0.7037E-01	0.1072E+00

Table 6. Exponential Model Predictions of Radiant Energy Flux for s/a = 2.28.

Range (attenuation lengths)	Aperture Cone Half-Angle γ (degrees)						
	0.10	1.60	2.51	6.31	10.00	25.11	100.00
1.0	0.3777E+00	0.4309E+00	0.4877E+00	0.5753E+00	0.6213E+00	0.6905E+00	0.7242E+00
2.0	0.1427E+00	0.1857E+00	0.2378E+00	0.3309E+00	0.3861E+00	0.4768E+00	0.5244E+00
3.0	0.5388E-01	0.8603E-01	0.1160E+00	0.1904E+00	0.2399E+00	0.3293E+00	0.3798E+00
4.0	0.2035E-01	0.3449E-01	0.5656E-01	0.1095E+00	0.1490E+00	0.2274E+00	0.2750E+00
5.0	0.7687E-02	0.1486E-01	0.2759E-01	0.6300E-01	0.9260E-01	0.1570E+00	0.1992E+00
6.0	0.2903E-02	0.6405E-02	0.1345E-01	0.3624E-01	0.5754E-01	0.1084E+00	0.1442E+00
7.0	0.1097E-02	0.2760E-02	0.6561E-02	0.2085E-01	0.3575E-01	0.7487E-01	0.1044E+00
8.0	0.4142E-03	0.1189E-02	0.3200E-02	0.1199E-01	0.2221E-01	0.5170E-01	0.7563E-01
9.0	0.1564E-03	0.5125E-03	0.1560E-02	0.6899E-02	0.1380E-01	0.3570E-01	0.5477E-01
10.0	0.5908E-04	0.2209E-03	0.7610E-03	0.3969E-02	0.8575E-02	0.2465E-01	0.3966E-01

Table 7. Monte Carlo Model Predictions of Radiant Energy Flux for s/a = 2.28.

Range (attenuation lengths)	Aperture Cone Half-Angle γ (degrees)						
	0.10	1.00	2.51	6.31	10.00	25.11	100.00
1.0	0.4282E+00	0.4594E+00	0.5168E+00	0.5936E+00	0.6324E+00	0.6937E+00	0.7280E+00
2.0	0.1742E+00	0.2035E+00	0.2619E+00	0.3502E+00	0.3985E+00	0.4772E+00	0.5261E+00
3.0	0.6523E-01	0.9198E-01	0.1347E+00	0.2071E+00	0.2499E+00	0.3266E+00	0.3774E+00
4.0	0.2306E-01	0.4237E-01	0.7007E-01	0.1228E+00	0.1562E+00	0.2225E+00	0.2689E+00
5.0	0.7906E-02	0.1983E-01	0.3692E-01	0.7296E-01	0.9743E-01	0.1510E+00	0.1904E+00
6.0	0.2696E-02	0.9143E-02	0.1967E-01	0.4345E-01	0.6072E-01	0.1021E+00	0.1341E+00
7.0	0.9394E-03	0.4552E-02	0.1059E-01	0.2593E-01	0.3787E-01	0.6878E-01	0.9388E-01
8.0	0.3432E-03	0.2220E-02	0.5752E-02	0.1551E-01	0.2366E-01	0.4625E-01	0.6541E-01
9.0	0.1349E-03	0.1093E-02	0.3150E-02	0.9297E-02	0.1483E-01	0.3103E-01	0.4538E-01
10.0	0.5862E-04	0.5423E-03	0.1738E-02	0.5584E-02	0.9337E-02	0.2080E-01	0.3135E-0

Table 8. Experimental Data of Radiant Energy Flux for s/a = 2.28.

Range (attenuation lengths)	Aperture Cone Half-Angle γ (degrees)						
	0.100	1.000	2.511	6.309	10.000	25.110	100.000
1.0	0.3895E·00	0.3795E·00	0.4770E·00	0.5965E·00	0.6481E·00	0.7195E·00	0.7449E·00
2.0	0.1538E·00	0.1559E·00	0.2355E·00	0.3560E·00	0.4160E·00	0.5121E·00	0.5500E·00
3.0	0.5986E-01	0.6560E-01	0.1176E·00	0.2111E·00	0.2642E·00	0.3594E·00	0.4003E·00
4.0	0.2304E-01	0.2832E-01	0.5944E-01	0.1245E·00	0.1665E·00	0.2493E·00	0.2878E·00
5.0	0.8813E-02	0.1255E-01	0.3047E-01	0.7333E-01	0.1043E·00	0.1711E·00	0.2047E·00
6.0	0.3362E-02	0.5717E-02	0.1585E-01	0.4317E-01	0.6508E-01	0.1165E·00	0.1443E·00
7.0	0.1285E-02	0.2678E-02	0.8382E-02	0.2548E-01	0.4055E-01	0.7887E-01	0.1010E·00
8.0	0.4939E-03	0.1291E-02	0.4510E-02	0.1511E-01	0.2529E-01	0.5314E-01	0.7037E-01
9.0	0.1918E-03	0.6414E-03	0.2472E-02	0.9026E-02	0.1581E-01	0.3571E-01	0.4884E-01
10.0	0.7553E-04	0.3286E-03	0.1382E-02	0.5442E-02	0.9940E-02	0.2399E-01	0.3385E-01

Table 9. Exponential Model Predictions of Radiant Energy Flux for s/a = 1.48.

Range (attenuation lengths)	Aperture Cone Half-Angle γ (degrees)						
	0.10	1.00	2.51	6.31	10.00	25.11	100.00
1.0	0.3763E+00	0.4214E+00	0.4686E+00	0.5400E+00	0.5769E+00	0.6317E+00	0.6580E+00
2.0	0.1416E+00	0.1776E+00	0.2196E+00	0.2916E+00	0.3328E+00	0.3990E+00	0.4330E+00
3.0	0.5328E-01	0.7483E-01	0.1029E+00	0.1575E+00	0.1920E+00	0.2520E+00	0.2849E+00
4.0	0.2005E-01	0.3153E-01	0.4822E-01	0.8503E-01	0.1108E+00	0.1592E+00	0.1875E+00
5.0	0.7545E-02	0.1329E-01	0.2260E-01	0.4592E-01	0.6391E-01	0.1006E+00	0.1233E+00
6.0	0.2839E-02	0.5500E-02	0.1059E-01	0.2480E-01	0.3687E-01	0.6353E-01	0.8116E-01
7.0	0.1068E-02	0.2360E-02	0.4962E-02	0.1339E-01	0.2127E-01	0.4013E-01	0.5340E-01
8.0	0.4020E-03	0.9944E-03	0.2325E-02	0.7230E-02	0.1227E-01	0.2535E-01	0.3514E-01
9.0	0.1513E-03	0.4190E-03	0.1090E-02	0.3904E-02	0.7081E-02	0.1601E-01	0.2312E-01
10.0	0.5692E-04	0.1766E-03	0.5107E-03	0.2108E-02	0.4085E-02	0.1011E-01	0.1521E-01

Table 10. Monte Carlo Model Predictions of Radiant Energy Flux for s/a = 1.48.

Range (attenuation lengths)	Aperture Cone Half-Angle γ (degrees)						
	0.10	1.00	2.51	6.31	10.00	25.11	100.00
1.0	0.4184E+00	0.4483E+00	0.4944E+00	0.5552E+00	0.5856E+00	0.6342E+00	0.6604E+00
2.0	0.1706E+00	0.1925E+00	0.2386E+00	0.3059E+00	0.3419E+00	0.3990E+00	0.4325E+00
3.0	0.6511E-01	0.8398E-01	0.1164E+00	0.1689E+00	0.1989E+00	0.2499E+00	0.2814E+00
4.0	0.2365E-01	0.3718E-01	0.5738E-01	0.9343E-01	0.1153E+00	0.1558E+00	0.1819E+00
5.0	0.8312E-02	0.1688E-01	0.2855E-01	0.5177E-01	0.6672E-01	0.9678E-01	0.1168E+00
6.0	0.2872E-02	0.7576E-02	0.1433E-01	0.2873E-01	0.3854E-01	0.5989E-01	0.7465E-01
7.0	0.9917E-03	0.3479E-02	0.7250E-02	0.1547E-01	0.2224E-01	0.3695E-01	0.4744E-01
8.0	0.3479E-03	0.1613E-02	0.3695E-02	0.8885E-02	0.1284E-01	0.2273E-01	0.3001E-01
9.0	0.1260E-03	0.7545E-03	0.1895E-02	0.4950E-02	0.7417E-02	0.1395E-01	0.1890E-01
10.0	0.4790E-04	0.3553E-03	0.9776E-03	0.2760E-02	0.4292E-02	0.8539E-02	0.1185E-01

Table 11. Experimental Data of Radiant Energy Flux for s/a = 1.48.

Range (attenuation lengths)	Aperture Cone Half-Angle ν (degrees)						
	0.100	1.000	2.511	6.309	10.000	25.110	100.000
1.0	0.3751E+00	0.3691E+00	0.4246E+00	0.5075E+00	0.5489E+00	0.6118E+00	0.6336E+00
2.0	0.1391E+00	0.1448E+00	0.1921E+00	0.2673E+00	0.3113E+00	0.3859E+00	0.4136E+00
3.0	0.5117E-01	0.5502E-01	0.9032E-01	0.1451E+00	0.1813E+00	0.2484E+00	0.2751E+00
4.0	0.1874E-01	0.2486E-01	0.4385E-01	0.8064E-01	0.1077E+00	0.1622E+00	0.1852E+00
5.0	0.6856E-02	0.1078E-01	0.2185E-01	0.4565E-01	0.6494E-01	0.1067E+00	0.1255E+00
6.0	0.2516E-02	0.4790E-02	0.1110E-01	0.2617E-01	0.3945E-01	0.7033E-01	0.8505E-01
7.0	0.9293E-03	0.2172E-02	0.5719E-02	0.1511E-01	0.2400E-01	0.4612E-01	0.5729E-01
8.0	0.3468E-03	0.1001E-02	0.2967E-02	0.8727E-02	0.1453E-01	0.2991E-01	0.3813E-01
9.0	0.1312E-03	0.4670E-03	0.1541E-02	0.5018E-02	0.8704E-02	0.1907E-01	0.2491E-01
10.0	0.5054E-04	0.2194E-03	0.7964E-03	0.2855E-02	0.5124E-02	0.1187E-01	0.1588E-01

Table 12. Average Errors Between the Two Models and Experimental Data as a Function of Range.

		Range (scattering lengths)									
s.a.	3.56	0.78	1.56	2.34	3.12	3.90	4.68	5.46	6.25	7.03	7.81
	E-D	0.1952E-01	0.2120E-01	0.4022E-01	0.4974E-01	0.6294E-01	0.8205E-01	0.1062E-00	0.1107E-00	0.1807E-00	0.2276E-00
	M-D	0.2193E-01	0.3151E-01	0.4681E-01	0.6088E-01	0.7662E-01	0.9170E-01	0.1022E-00	0.1061E-00	0.1057E-00	0.1109E-00
		Range (scattering lengths)									
s.a.	2.28	0.70	1.39	2.08	2.78	3.48	1.17	1.87	5.56	6.26	6.95
	E-D	0.2174E-01	0.3338E-01	0.4070E-01	0.4128E-01	0.4372E-01	0.4789E-01	0.5155E-01	0.6878E-01	0.9122E-01	0.1213E-00
	M-D	0.3816E-01	0.4670E-01	0.5641E-01	0.6565E-01	0.7619E-01	0.8746E-01	0.9721E-01	0.1025E-00	0.1097E-00	0.3019E-01
		Range (scattering lengths)									
s.a.	1.48	0.60	1.19	1.79	2.39	2.98	3.58	4.18	4.77	5.37	5.97
	E-D	0.2713E-01	0.3916E-01	0.4129E-01	0.3891E-01	0.3446E-01	0.3534E-01	0.4515E-01	0.6058E-01	0.7712E-01	0.9364E-01
	M-D	0.4212E-01	0.6386E-01	0.7516E-01	0.8026E-01	0.8342E-01	0.8891E-01	0.8750E-01	0.9303E-01	0.9838E-01	0.1011E-00

Table 13. Average Errors Between the Two Models and Experimental Data as a Function of Aperture Angle.

		Aperture Cone Half-Angle γ (degrees)						
		0.10	1.00	2.51	6.31	10.00	25.11	100.00
s a	3.56							
	E D	0.5073E-01	0.1077E-00	0.1580E-00	0.1159E-00	0.8663E-01	0.5748E-01	0.3406E-01
	M D	0.6337E-01	0.1061E-00	0.3364E-01	0.4148E-01	0.6344E-01	0.8238E-01	0.6294E-01
s a	2.28							
	E D	0.4809E-01	0.6183E-01	0.8864E-01	0.5941E-01	0.3624E-01	0.1092E-01	0.2306E-01
	M D	0.7150E-01	0.1399E-00	0.6096E-01	0.5869E-01	0.1903E-01	0.3736E-01	0.2078E-01
s a	1.48							
	E D	0.3254E-01	0.5533E-01	0.6737E-01	0.4785E-01	0.3911E-01	0.3458E-01	0.1626E-01
	M D	0.4787E-01	0.1315E-00	0.7299E-01	0.3166E-01	0.3249E-01	0.6084E-01	0.5307E-01

REFERENCES

1. C. Funk, "Monte Carlo Simulation of the Underwater Light Field Distribution from a Point Source," Naval Undersea Warfare Center, Pasadena, California, NUWC TN 138, September 1968.

2. C. Funk, "Computer Simulation of the Performance of Advanced Underwater Optical Viewing Systems," *Engineering in the Ocean Environment, Record of the 1971 IEEE Conference held at San Diego, Calif., 21-24 September 1971,* Institute of Electrical and Electronic Engineers, New York, 1971.

3. S. Q. Duntley, "Underwater Lighting by Submerged Lasers and Incandescent Sources," University of California, San Diego, Scripps Institution of Oceanography, Visibility Laboratory, San Diego, California, SIO Ref. 71-1, June 1971.